7 mif

X-621-73-223

SUPERCEDES
X-621-72-480

X-70441

THERMOSPHERIC WIND EFFECTS ON THE GLOBAL DISTRIBUTION OF HELIUM IN THE EARTH'S UPPER ATMOSPHERE

CARL A. REBER

(NASA-TM-X-70441) THERMOSPHERIC WIND EFFECTS ON THE GLOBAL DISTRIBUTION OF HELIUM IN THE EARTH'S UPPER ATMOSPHERE Ph.D. Thesis - Michigan Univ., Ann Arbor (NASA) ~~156~~ 152 p HC $10.00 CSCL 04A

N73-29391

Unclas

G3/13 11975

JULY 1973

GSFC

GODDARD SPACE FLIGHT CENTER
GREENBELT, MARYLAND

X-621-73-223
Supersedes
X-621-71-480

THERMOSPHERIC WIND EFFECTS ON THE GLOBAL DISTRIBUTION OF HELIUM IN THE EARTH'S UPPER ATMOSPHERE

Carl A. Reber

July 1973

This report was also a dissertation submitted in partial fulfillment of the requirements for the degree of Doctor of Philosophy in the Horace H. Rackham School of Graduate Studies at The University of Michigan, 1973.

Goddard Space Flight Center

Greenbelt, Maryland

ABSTRACT

The momentum and continuity equations for a minor gas are combined with the momentum equation for the major constituents to obtain the time dependent continuity equation for the minor species reflecting a wind field in the background gas. This equation is used to study the distributions of helium and argon at times of low, medium, and high solar activity for a variety of latitudinal-seasonal wind cells. For helium, the exospheric return flow at the higher thermospheric temperatures dominates the distribution to the extent that much larger latitudinal gradients can be maintained during periods of low solar activity than during periods of high activity. By comparison to the exospheric flow, the smoothing effect of horizontal diffusion is almost negligible. The latitudinal variation of helium observed by satellite mass spectrometers can be reproduced by the effect of a wind system of air rising in the summer hemisphere, flowing across the equator with speeds on the order of 100 to 200 m/sec, and descending in the winter hemisphere. Argon, being heavier than the mean mass in the lower thermosphere, reacts oppositely to helium in that it is enhanced in the summer hemisphere and depleted in the winter. By using winds which are effective in the lower thermosphere, the anomalous vertical helium profiles observed from rockets can be reproduced. The time response of the helium density distribution following the initiation of a wind field implies the likelihood of a factor of two to four density enhancement at night over the daytime values.

The author wishes to express his appreciation to Professor Paul B. Hays for his guidances, assistance and encouragement throughout this study. The author also appreciates the thoughtful comments and the time taken by the various other members of his committee including Professors William R. Kuhn, Leslie M. Jones, Andrew F. Nagy, and James C. G. Walker, and Doctor Ernest G. Fontheim. He is also indebted to the many people in the Laboratory for Planetary Atmospheres of the Goddard Space Flight Center and in the Space Physics Research Laboratory of the University of Michigan who contributed to making the OGO-6 mass spectrometer a success. In particular, the efforts of George R. Carignan are gratefully acknowledged; he more than anyone else, by his untiring efforts in all phases of experiment preparation, helped to insure the success of the experiment.

At Goddard Space Flight Center, the author is indebted to Dr. Alan E. Hedin and Miss Georgiann Batluck for helpful discussions during the development of the computer program, as well as to Dr. Frank Huang for helping to streamline the program so that it would run in a finite length of time on the GSFC 360/75.

TABLE OF CONTENTS

ILLUSTRATIONS

Figure		Page

Figure		Page

Figure		Page

NOMENCLATURE

$A_{\ell nm}$	=	coefficient defined in Appendix D
B_{ℓ}	=	coefficient defined in II.B.2
$B_{\ell nm}$	=	coefficient defined in Appendix D
b	=	radius to base of exosphere
C_{nm}	=	coefficient defined in Appendix D
D	=	molecular diffusion coefficient
g	=	local acceleration of gravity
H	=	$\frac{kT}{mg}$ = scale height of minor gas
H^1	=	$\frac{kT}{Mg}$ = scale height of major gas
J	=	coefficient defined in Section II D
k	=	Boltzmann's constant
K	=	eddy diffusion coefficient
m	=	molecular mass of minor gas
M	=	molecular mass of major gas
n	=	number density of minor gas
N	=	number density of major gas
p	=	pressure
$P_m(\theta)$	=	Legendre polynomial
r	=	radial coordinate
S	=	shape factor in exponential temperature profile
T	=	temperature
t	=	time

v = flow velocity of minor gas

V = flow velocity of major gas

$\langle v \rangle$ = mean molecular speed = $(2.55\ k\ T/m)^{1/2}$

α = thermal diffusion factor

β_ℓ^1 = factor determining wind velocity gradient

β_ℓ = $\beta^1 \times 10^2$ (defined in III.B.1.a)

$\Gamma(\ell)$ = gamma function = $(\ell - 1)!$ for n = integer > 0

ϵ = coefficient defined in II.D.

θ = polar angle (colatitude)

μ = cosine θ

ν = momentum transfer collision frequency for gas n in a background gas

σ = coefficient defined in Appendix B

THERMOSPHERIC WIND EFFECTS ON THE GLOBAL DISTRIBUTION OF HELIUM IN THE EARTH'S UPPER ATMOSPHERE

I. INTRODUCTION

The enhancement of upper atmospheric helium in the winter hemisphere has been noted from satellite mass spectrometers (Reber and Nicolet, 1965; Reber, et al., 1968) and has been suggested to explain anomalies in satellite drag data (Keating and Prior, 1968; Jacchia, 1968). The best mapping of this phenomena has come recently from the quadrupole mass spectrometer flown on the OGO-6 satellite (Reber, et al., 1971). Figure 1 shows the distribution of helium from this measurement taken over half an orbit near sunrise on 7 June 1969. As the data are taken over a range of altitudes, this parameter is normalized out by dividing each measured density by the predicted density from the appropriate Jacchia model atmosphere (Jacchia, 1965, hereafter referred to as J65),

$$[\mathrm{He}]_N = \frac{\text{Measured helium density}}{\text{Model helium density}}.$$

To the extent that J65 correctly represents the real temperature profile, and the atmosphere is in diffusive equilibrium, $[\mathrm{He}]_N$ is the ratio of the actual helium density at 120 km to the constant boundary density of the model. The data in

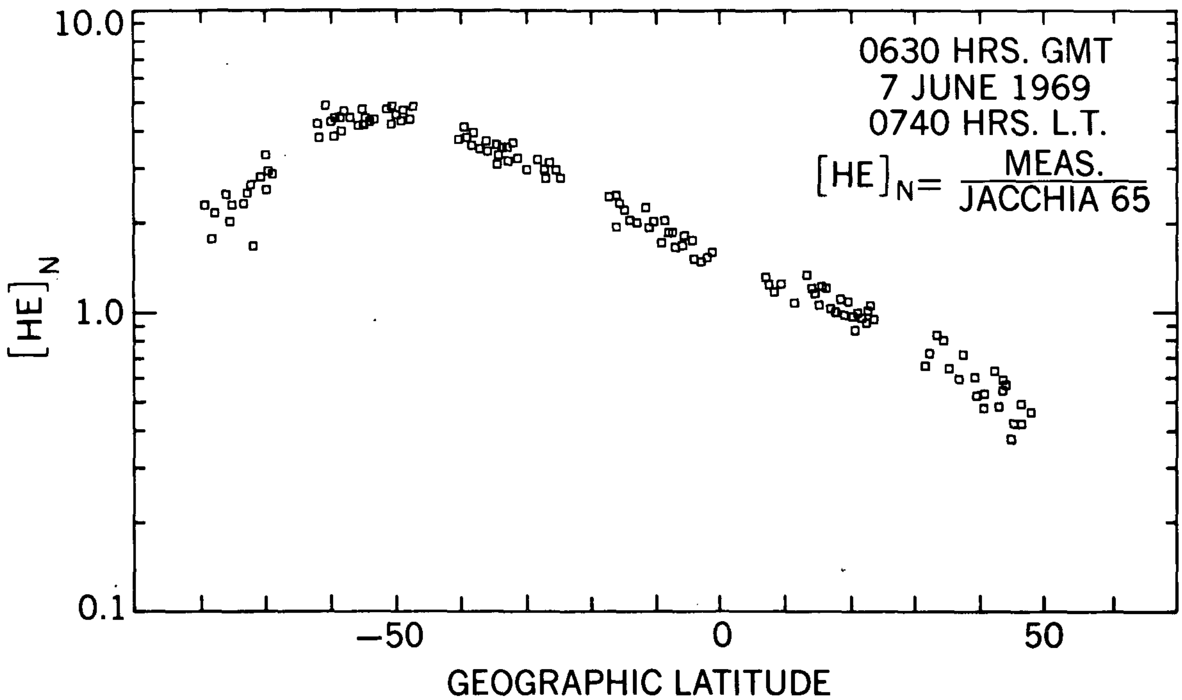

Figure 1. Ratio of the measured helium number density to Jacchia 65 model atmosphere density as a function of geographic latitude (Reber, et al., 1971).

Figure 1 shows that this ratio varies by an order of magnitude over the geographic latitude range 50°N to 80°S, with a peak near 55°S. It is further shown that the location of the peak in the helium density is closely correlated with the geomagnetic dipole field, with peak locations falling quite close to the 53° south magnetic dipole latitude.

Vertical profiles of constituent densities obtained from rocket measurements consistently show departures from diffusive equilibrium profiles for helium and occasionally for argon as well. Kasprzak (1969) summarizes seven of these flights and attributes the profiles to an upward flux of helium ranging from $2.0 \times 10^8\,cm^{-2}\,sec^{-1}$ to $2.6 \times 10^{10}\,cm^{-2}\,sec^{-1}$. He notes that these values are consistent with fluxes calculated by McAfee (1967) for lateral transport of helium at the base of the exosphere due to diurnal temperature variations. Hartmann, et al. (1968) reports an enhanced helium distribution in the winter thermosphere and decreased argon concentrations. They attribute their results to a lowering of the turbopause level below that assumed by the COSPAR International Reference Atmosphere (CIRA, 1965). Reber (1968) interpretes the deviations from diffusive equilibrium profiles in terms of the long diffusion times in the lower atmosphere and the combination of this phenomenon with changes in time of either the turbopause level or the exospheric temperature.

In the discussion of helium data from Explorer 17, Reber and Nicolet (1965) suggest that the observed latitudinal/seasonal (spring-fall) variation of a factor of two could be explained by a seasonally dependent change of 5 km in the turbopause altitude. The variation of helium density with turbopause altitude has been studied in detail by Kockarts and Nicolet (1962); Kockarts (1971), exploring this mechanism further, points out that a factor of 20 variation in the eddy diffusion coefficient is required to explain the OGO-6 data. However, Colegrove, Hanson and Johnson (1965) comment that the molecular oxygen to atomic oxygen ratio at 120 km is proportional to the eddy diffusion coefficient. As an oxygen variation of this magnitude is not observed, there is an apparent inconsistency in the use of this mechanism to explain the entire helium variation.

Johnson and Gottlieb (1969, 1970) suggest that the source of the winter enhancement of helium is a large scale meridional circulation system, with air moving from the summer polar regions toward the winter pole. They infer a downward flow on the order of 100 cm/sec between 150 and 200 km altitude in the winter polar region from the compressional heating required to maintain the temperature in this region. Taking into account the upward flux required to support exospheric transport (McAfee, 1967) due to the density enhancement, they arrive at a concentration buildup of about a factor of two at the winter pole. They state further that there is probably an inverse effect over the summer pole so the circulation mechanism would support a pole-to-pole ratio of about four.

To investigate the effect of winds on minor constituents in more detail, Reber, Mayr and Hays (1970) studied the continuity equation for a minor gas modified to include the effects of winds. The simplified wind system used in their calculation consists of a constant vertical velocity above 200 km and zero wind below that altitude, along with a cosine distribution in latitude. They conclude that the global helium distribution can be explained on the basis of upper thermospheric winds and that these winds would affect the vertical distribution to altitudes below 100 km.

In the present work these calculations are expanded in several ways to reflect a more realistic physical situation. Basically, the analytical approach involves combining the momentum and continuity equations for a minor gas (e.g. helium) with the continuity equation for the major background gas (in this case, the total of 0, 0_2 and N_2). The result is the three-dimensional time-dependent continuity equation for the minor gas, modified from the usual version by the addition of motion in the background gas through which the minor gas is diffusing. The horizontal component of the meridional wind field is expressed in terms of the vertical component through the major gas continuity equation, while the analytic form of the vertical wind permits a more realistic and easily varied circulation cell to be described. The calculation includes the smoothing effect of horizontal diffusion at all altitudes, and in addition, the upper boundary condition reflects the exospheric transport discussed by McAfee (1967) and Hodges and Johnson (1968).

The resulting differential equation is integrated numerically, using an IBM 360-75 computer. The results, presented in the following chapters, permit the effects of vertical wind profile, exospheric temperature, horizontal diffusion and exospheric transport to be examined in detail with respect to their influence on the horizontal and vertical distribution of helium. In a later chapter, the types of wind fields which produce distributions consistent with satellite and rocket observations are described. The majority of the study is carried out for the steady state situation (primarily to reduce computer time), but the time response following a sudden initiation of a wind field is investigated for a number of typical systems. Finally, the behavior of argon (which exhibits an opposite reaction to winds compared to helium) is examined from the point of view of (1) comparison with measurements and (2) emphasizing the physical processes important in the redistribution of gases in the upper atmosphere.

II. DYNAMIC MODEL FOR A MINOR GAS

The problem of studying the three dimensional distribution of a minor gas, when a motion field is impressed on the major (background) gas, is approached by combining the momentum and continuity equations for the minor gas with the continuity equation for the major species. The result is the minor gas continuity equation, modified from the usual form by the addition of terms reflecting winds in the major species.

The calculation is simplified considerably by the assumption (discussed in detail in IIB) that the wind fields and minor gas distribution can be averaged over a day; thus, any longitudinal variations are neglected. A solution to the continuity equation is obtained by expanding the minor gas distribution and the wind field in terms of Legendre polynomials and solving for the coefficients of the gas distribution for a given wind field. The remainder of this chapter is devoted to a discussion of this calculation; detailed derivations are found in the appendix.

A. Combined Continuity and Momentum Equations

In spherical coordinates, with no longitudinal variation and no sources or sinks, the continuity equation for the minor species (n) becomes

$$\frac{\partial n}{\partial t} + \frac{\partial}{\partial r}(n\,v_r) + \frac{2\,n\,v_r}{r} + \frac{1}{r\sin\theta}\frac{\partial}{\partial\theta}(\sin\theta\, n\, v_\theta) = 0, \tag{1}$$

where

n = number density of minor gas,

t = time,

v = flow velocity of minor gas,

r = radial coordinate,

θ = polar angle.

Similarly, the radial and latitudinal components of the momentum equation become

$$n\,[v_r - V_r] = -D\left[\frac{\partial n}{\partial r} + \frac{n\,(1+\alpha)}{T}\frac{\partial T}{\partial r} + \frac{n}{H}\right] - K\left[\frac{\partial n}{\partial r} + \frac{n}{T}\frac{\partial T}{\partial r} + \frac{n}{H'}\right] \tag{2}$$

and

$$n\,[v_\theta - V_\theta] = -\frac{D}{r}\left[\frac{\partial n}{\partial\theta} + \frac{n\,(1+\alpha)}{T}\frac{\partial T}{\partial\theta}\right], \tag{3}$$

where

V = flow velocity of background (major) gas

D = molecular diffusion coefficient,

α = thermal diffusion factor,

T = temperature,

$H = \dfrac{kT}{mg}$ = scale height of minor gas,

k = Boltzmann's constant,

m = molecular mass of minor gas,

g = local acceleration of gravity,

K = eddy diffusion coefficient,

$H' = \dfrac{kT}{Mg}$ = scale height of major gas,

M = mean molecular mass of major gas.

The eddy diffusion term,

$$K \left[\frac{\partial n}{\partial r} + \frac{n}{T}\frac{\partial T}{\partial r} + \frac{n}{H'}\right],$$

is added to the expression for the radial momentum by considering the flux to be composed of diffusive and eddy components, after the development by Colegrove, et al. (1965). (Horizontal eddy diffusion effects are not included in the present calculation.) By combining equations (1), (2) and (3) with the continuity equation for the background gas one can obtain a form of the minor gas continuity equation which contains the effect of motion in the background gas (see Appendix A):

$$\begin{aligned}
\frac{\partial n}{\partial t} = \frac{\partial}{\partial r} & \left\{ D \left[\frac{\partial n}{\partial r} + \frac{n(1+\alpha)}{T}\frac{\partial T}{\partial r} + \frac{n}{H}\right] + K \left[\frac{\partial n}{\partial r} + \frac{n}{T}\frac{\partial T}{\partial r} + \frac{n}{H'}\right]\right\} \\
& + \frac{2}{r}\left\{ D \left[\frac{\partial n}{\partial r} + \frac{n(1+\alpha)}{T}\frac{\partial T}{\partial r} + \frac{n}{H}\right] + K \left[\frac{\partial n}{\partial r} + \frac{n}{T}\frac{\partial T}{\partial r} + \frac{n}{H'}\right]\right\} \\
& + V_r \left[\frac{n}{N}\frac{\partial N}{\partial r} - \frac{\partial n}{\partial r}\right] + V_\theta \frac{1}{r}\left[\frac{n}{N}\frac{\partial N}{\partial \theta} - \frac{\partial n}{\partial \theta}\right] \\
& + \frac{1}{r^2 \sin\theta}\frac{\partial}{\partial \theta}\left[D \sin\theta \left(\frac{\partial n}{\partial \theta} + \frac{n(1+\alpha)}{T}\frac{\partial T}{\partial \theta}\right)\right],
\end{aligned} \tag{4}$$

where N = background gas number density. The first two terms on the right represent the effect of radial diffusive flow in a spherically symmetric atmosphere; solution of the equation containing only these two terms, with the diffusive flux, $n(v_r - V_r)$, set equal to zero yields the usual static diffusive-equilibrium vertical distribution. The fifth term reflects the smoothing effect of horizontal diffusion.

The third and fourth terms represent the perturbations introduced by vertical and horizontal winds, V_r and V_θ, on the minor gas distribution. The physical effect of this type of term can be better seen by using the approximations

$$\frac{1}{N}\frac{\partial N}{\partial r} \cong -\frac{1}{H'}$$

and

$$\frac{1}{n}\frac{\partial n}{\partial r} \cong -\frac{1}{H}.$$

With these, the vertical wind term becomes

$$nV_r\left(\frac{1}{H}-\frac{1}{H'}\right) = \frac{nV_r}{H'}\left(\frac{m}{M}-1\right). \tag{5}$$

Thus, an upward wind will cause a decrease in density for gases whose mass is less than the mean mass, and an increase in density for gases whose mass is greater than the mean mass; for gases whose mass is close to the mean mass in regions where the wind is important (e.g. N_2) there is little effect. The opposite sense holds true, of course, for a vertically downward wind.

One can also study the reaction to a vertical wind in terms of its effect on the composition of a cell of air moving with the wind. A cell moving upward in the region where mixing is no longer important will maintain the relative composition of air at a lower altitude. For a light gas such as helium, this results in a decrease in the relative number density at higher altitudes. Again, the opposite holds true for a downward wind: a cell of air transported to lower altitudes reflects the relative composition of the higher altitude, resulting in an enhancement of the lighter species and a depletion of the heavier gases. While the vertical wind is distorting the vertical profile from a diffusive distribution, molecular diffusion is attempting to re-establish this profile. Thus, to be effective, the vertical wind speed must be significant relative to the local diffusion velocity, v_D, where

$$v_D = \frac{D}{H} .$$

In this sense, the process may be considered analogous to the competition between eddy and molecular diffusion in establishing the transition from the mixed to the diffusive atmosphere (the "turbopause").

B. Assumptions and Approximations

1. Longitudinal averaging

In the derivation of equation 4 one assumption has already been made and noted, that of no longitudinal (or diurnal) variation in the quantities of interest. This is done on the basis that the phenomenon being studied is an averaged, relatively long term, effect (namely a latitudinal-seasonal phenomenon) as opposed to a diurnal effect. The wind system postulated is also a diurnal average and is divergence free in the east-west direction; the only requirement is that outflow during the day near the summer pole must exceed the inflow during the night, while at the winter pole the inflow must exceed the outflow. A wind system of this general nature is discussed in some detail by Johnson and Gottlieb

(1970) as being required to explain the relative warmth of the mesosphere and thermosphere over the winter pole in the absence of direct solar heating. There is also no indication from available data that there exists a persistent longitudinal variation in the helium distribution.

2. Polynomial expansion of minor gas distribution and wind field

Equation (4) is solved by expressing the latitudinal wind field and minor gas (hereafter specified as helium) distribution as an expansion in Legendre polynomials:

$$V_r(r, \theta) = \sum_{\ell} V_{\ell}(r) P_{\ell}(\theta) \tag{5}$$

and

$$n(r, \theta) = \sum_{n} n_n(r) P_n(\theta). \tag{6}$$

The horizontal wind components are related to the vertical components through the major gas continuity equation.

$$\frac{\partial N}{\partial t} + \frac{\partial}{\partial r}(NV_r) + \frac{2NV_r}{r} + \frac{1}{r \sin\theta} \frac{\partial}{\partial \theta}(\sin\theta N V_\theta) = 0. \tag{7}$$

For a steady state the latitudinal components become (see Appendix C)

$$V_\theta(r, \theta) = -\sum_{\ell} B_{\ell}(r) P_{\ell}^{-1}(\theta), \tag{8}$$

where

$$B_{\ell}(r) = r\frac{\partial V_{\ell}}{\partial r} + r\frac{V_{\ell}}{N}\frac{\partial N}{\partial r} + 2V_{\ell}, \tag{9}$$

$$P_{\ell}^{-1}(\theta) = -\frac{\Gamma(\ell)}{\Gamma(\ell + 2)} P_{\ell}^{1}(\theta),$$

and

$$\Gamma(\ell) = \int_0^\infty x^{\ell - 1} e^{-x} dx = (\ell - 1)! \quad \text{for } n = \text{integer} > 0.$$

3. Model atmosphere

The molecular and eddy diffusion coefficients (D and K), the major gas number density (N), and atmospheric temperature (T) are assumed to be independent of latitude. Between 80 kilometers and 120 kilometers the atmospheric parameters of number densities and temperature are taken in tabular form from the CIRA 1965 model atmosphere (CIRA, 1965). (For the numerical solution, it was found desirable to modify the temperature profile slightly to eliminate discontinuities in the slope. (See Appendix B.) Above 120 kilometers the analytic expressions for the temperature and major constituent density profiles are taken from the 1965 Jacchia model atmosphere as modified by Walker (1965). The major (background) gas is taken to consist of molecular nitrogen (N_2), molecular oxygen (O_2) and atomic oxygen (O).

C. Solution of the Minor Gas Continuity Equation

Using in Equation (4) the expansions from Section IIB, multiplying each term by $P_m(\theta) \sin\theta$, and integrating over the polar angle from 0 to π, we find the continuity equation for the m^{th} harmonic in the expansion of the helium distribution (for details, see Appendix D):

$$\frac{2}{2m+1}\frac{\partial n_m}{\partial t} = \frac{2}{2m+1}\frac{\partial}{\partial r}\left\{\quad\right\}_m + \frac{2}{2m+1}\delta_{nm}\frac{2}{r}\left\{\quad\right\}_m$$

$$- \sum_{\ell,n} v_\ell \left[\frac{n_n}{H^*} + \frac{\partial n_n}{\partial r}\right] A_{\ell nm} - \frac{1}{r}\sum_{\ell,n} B_\ell\, n_n\, B_{\ell nm} + \frac{D}{r^2}\sum_n n_n\, C_{nm}, \tag{10}$$

where

$$\left\{\ \right\}_m = D\left[\frac{\partial n_m}{\partial r} + \frac{n_m(1+\alpha)}{T}\frac{\partial T}{\partial r} + \frac{n_m}{H}\right] + K\left[\frac{\partial n_m}{\partial r} + \frac{n_m}{T}\frac{\partial T}{\partial r} + \frac{n_m}{H'}\right]$$

$$H^* = \frac{1}{T}\frac{\partial T}{\partial r} + \frac{1}{H'},$$

$$A_{\ell nm} = \int_{-1}^{+1} P_\ell(\mu)\, P_n(\mu)\, P_m(\mu)\, d\mu,$$

$$B_{\ell nm} = \int_{-1}^{+1} P_\ell^{-1}(\mu)\, \frac{\partial P_n(\mu)}{\partial \theta}\, P_m(\mu)\, d\mu,$$

$$C_{nm} = \int_{-1}^{+1} \frac{1}{\sin\theta}\, P_m(\mu)\, \frac{\partial}{\partial\theta}\left(\sin\theta\, \frac{\partial P_n(\mu)}{\partial\theta}\right) d\mu,$$

and

$$\mu = \cos\theta.$$

A numerical solution to Equation (10) is obtained using an integration technique described by Lindzen and Kuo (1969). Details on the method of solution are given in Appendix D.

D. Boundary Conditions

The helium density at the lower boundary (80 km) is taken to be 1.989×10^9 cm^{-3} from CIRA,1965, and assumed to be independent of latitude. This implies that there is a sufficiently large reservoir at this altitude to supply or accept the amount transported horizontally in the thermosphere, with no modification of the lower boundary density.

At the upper boundary (500 km, the base of the exosphere) the slope of the helium profile is determined from the vertical flux across this level:

$$n\,(v_r - V_r) = -D \left[\frac{\partial n}{\partial r} + \frac{n\,(1+\alpha)}{T}\,\frac{\partial T}{\partial r} + \frac{n}{H}\right] - K \left[\frac{\partial n}{\partial r} + \frac{n}{T}\,\frac{\partial T}{\partial r} + \frac{n}{H'}\right], \tag{11}$$

where all the quantities are evaluated at 500 km. Above this altitude, molecules are assumed to be describing ballistic trajectories and returning without experiencing collisions. This results in a horizontal flow (exospheric transport), related to horizontal temperature and density gradients, which has been studied extensively by McAfee (1967) and Hodges and Johnson (1968). The expression developed by the latter authors is used here to express the vertical helium flow in terms of atmospheric properties at 500 km:

$$n v_r \cong - \left(1 + \frac{8.4}{\epsilon}\right) \nabla^2 \left(n \langle v \rangle H^2\right), \tag{12}$$

where

$$\epsilon = \frac{b}{H},$$

$\langle v \rangle$ = mean molecular speed, and

b = radius to base of exosphere.

Going through a development similar to that outlined in IIC, and setting

$$J = - \left(1 + \frac{8.4}{\epsilon}\right) \frac{\langle v \rangle}{\epsilon^2},$$

Equation (11) reduces to

$$
-2J \sum_{n} \frac{n(n+1)}{2n+1} \delta_{nm} n_n - \sum_{n,\ell} n_n v_\ell A_{\ell nm}
$$

$$
+D \left[\sum_{n} \frac{2}{2n+1} \delta_{nm} \left(\frac{\partial n_n}{\partial r} + \frac{n_n (1+\alpha)}{T} \frac{\partial T}{\partial r} + \frac{n_n}{H} \right) \right] = 0, \tag{13}
$$

for the coefficient of the mth term at the boundary. (Terms reflecting the effect of eddy diffusion are dropped, since at 500 km altitude $K \ll D$.)

III. MINOR GAS RESPONSE TO LARGE SCALE MOTIONS IN THE MAJOR SPECIES

A. Eddy Diffusion Coefficient

The individual component density in the upper thermosphere and exosphere is extremely sensitive to the value of the eddy diffusion coefficient in the region of transition from a mixed atmosphere to one controlled by molecular diffusion (Lettau, 1951; Kockarts and Nicolet, 1962; Mange, 1961; Colegrove, Johnson and Hanson, 1966). In particular, the effect is enhanced for minor species (such as helium) whose mass differs greatly from the mean mass of the mixed atmosphere. Also, the sense of the effect for a particular gas depends on the difference in mass between the gas and the mixed mean mass: for a heavier gas such as argon, an increase in eddy diffusion coefficient will result in an increased density at higher altitudes, while for helium an increased eddy diffusion coefficient will decrease the density. These effects are discussed in detail in the references cited above.

For the study of a minor gas response to winds, it is necessary to include a realistic function for the eddy diffusion coefficient. A number of profiles were

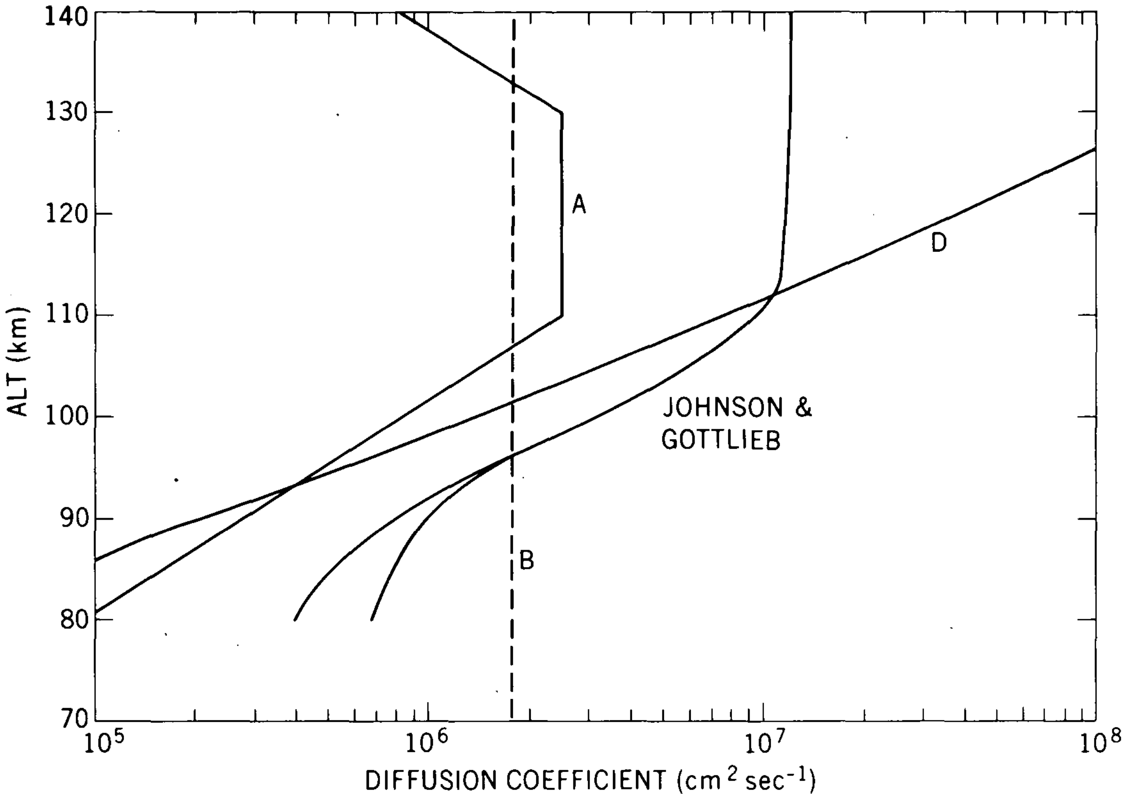

Figure 2. Diffusion coefficients as a function of altitude: (A) eddy diffusion coefficients used in the calculations presented here; (B) constant eddy diffusion coefficient which produces same high altitude helium density as (A); Johnson and Gottlieb (1970) eddy diffusion coefficient based on thermal considerations; (D) molecular diffusion coefficient for T_∞ = 1200.

tried, from a constant to an approximation of a profile suggested by Johnson and Gottlieb (1970) based on thermal considerations, consisting of a constant value over an altitude interval with an exponential decrease above and below this interval. These two profiles are shown in Figure 2 along with the Johnson and Gottlieb profile and the molecular diffusion coefficient (for an exospheric temperature of 1200°). The profile A falls off from 130 km rather than 150 km as suggested by Johnson and Gottlieb due to the lower absolute maximum value; they state that the decrease should begin about a scale height above the altitude where the eddy diffusion and molecular diffusion are comparable.

To determine a realistic value for the eddy diffusion coefficient, helium densities obtained from the mass spectrometer on OGO-6 are compared against several calculated values for each of the two diffusion coefficient profiles (Figure 3). The influence of dynamics on the distribution of helium is most likely minimal during quiet periods near equinox. Thus, the mass spectrometer densities are taken from a magnetically quiet period ($A_p = 5$) on 24 September 1969 at latitudes of +48° and -41° and at 500 km altitude. The exospheric temperature, determined from the molecular nitrogen density (measured by the mass spectrometer), was 1176°K and 1235°K at +48° and -41° latitudes respectively. Helium densities at these two locations were 2.73×10^6 cm^{-3} and

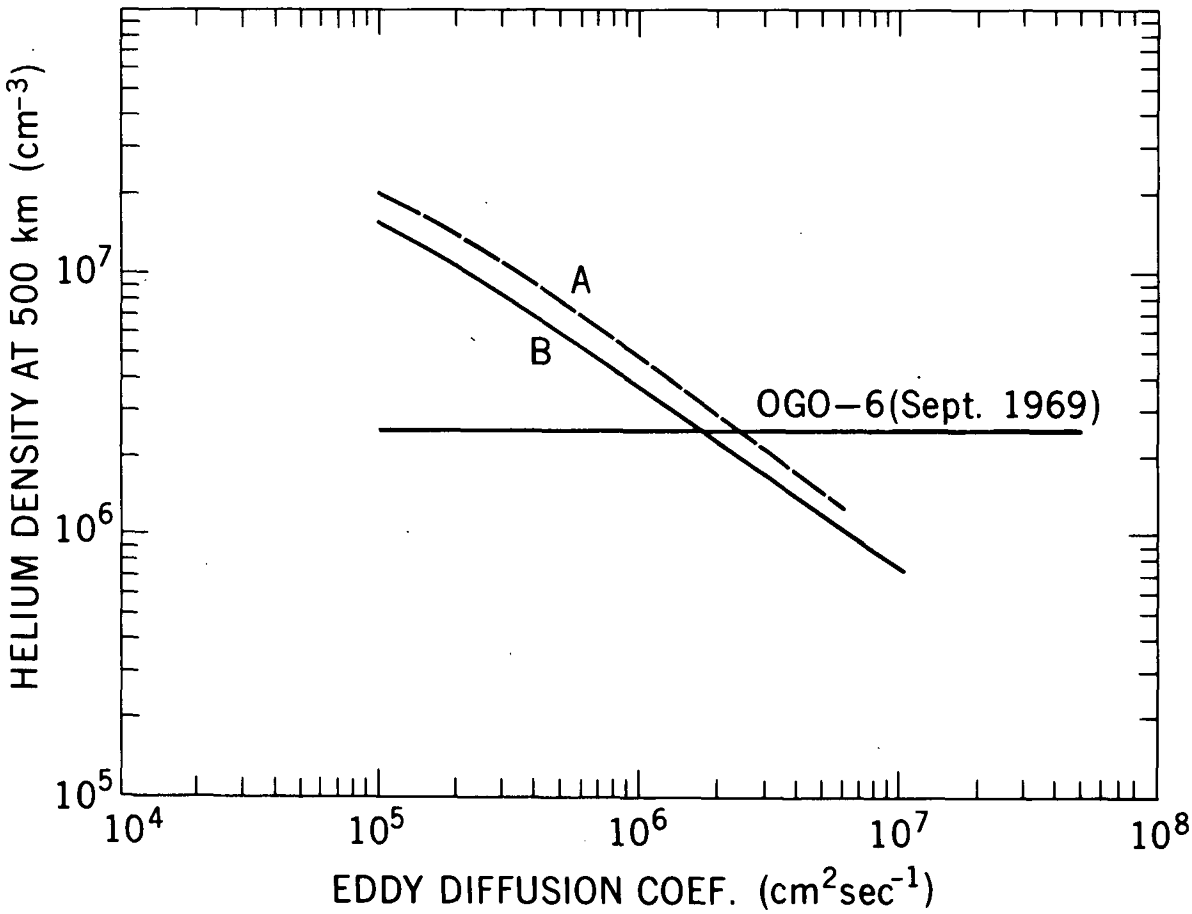

Figure 3. Helium density at 500 km for $T_\infty = 1200°$ as a function of eddy diffusion coefficient. The two curves correspond to the eddy diffusion coefficient profiles shown in Figure 2.

2.19×10^6 cm^{-3}. The calculated values are obtained by using the same computer program used in the dynamic-diffusion calculations, setting the wind equal to zero, and using 1200° for the exospheric temperature. It can be seen from Figure 3 that either of the two eddy diffusion profiles mentioned can produce satisfactory agreement with the high altitude data and one need only choose the appropriate constant value; either 1.8×10^6 $cm^2 sec^{-1}$ for the constant profile or 2.5×10^6 $cm^2 sec^{-1}$ for the Johnson and Gottlieb profile satisfy the data.

The shape of the vertical profile for helium is not affected by the eddy diffusion coefficient used in the calculation. This can be seen in Figure 4 where helium density profiles for various constant eddy diffusion coefficients are shown

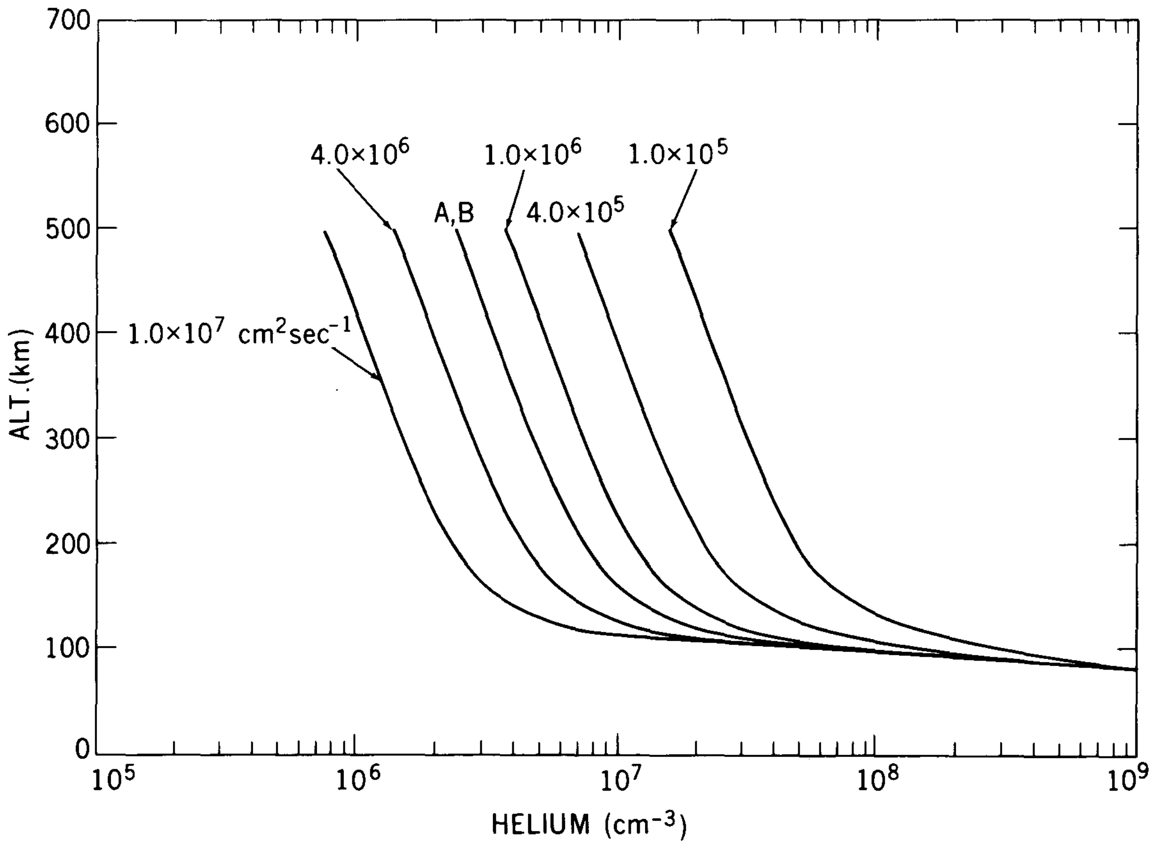

Figure 4. Helium density as a function of altitude for various constant values of the eddy diffusion coefficient and for the eddy diffusion coefficients of Figure 2 (marked A and B). The exospheric temperature, T_∞, is 1200°.

along with the two profiles which best match the high altitude data (marked A and B in the figure). Figure 5 shows the expanded display of the same set of calculations where now the dependent variable is the ratio of the number density of helium to the sum of the major gases (molecular nitrogen, molecular oxygen and atomic oxygen). For the remainder of the calculations, the Johnson and Gottlieb eddy profile is used, with a maximum value of 2.5×10^6 cm^2 sec^{-1}, and a scale height of 9.1 km for the exponential regions. It is assumed that the eddy diffusion coefficient determined during equinox conditions can be applied globally during solstace conditions.

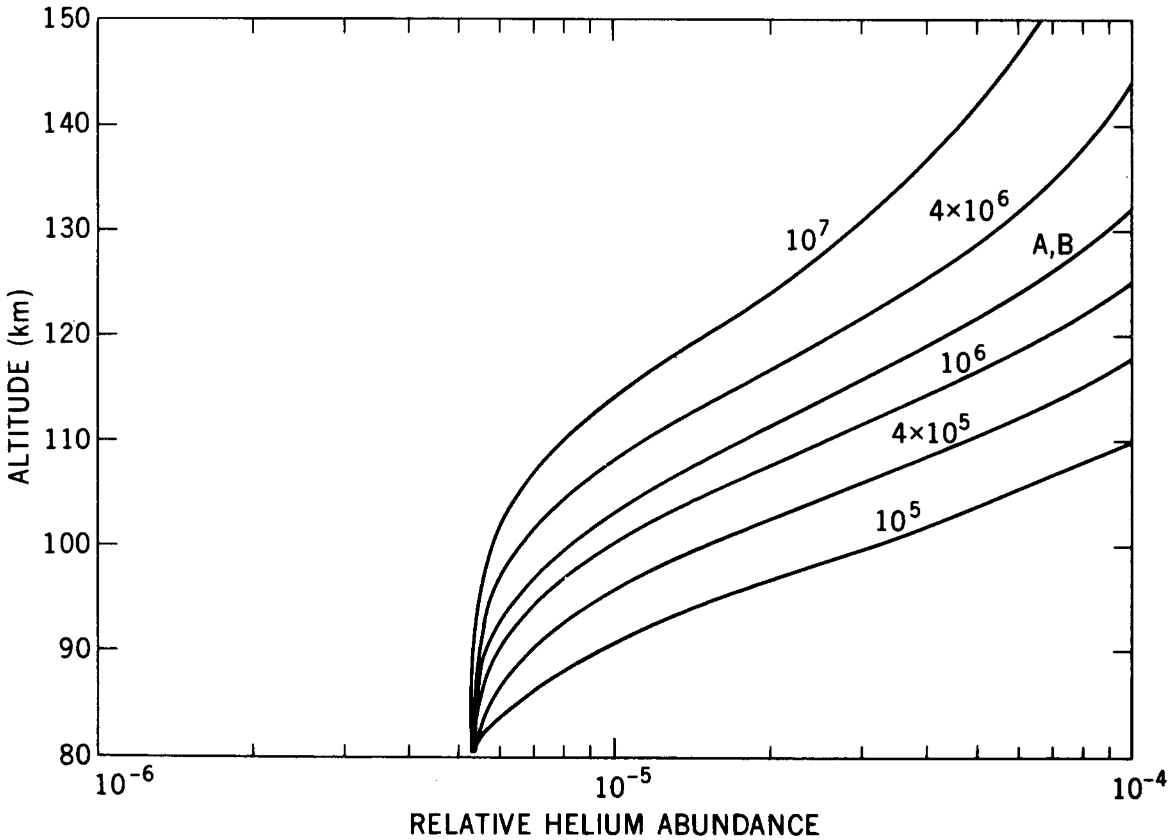

Figure 5. Relative abundance of helium as a function of altitude for various eddy diffusion coefficients; the curves A and B refer to the eddy diffusion coefficient profiles of Figure 2. $T_\infty = 1200°$.

B. Effect of Latitudinal – Seasonal Circulation

There are no direct measurements of vertical velocities in the upper mesosphere and thermosphere, nor are there any measurements of large scale latitudinal-seasonal circulation cells in these regions. That high winds exist in the thermosphere and mesosphere is in little doubt, however, and many analytical studies have been published concerning various aspects of upper air wind systems based on assumed pressure gradients (Geisler, 1966, 1967; Dickinson and Geisler, 1968; Dickinson, Lagos, and Newell, 1968; Lindzen, 1966, 1967; Chapman and Lindzen, 1970; Volland, 1969; Volland and Mayr, 1970; Mayr and Volland, 1971; Kohl and King, 1967a, 1967b, 1968; Challinor, 1968, 1969; Bailey, Moffett and Rishbeth, 1969; Rishbeth, Moffett and Bailey, 1969) or thermal requirements (Johnson and Gottlieb, 1970). A number of general features of these studies have been extracted and incorporated into a large scale, easily parameterized circulation cell: (1) the air flows from regions of relatively high pressure to regions of low pressure (in this case, from the summer to the winter hemisphere); (2) the vertical profile of the vertical component of the wind field consists of a rapid increase with altitude up to heights where viscous effects may be expected to become important, at which point the velocity tends toward a constant value (the profile and magnitude are consistent with those of Kohl and King (1967) and Volland and Mayr (1970)); (3) the horizontal component of the wind field is determined from the vertical component through the major gas continuity equation (see Sec. IIB and Appendix C). Studying the effect of thermospheric wind cells of this type on the distribution of minor species is the object of the present work. This investigation comprises three general areas: (1) a broad parametric steady state analysis corresponding to periods of low, medium and high solar activity, and demonstrating the effects of such phenomena as exospheric transport, horizontal diffusion and wind profiles; (2) a specific comparison with OGO-6 mass spectrometer helium measurements near the June 1969 solstace, showing the types of wind systems which are compatible with the observations; (3) the results of time-dependent calculations showing rates of generation of various minor gas distributions when a wind system is suddenly "turned-on".

1. Cellular Motion

a. Vertical Profile

The adoption of an arbitrary, easily parameterized wind system is facilitated by the reduction of the horizontal and vertical components of this system to expressions in terms of the vertical components only (see Section IIB and Appendix C). This reduction, accomplished by using the major gas continuity equation and expanding the wind field in Legendre polynomials, greatly simplifies the analysis as it permits a complete description of a circulation cell with a minimum number of parameters.

The general vertical velocity profile imposed on the circulation cells consists of a rapid increase with height up to altitudes where viscous effects begin to dominate, at which point the velocity tends to become constant with altitude. This shape can be expressed as

$$V_\ell = \frac{W_\ell}{2} \left\{1 + \mathrm{erf}\,[\beta'_\ell(z - z_{0\ell})]\right\}, \tag{14}$$

where V_ℓ = vertical major gas velocity $\left(\frac{\text{cm}}{\text{sec}}\right)$,

W_ℓ = maximum value of $V_\ell \left(\frac{\text{cm}}{\text{sec}}\right)$,

erf(x) = error function $\left(\mathrm{erf}(x) = 2/\sqrt{\pi} \int_0^x e^{-t^2}\, dt\right)$,

$z_{0\ell}$ = reference altitude (where slope, $dv/\partial z$, is equal to $1/\sqrt{\pi}\, w\, \beta$ or where $V_\ell = W_\ell/2$), km),

β'_ℓ = factor determining altitude gradient (equal to $\sqrt{\pi}/w_\ell\ \partial V_\ell/\partial z$ at $z = z_{0\ell}$) (km^{-1}).

Thus, by defining W_ℓ, $z_{0\ell}$ and β'_ℓ, the complete circulation cell is determined (for a given density profile; see below). The generalized altitude profile is shown in Figure 6; Figure 7 shows representative vertical velocity profiles for w = 100 cm sec^{-1}, z_0 - 200 km and several values for β_ℓ ($\beta_\ell = \beta'_\ell \times 10^2$). Also shown for comparison is the vertical profile deduced by Johnson and Gottleib (1970) from thermal considerations for the winter mesosphere and thermosphere.

b. Cell Shape

Using the assumptions of Section II.B.1, the air motion is approximated by a pole-to-pole circulation cell, with air rising in the summer hemisphere ($0 \leq \theta \leq 90°$), flowing across the equator and descending in the winter hemisphere ($90° \leq \theta \leq 180°$). This distribution can be described by using only the first Legendre polynomial in the expansion of the vertical component of motion (see Section II.B.2.):

$$V_r(r, \theta) = V_1(r) \cos\theta. \tag{15}$$

The latitudinal component then becomes (Appendix C).

$$V_\theta(r, \theta) = -1/2\, B_1(r) \sin\theta, \tag{16}$$

where

$$B_1(r) = r\frac{\partial V_1}{\partial r} + r\frac{V_1}{N}\frac{\partial N}{\partial r} + 2V_1. \tag{17}$$

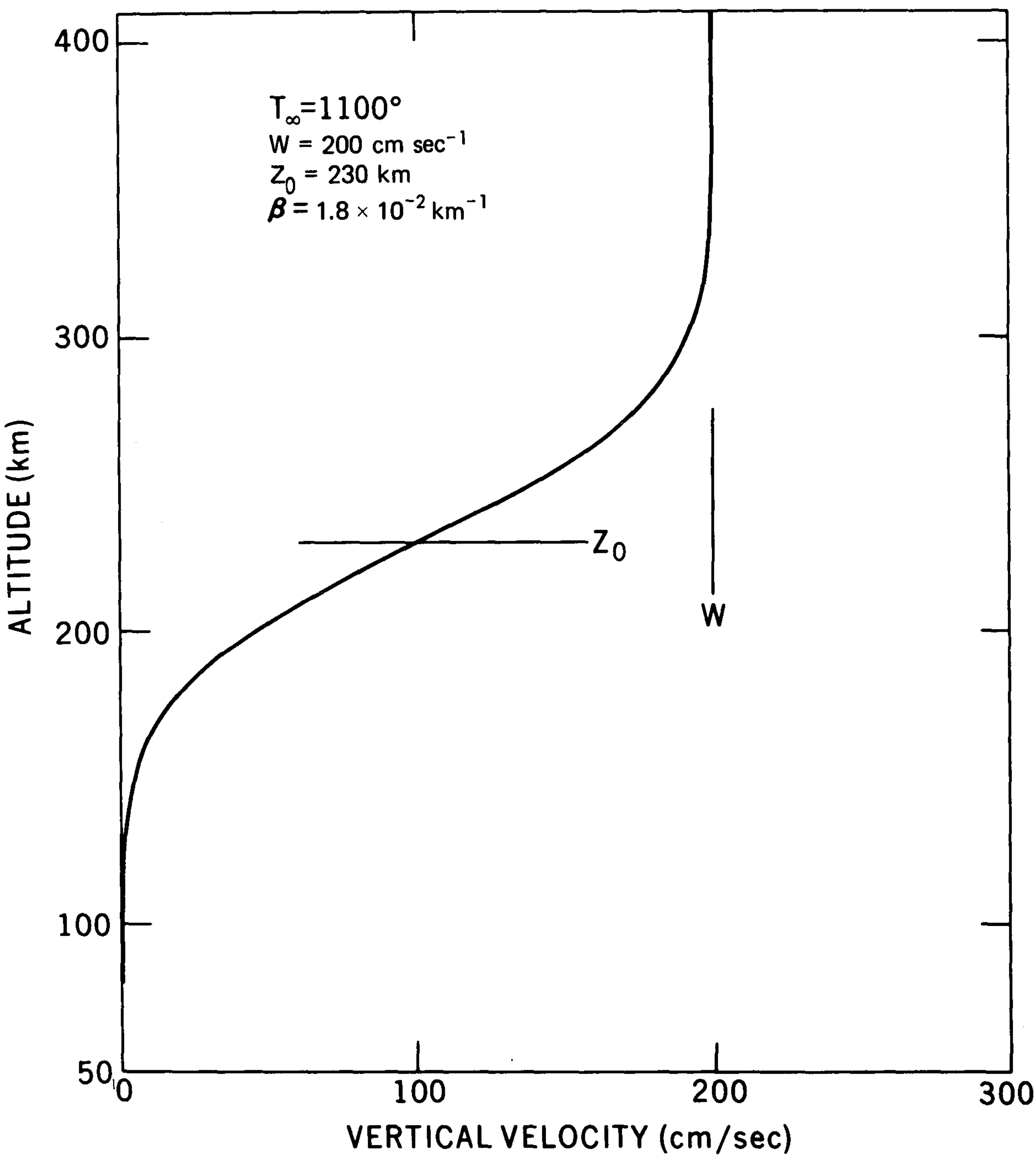

Figure 6. General vertical profile of the vertical wind used in the calculations. This specific profile is characterized by T_∞ = 1100°, W = 200 cm/sec, Z_0 =230 km, and $\beta = 1.8 \times 10^{-2}$ km^{-1}

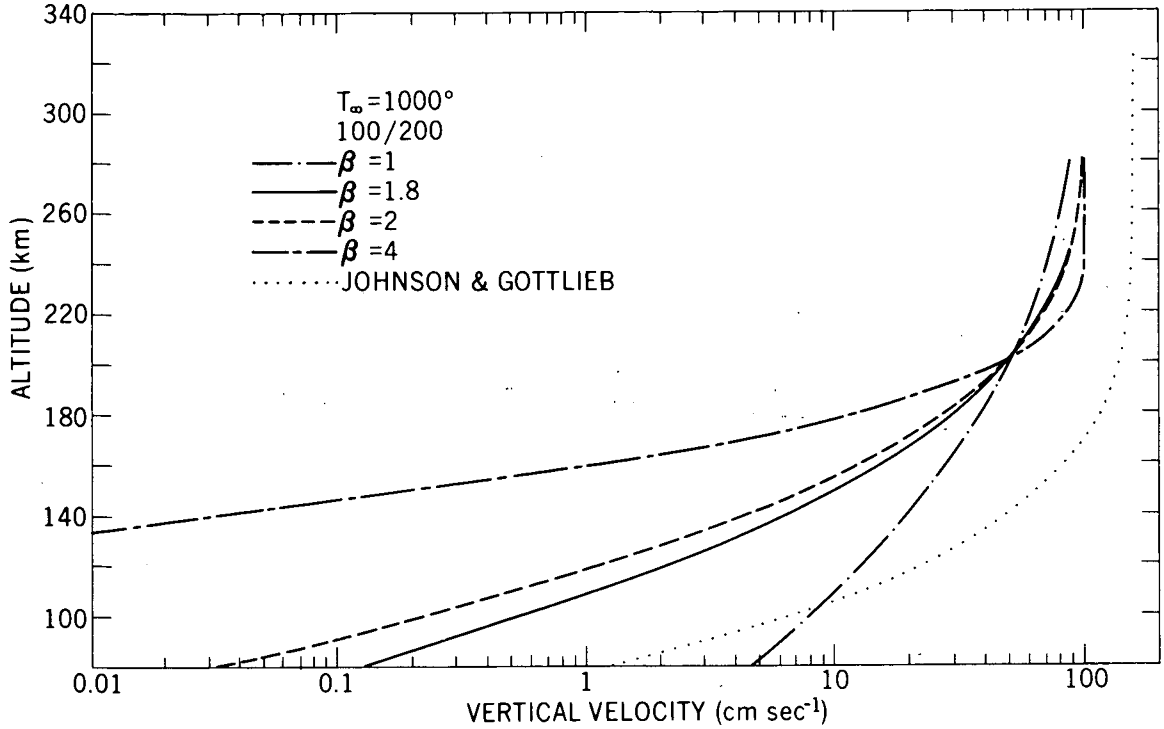

Figure 7. Vertical wind profiles for several values of β, with T_{∞} =1000°, W = 100 cm/sec and Z_0 =200 km. Also shown for comparison is the vertical wind profile deduced by Johnson and Gottlieb (1970) from thermal considerations.

Thus, the complete circulation cell is defined in terms of cosine and sine functions and the profiles of the vertical wind component and major gas number density.

It can be seen by inspection of equation (16) that the direction of latitudinal flow will be determined by a balance of the density gradient term on the right (always negative) against the positive first and third terms. In regions where the density gradient term dominates, the flow will be toward increasing values of θ(i.e., toward the winter pole); in regions where the wind gradient and amplitude dominates, V_θ (r, θ) is negative and the flow is toward decreasing θ (the summer pole). Figure 8 shows the vertical profiles of the vertical and horizontal components for a typical wind system, with w = 100 cm sec^{-1}, z_0 = 200 km, β = 2.0 and an exospheric temperature, T_∞, of 1100°. (Henceforth,

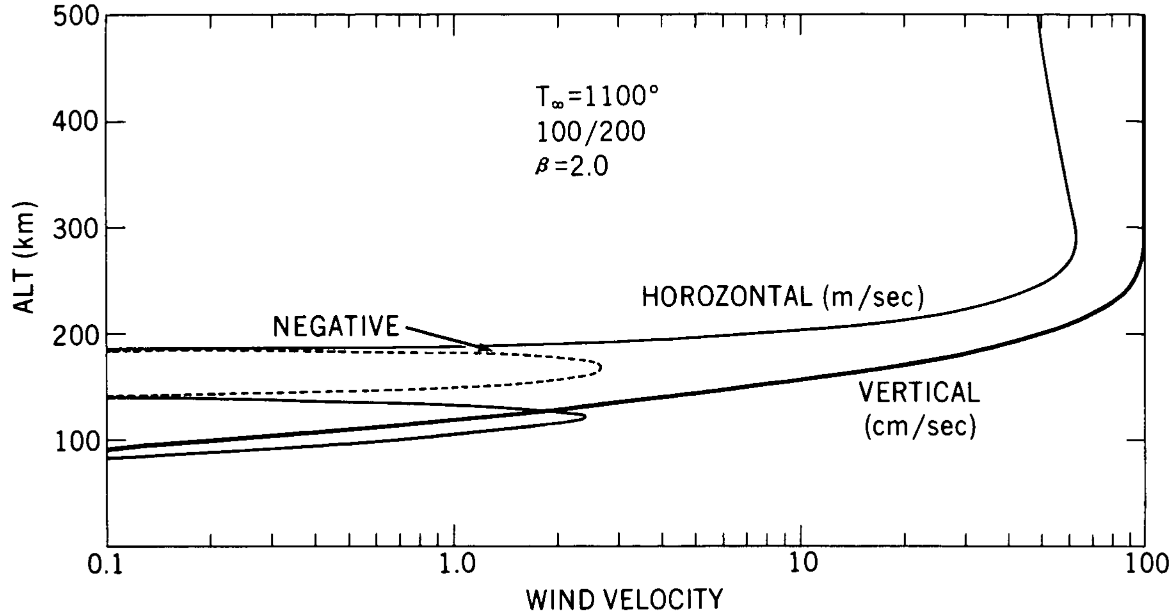

Figure 8. Vertical and horizontal wind profiles for T_∞ = 1100°, W = 100 cm/sec, Z_0 = 200 km and β=2.0. Note that the horizontal wind becomes negative (toward the summer pole) between 140 and 185 km.

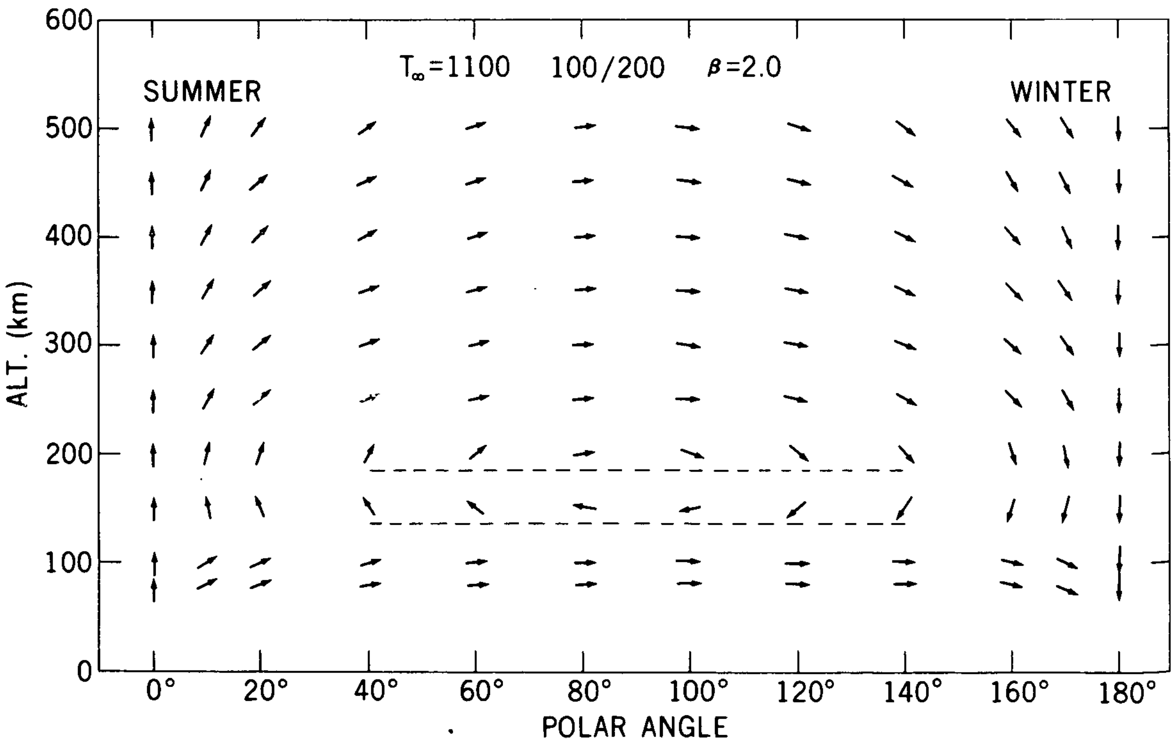

Figure 9. Direction of the wind vectors associated with the vertical and horizontal profiles of Figure 8.

this nomenclature will be abbreviated, i.e. 100/200, $\beta = 2.0$). The region of return flow, toward decreasing θ, is seen to lie between 140 km and 185 km; the sharp break in horizontal velocity at 120 km is due to the change in slope of the density of the atmospheric model used. The shape of the circulation cell associated with these profiles is depicted in Figure 9.

Qualitatively, the relationship between the gradient of the vertical velocity component and the direction and amplitude of the horizontal flow can be seen by considering the requirements for continuity in a vertical column. If the vertical velocity, v, increases with altitude at exactly the same rate at which the density, N, decreases, the flux, Nv, is constant along the length of the column and there is no horizontal inflow or outflow (assuming that a diffusive vertical profile is maintained for the major species). If, however, the vertical velocity increases more rapidly than 1/N, the flux out the top of a small volume element in the column exceeds the flux coming in through the bottom and there is a need for compensating inflow through the sides of the volume element. Conversely, if V increases less rapidly than 1/N there is a net horizontal outflow.

The relationship of the altitude regime of reverse flow to the vertical profile parameters is shown in Figures 10, 11 and 12 for exospheric temperatures of 800°, 1100° and 1500°. These three temperatures were chosen as they approximate global averages for periods of low, medium and high solar activity. In these figures, the region of reverse flow is the area to the right of a particular β/altitude curve; the area to the left of a given curve indicates flow toward the winter pole. In general, as the height increases at which the vertical velocity levels off, there is a corresponding increase in the altitude of return flow. The

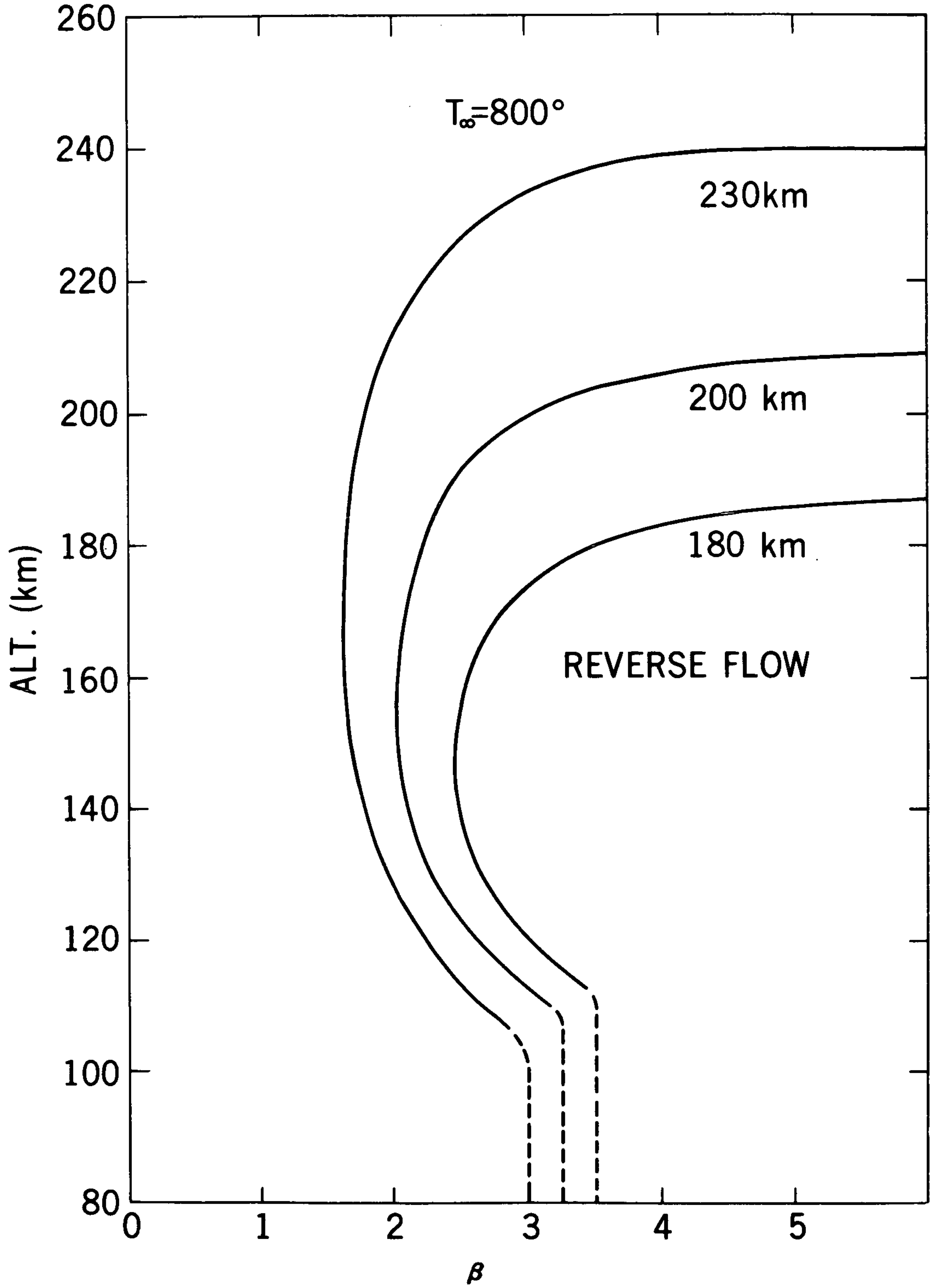

Figure 10. Altitude regions of reverse flow for Z_0 = 180, 200 and 230 km; T_∞ =800°. The horizontal wind is toward the summer pole for values in the altitude $-\beta$ plane to the right of a given curve.

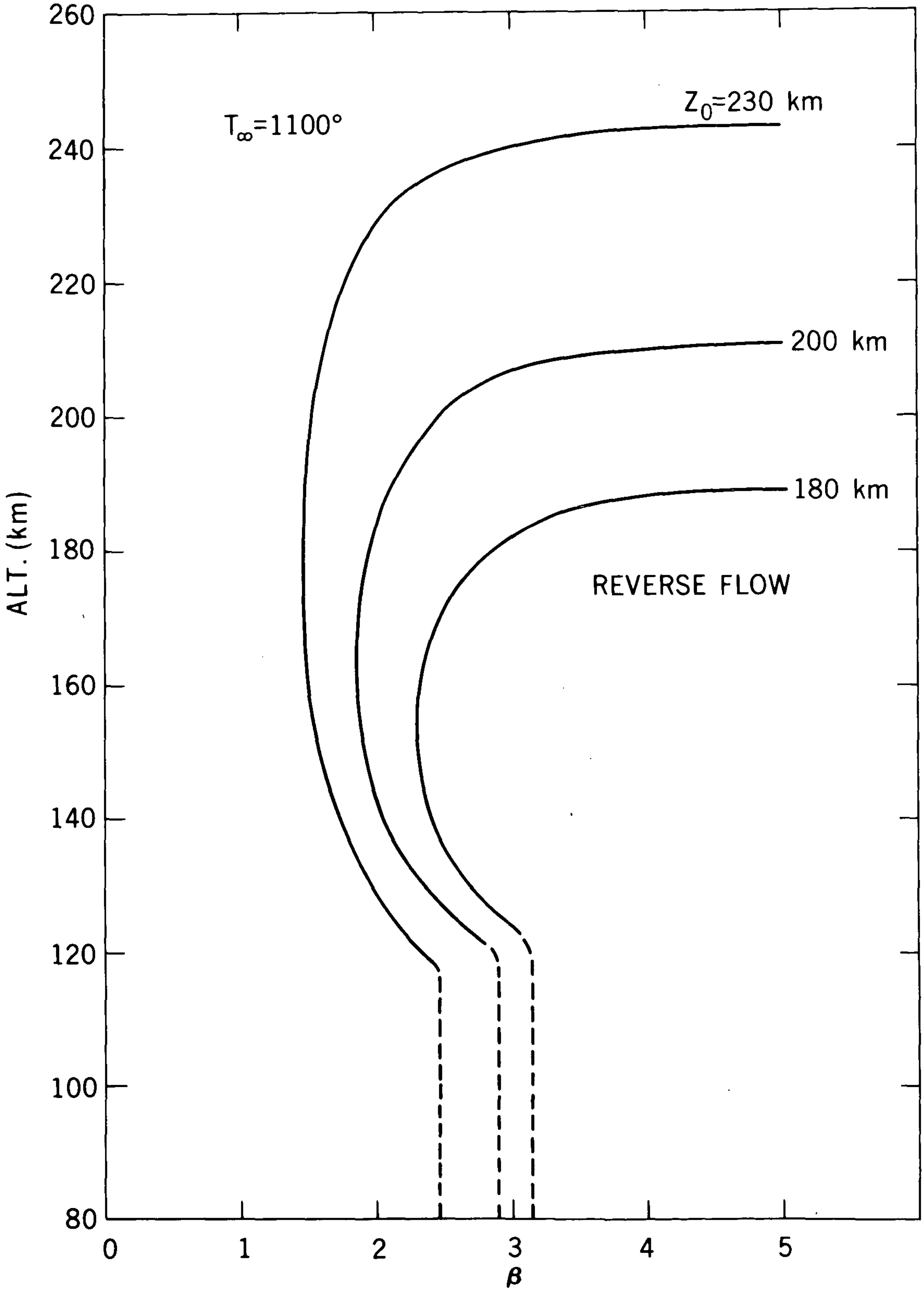

Figure 11. Altitude regions of reverse flow for T_∞ =1100°.

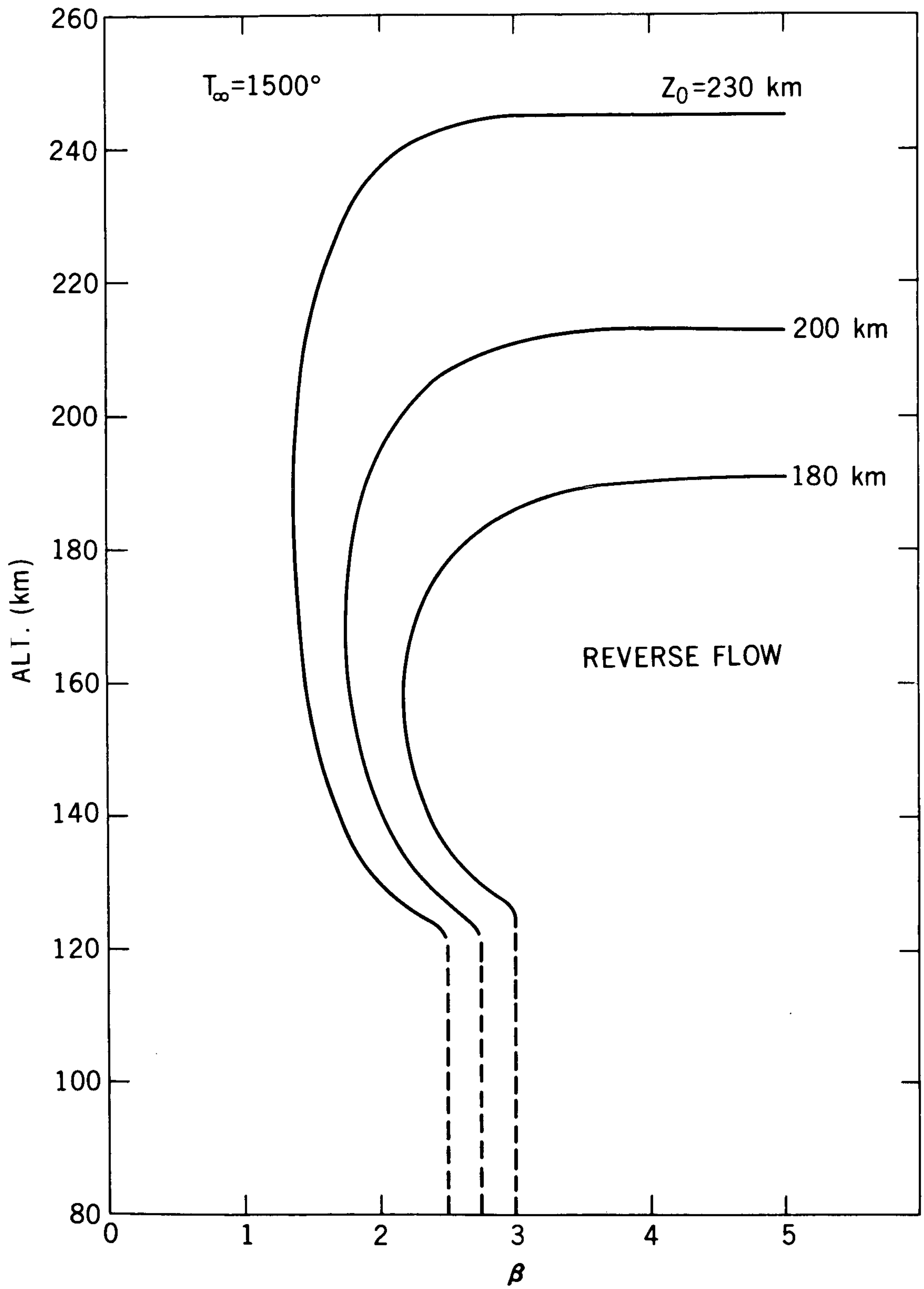

Figure 12. Altitude regions of reverse flow for T_∞ =1500°.

small variation in shape of these curves with exospheric temperature reflects the variation in the major constituent density profile which is balanced against the wind gradient in the calculation of B_1 (r).

2. Minor Gas Response to Cellular Motion: Helium

The response of minor gases to large scale dynamic systems shows up most dramatically in two ways that can be compared directly with observations: (1) the vertical profile as would be measured from a rocket borne mass spectrometer; and (2) large scale latitudinal distributions which can be compared with satellite observations. This discussion will emphasize helium as there are many more data applicable to this gas; argon will be discussed separately in a later section.

As the majority of the data on the large scale distribution of helium has been obtained at satellite altitudes, it is desirable to compare the results of the calculation directly to high altitude data. Figure 13 shows the calculated results of the helium density at fixed altitudes of 300 km and 500 km as a function of latitude for a typical wind system. It is seen that the distributions are smooth functions, increasing from the summer pole toward the winter pole, with a pole-to-pole ratio (R_p) of 8.7 at 500 km. (This parameter, the pole-to-pole density ratio, turns out to be a useful quality figure, and will be referred to frequently in later sections.)

Figure 14 displays the vertical helium number density profiles associated with the latitudinal distributions of the previous figure. Three profiles are given, representing the summer pole (0°), the winter pole (180°) and for comparison, the static-diffusion profile. In general, for the simple wind cells studied, the

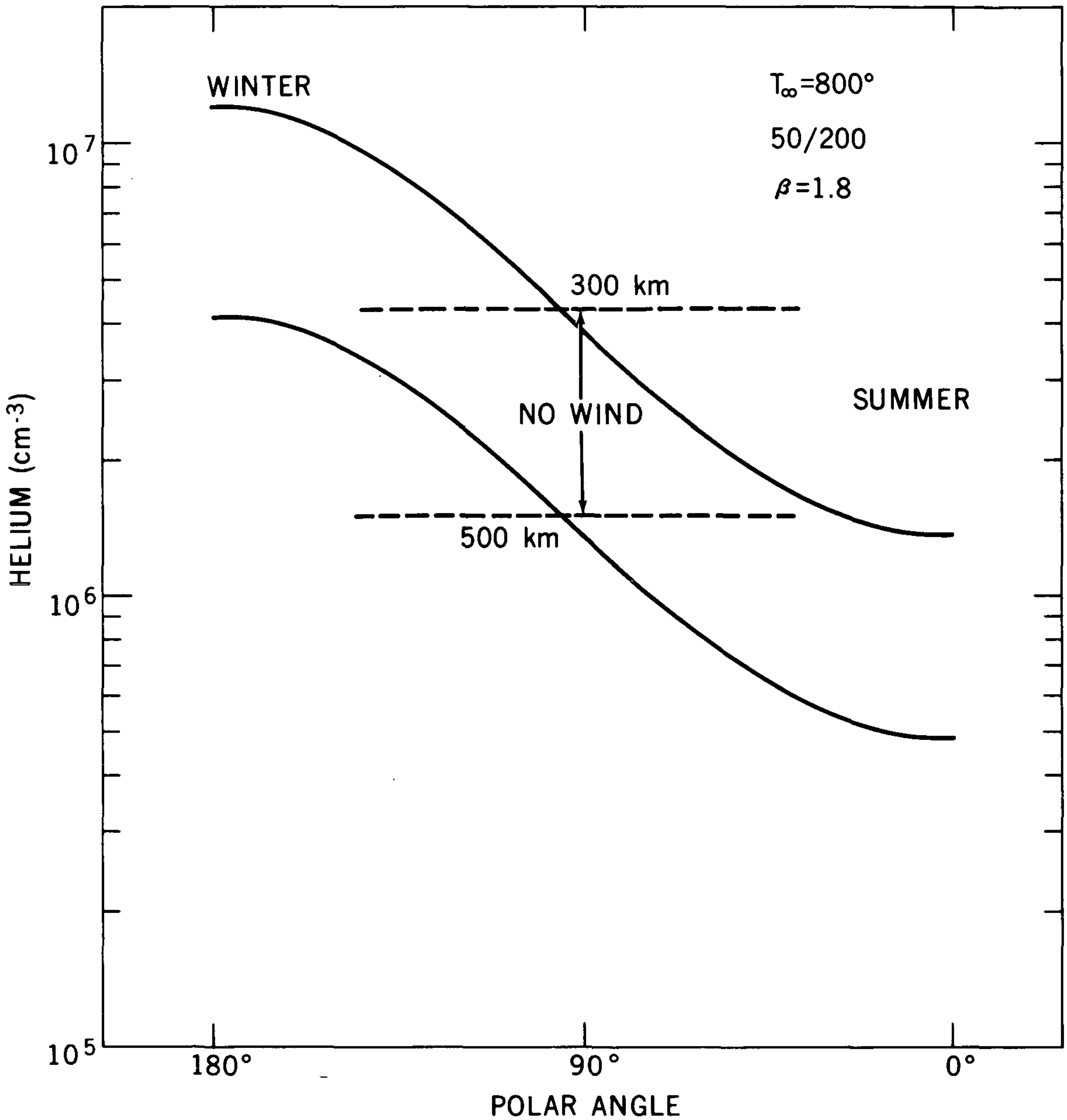

Figure 13. Helium density as a function of polar angle for the constant altitudes of 300 km and 500 km. The exospheric temperature is 800° (low solar conditions), W = 50 cm/sec, Z_0 = 200 km, β = 1 8. Also shown are the densities in the absence of winds.

polar profiles represent the extrema of the dynamic effects on the helium density.

The following three sections will examine the effects of exospheric lateral transport, exospheric temperature, and horizontal diffusion on the vertical and horizontal distributions of helium. Following these is a discussion of the

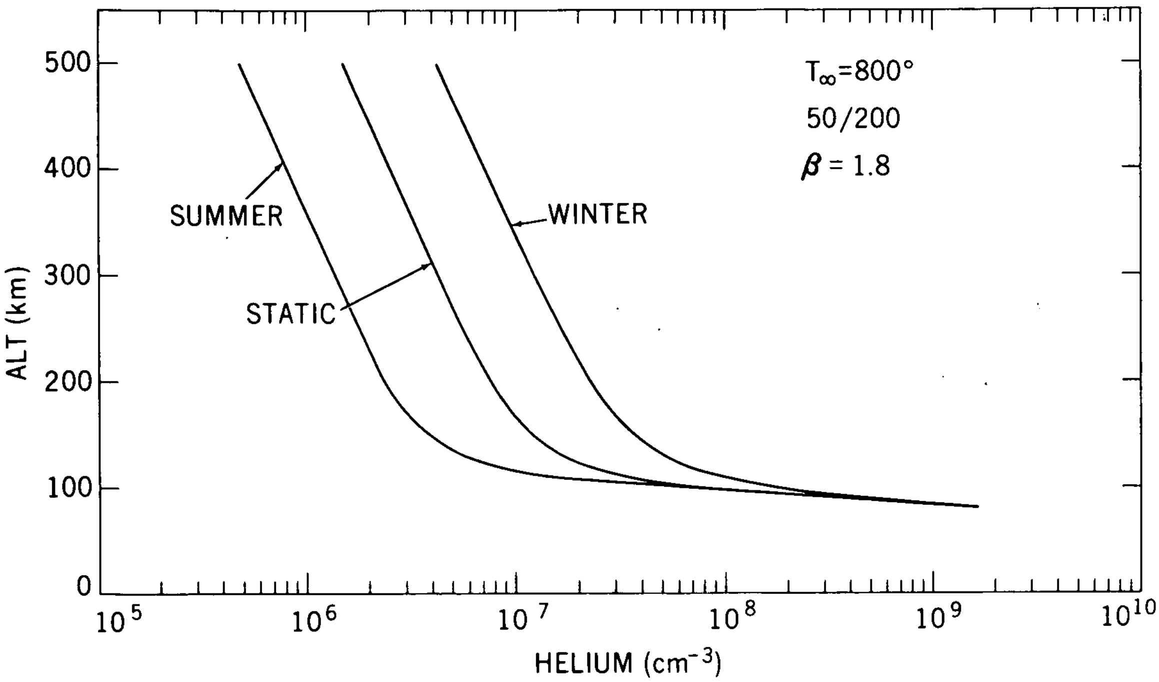

Figure 14. Helium density at the summer and winter poles as a function of altitude, for the 50/200, $\beta = 1.8$ wind system of Figure 13. Also shown is the static profile.

variations in the distribution as functions of the shape, amplitude and altitude of the wind cell.

a. Exospheric Transport

By far the largest effect tending to smooth out horizontal variations in helium density is that due to lateral flow in the exosphere. This transport is proportional to the quantity

$$J = -\left(1 + \frac{8.4}{\epsilon}\right) \frac{\langle v \rangle}{\epsilon^2}$$

(see equations (12) and (13), section II.D) where $\langle v \rangle$ is the mean molecular speed and $\epsilon = b/H$, where b is the geocentric distance and $H = kT/mg$. It can be seen that an increase in exospheric temperature will cause an increase in J, through both the mean molecular speed and the scale height, H. J is shown as a function of exospheric temperature in Figure 15, where it will be observed that an increase of more than a factor of five in exospheric flow has resulted from a temperature increase from 800° to 1500°. The net result of this transport mechanism is a flux up and out of the thermosphere in regions of comparatively high helium density (i.e. near the winter pole), high altitude flow over the equator toward the summer pole, and flow into the thermosphere from the top in the summer hemisphere.

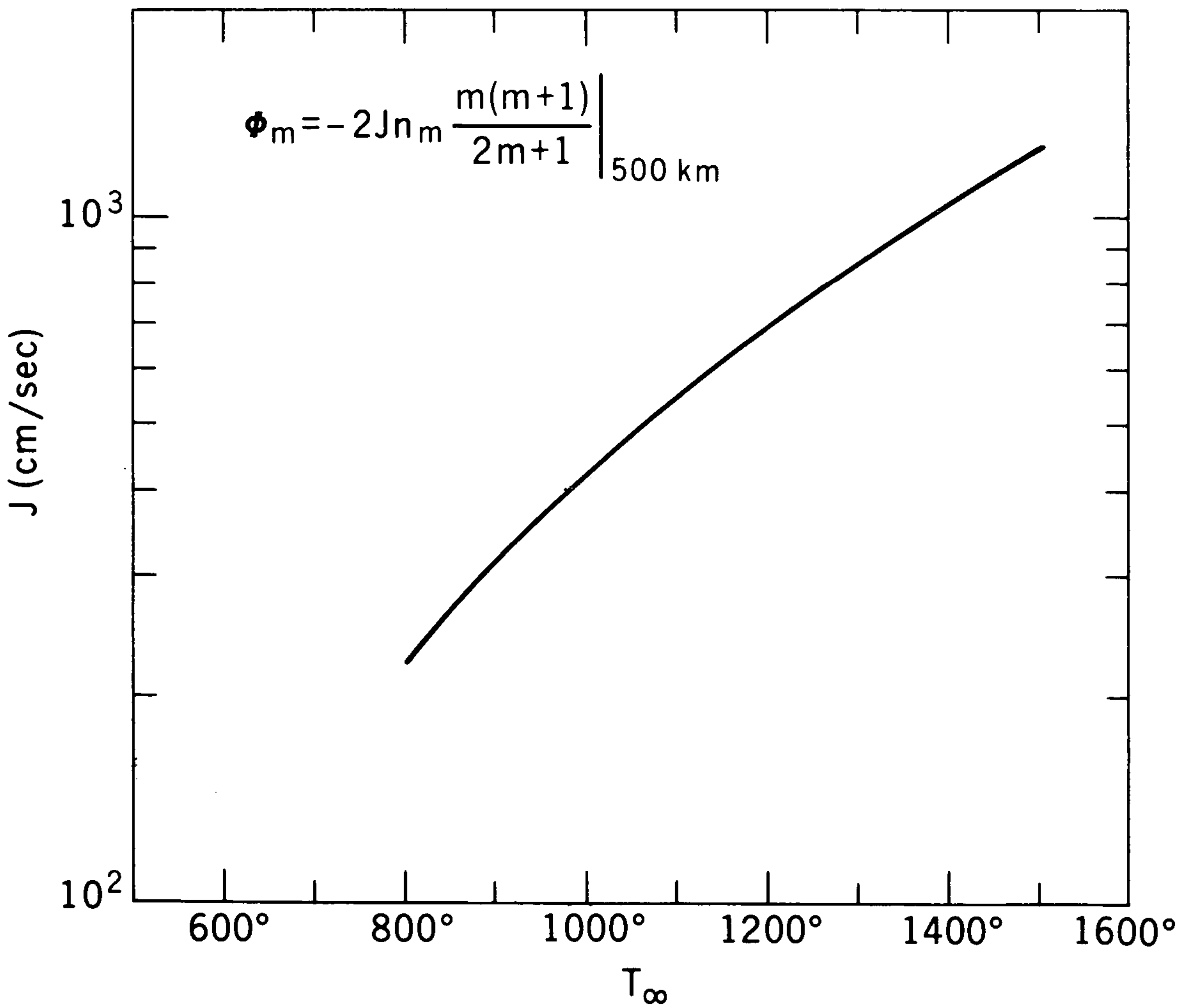

Figure 15. The exospheric transfer velocity function, J, as a function of exospheric temperature. The exospheric flux is related to J through the expression shown.

There are no measurements of this exospheric flux, but its existence can hardly be in doubt. The magnitude of the transport, however, might be questioned, so this quantity was varied from 0 up to 1.5 times the magnitude suggested by Hodges and Johnson. The results for two wind systems are shown in Figure 16, where it can be seen that the pole-to-pole ratios (R_p) vary only slightly when the exospheric flow is varied in the neighborhood of the Hodges and Johnson value.

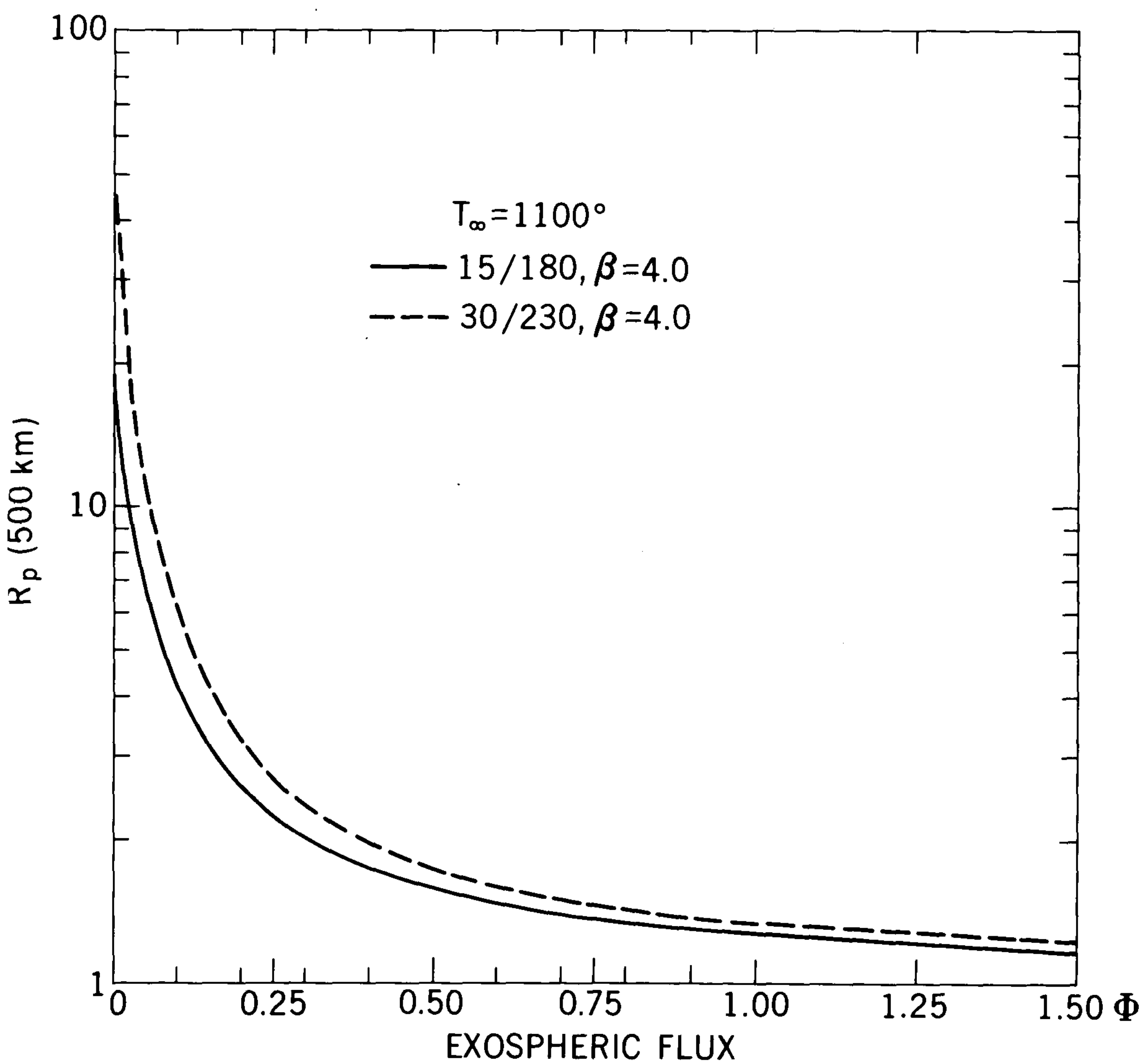

Figure 16. The pole-to-pole helium density ratio, R_p, at 500 km as a function of exospheric flux for average solar conditions (T_∞ = 1100°). The value 1.00 Φ represents the value calculated from Equation 12 for the Hodges and Johnson (1968) flux.

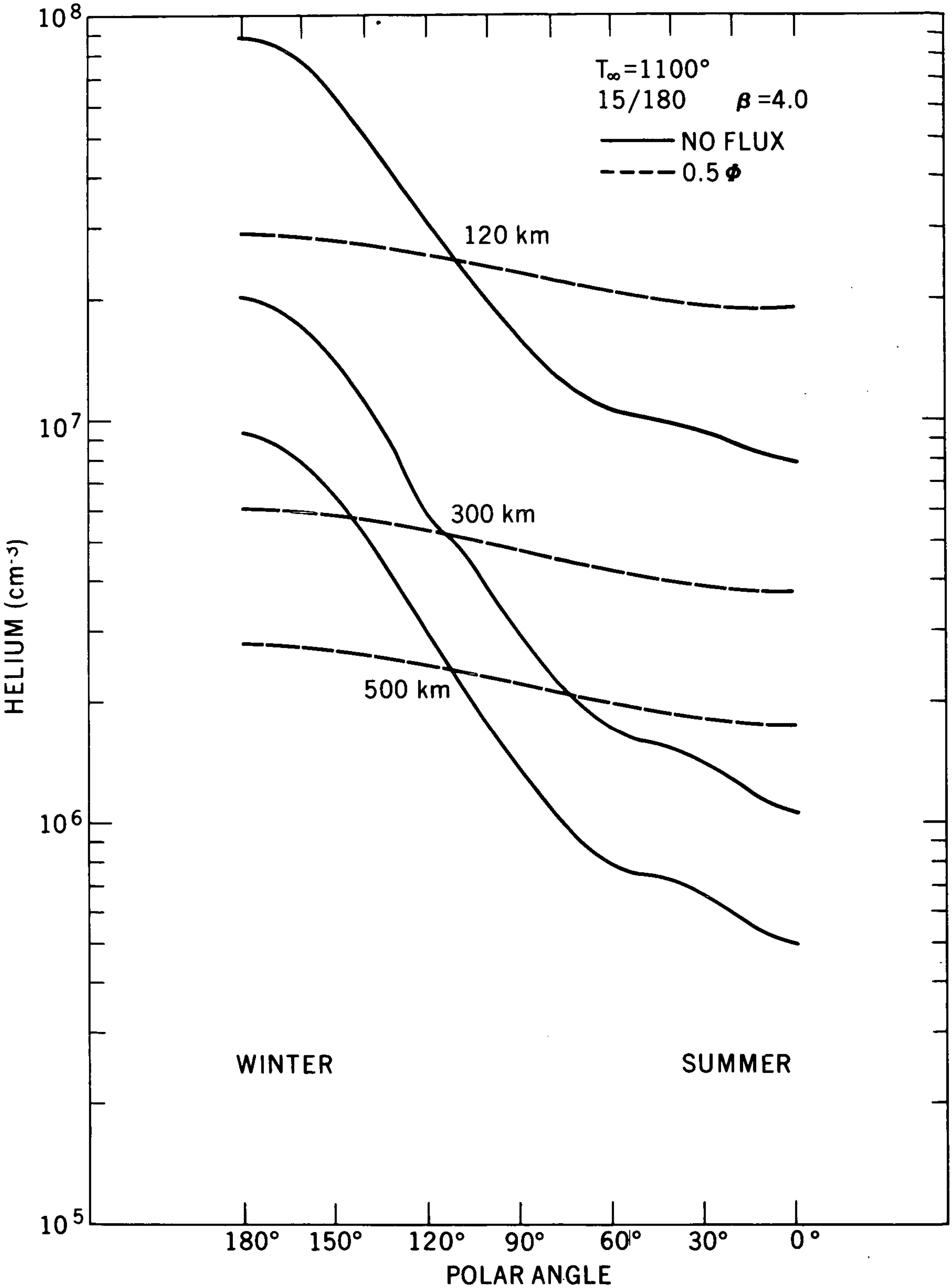

Figure 17. Helium densities at 120, 300 and 500 km as a function of polar angle for no exospheric flux and for half the Hodges and Johnson flux.

When the exospheric flow is removed, however, the pole-to-pole ratios increase by more than an order of magnitude. The smoothing effect on the large scale distribution can be seen in Figure 17, where the latitudinal variations of helium at altitudes of 120 km, 300 km and 500 km are shown for; (1) no exospheric flux and for; (2) half the Hodges and Johnson value. For the "no flux" case the higher harmonics are clearly present, while for the other case they are gone. The vertical profiles corresponding to these situations are shown in Figure 18. The calculations discussed in the remainder of this paper are performed using the Hodges and Johnson expression for the magnitude of the exospheric transport.

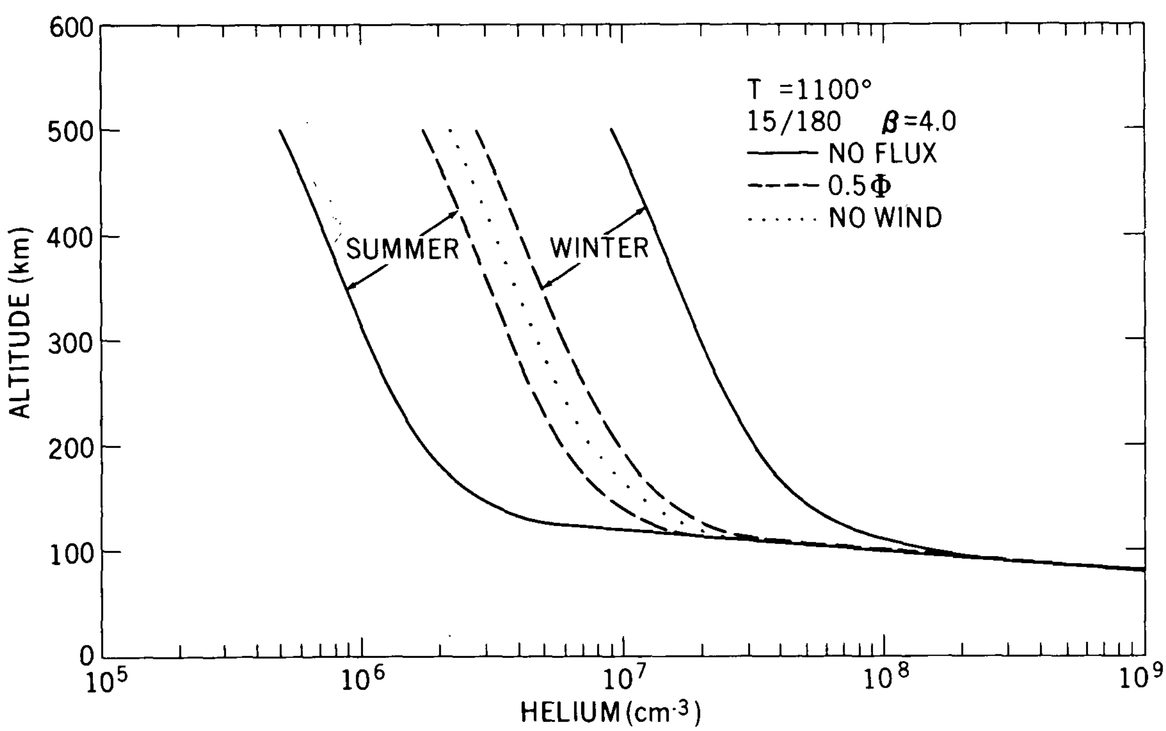

Figure 18. Helium density vertical profiles at the poles for no exospheric flux and half the Hodges and Johnson flux. Shown for comparison is the no wind helium profile.

b. Horizontal Diffusion

Lateral diffusion below the base of the exosphere is the other "restoring force" acting to smooth out horizontal variations in component density, but compared to exospheric flow its effect is minor. Figure 19 shows the variation in helium density at 500 km with latitude for a typical wind system, both with and without horizontal diffusion included in the calculation. The effect on the pole-to-pole ratio is 10%, certainly less than could be observed with present measuring

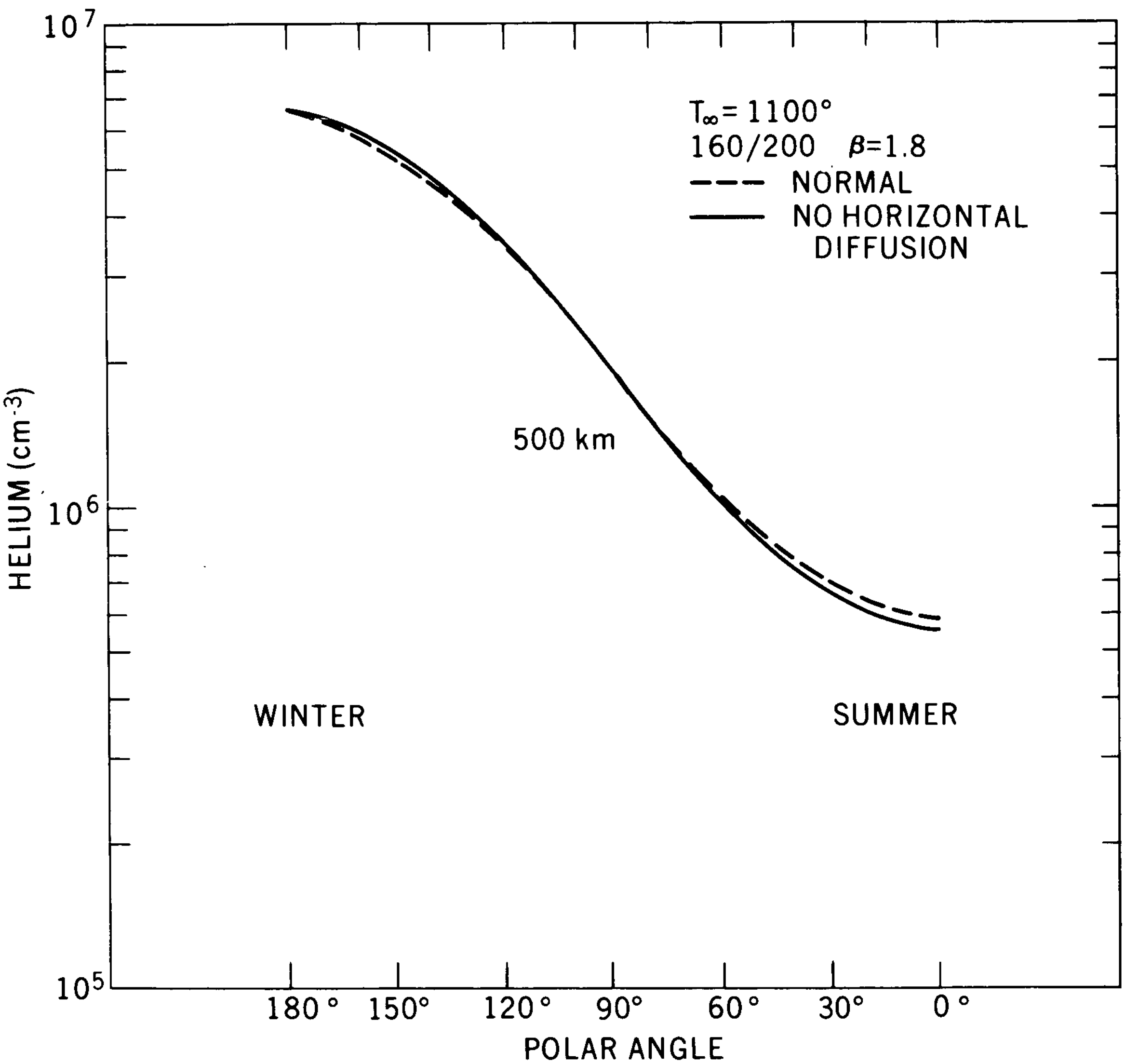

Figure 19. Helium density at 500 km versus polar angle for the case of no horizontal diffusion and including horizontal diffusion.

techniques. At 120 km the pole-to-pole ratio is increased by 16% by eliminating horizontal diffusion, but here again it would be difficult to observe. Figure 20 gives a comparison of vertical profiles with and without back diffusion. The amplitude of this effect would grow with increasing atmospheric temperature due to the temperature dependence of the molecular diffusion coefficient, but its relative importance as a smoothing mechanism would diminish compared to the much more temperature sensitive exospheric transport.

c. Exospheric Temperature

It is to be expected that increasing the amplitude of the winds in a circulation cell (as might be anticipated during periods of high solar activity) will produce a corresponding increase in their influence on the distribution of minor gases. Increasing the atmospheric temperature, however, has the opposite result, as the

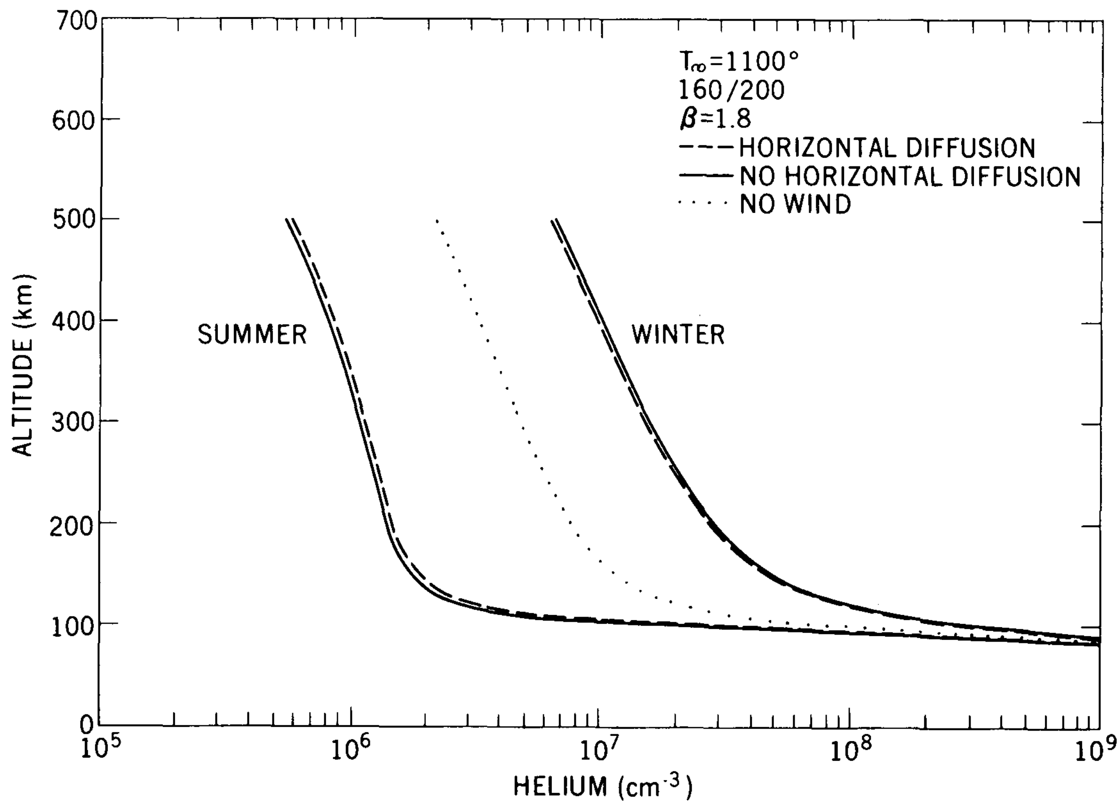

Figure 20. Helium density vertical profiles at the poles corresponding to Figure 19. Also shown is the static profile.

exospheric transport increases strongly with temperature and tends to reduce any variation. The competition between these two effects is such that at periods of high solar activity, much stronger winds are required to produce and maintain a given latitudinal variation than at periods of low solar activity. This relationship is illustrated in Figure 21 where the pole-to-pole ratios of helium (R_p) at altitudes of 120 km, 300 km and 500 km are shown as functions of the maximum vertical velocity in a cell; three exospheric temperatures are represented, corresponding again to periods of low, medium and high solar activity.

A number of interesting features are apparent here. First, a factor of two in R_p at 500 km requires an order of magnitude higher wind for an exospheric

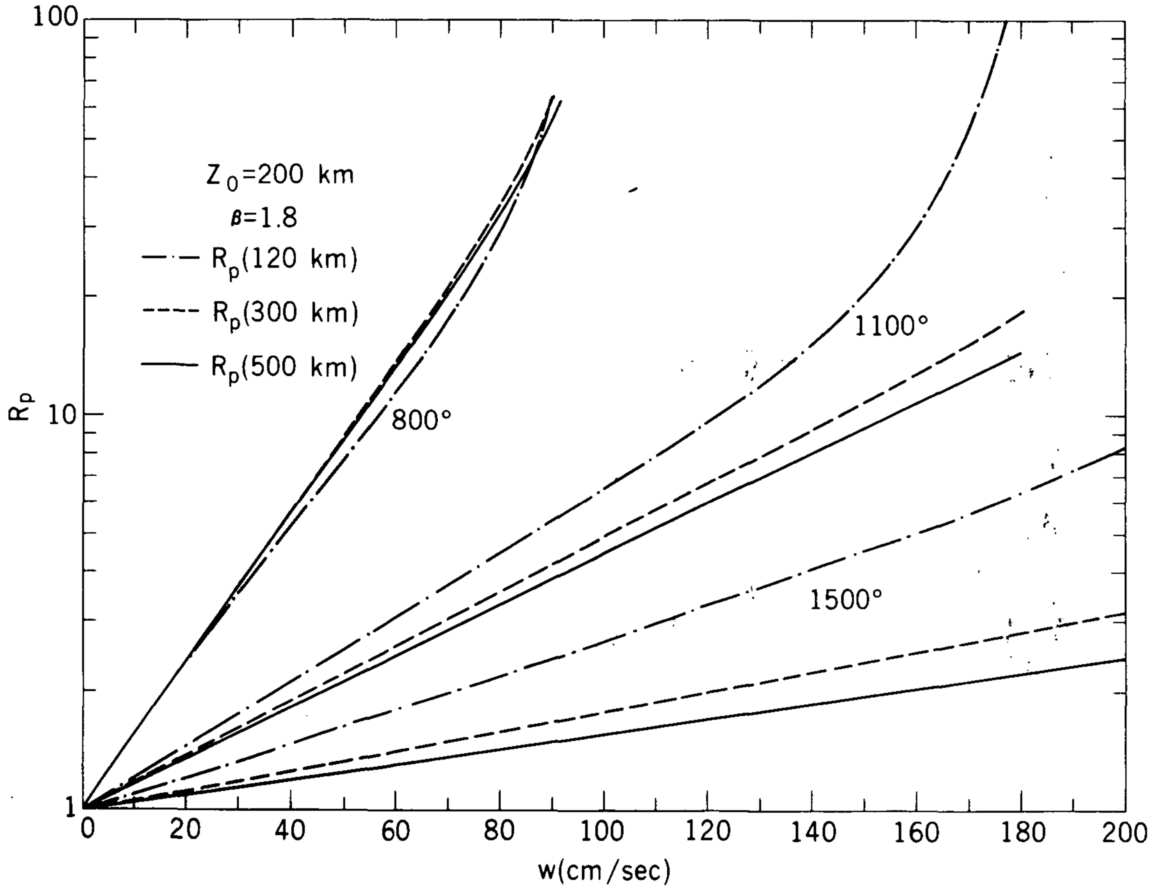

Figure 21. Pole-to-pole ratios, R_p, at 120, 300 and 500 km as functions of maximum vertical wind speed, w. Low, medium and high solar conditions are represented; Z_0 = 200 km and β = 1.8 for all the curves.

temperature of 1500° than for one of 800°, in agreement with the discussion in the previous paragraph. Second, for higher temperatures the latitudinal variation is suppressed at high altitude relative to 120 km. This is another consequence of the enhancement in exospheric return flow at high temperatures, which tends to smooth out latitudinal variations most significantly at higher altitudes. Thus, at times of low solar activity there should be much better agreement between low altitude measurements (e.g. from rockets) and satellite measurements than during periods of high solar activity. Also, it is not likely that the wind amplitude increases sufficiently (due only to increases in the pressure gradients), from periods of low to high solar activity, to maintain the same level of disturbance in the helium distribution; therefore, the observed pole-to-pole ratio should be highest at times of low solar activity.

d. Shape, Amplitude and Altitude of Wind Cell

While the effects discussed so far, particularly the exospheric transport, have an important bearing on the ultimate distribution of a minor gas, it is the wind field itself which sets up the variation from a uniform, static-diffusion distribution. In this section, we shall examine the effect of varying the characteristics of the wind field itself, specifically the altitude and amplitude of the cell and the altitude of the return flow.

The pole-to-pole ratios of the helium density as functions of maximum vertical wind speed are shown in Figures 22 through 27 for β's of 1.8 and 4.0, z_0's of 170 km, 200 km and 230 km, and exospheric temperatures of 800°, 1100°, and 1500°. The corresponding vertical profiles at the summer and winter poles and equator are given in Figures 28 through 33; Figures 28, 31

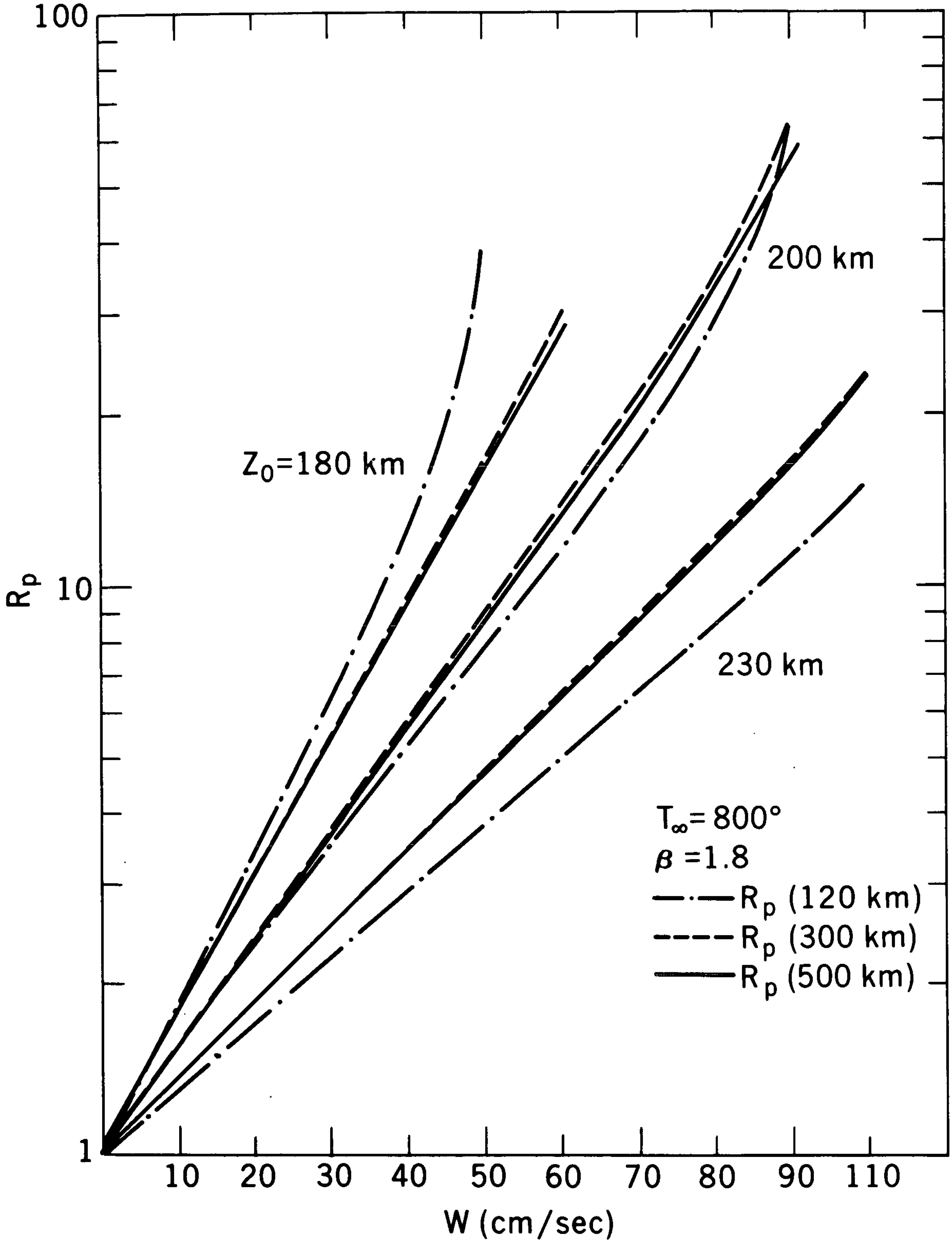

Figure 22. Pole-to-pole ratios, R_p, at 120, 300 and 500 km versus vertical wind speed w, for T_∞ =800°, Z_0 = 180, 200 and 230 km, and β = 1.8.

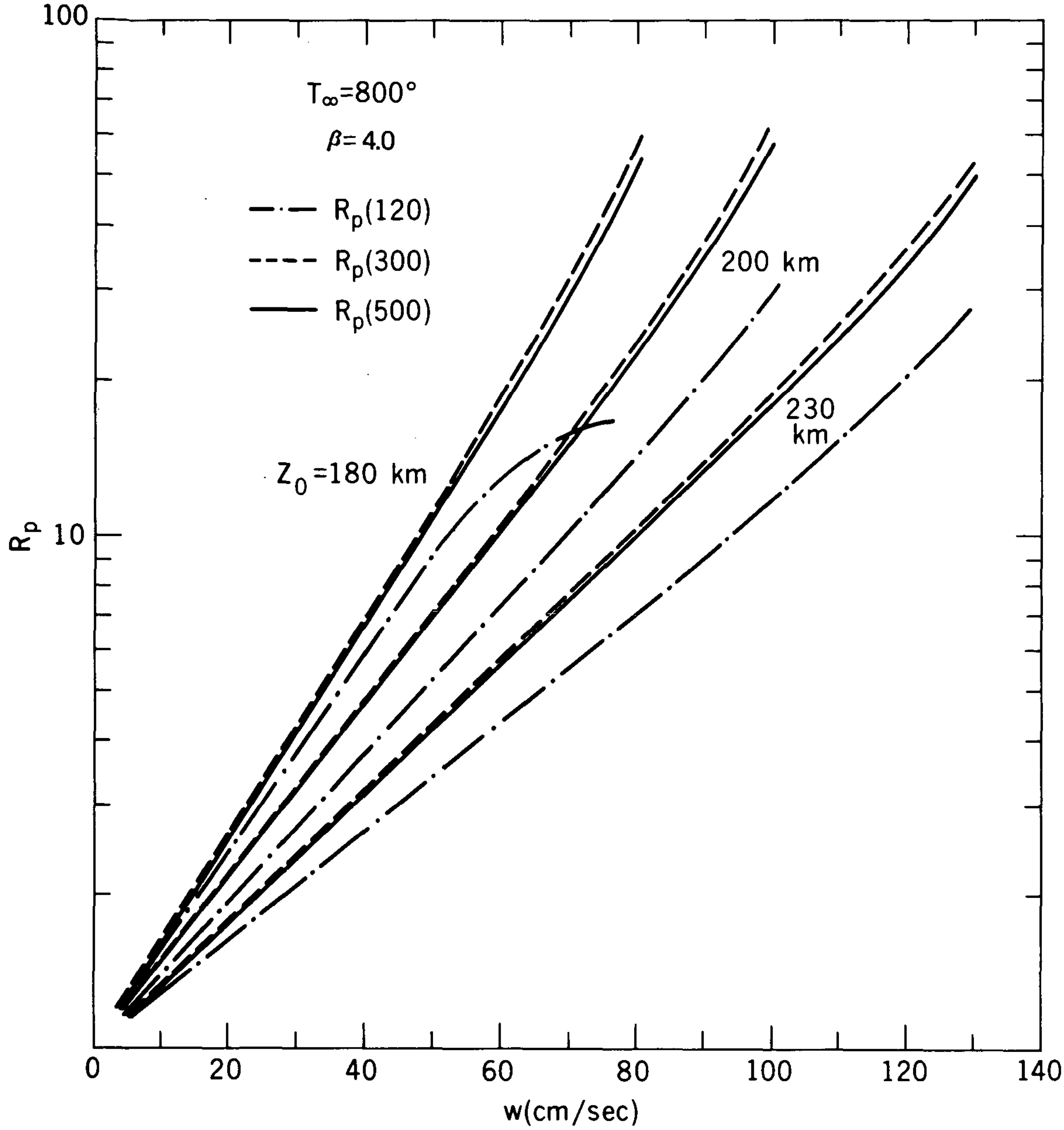

Figure 23. Pole-to-pole ratios, R_p, at 120 300 and 500 km versus vertical wind speed w, for T_∞ =800°, Z_0 =180, 200 and 230 km, and β = 4.0,

and 33 compare equal vertical amplitudes, while Figures 29, 30 and 32 give the profiles for approximately equal values of R_p. The latitudinal distributions at 120 km, 300 km and 500 km are given in Figures 34 through 39 for the same set of parameters. Representative horizontal and vertical wind profiles for these systems are shown in Figures 40 through 43, and Figures 44 through 47 picture the corresponding circulation cells. The plots of R_p versus wind speed indicate

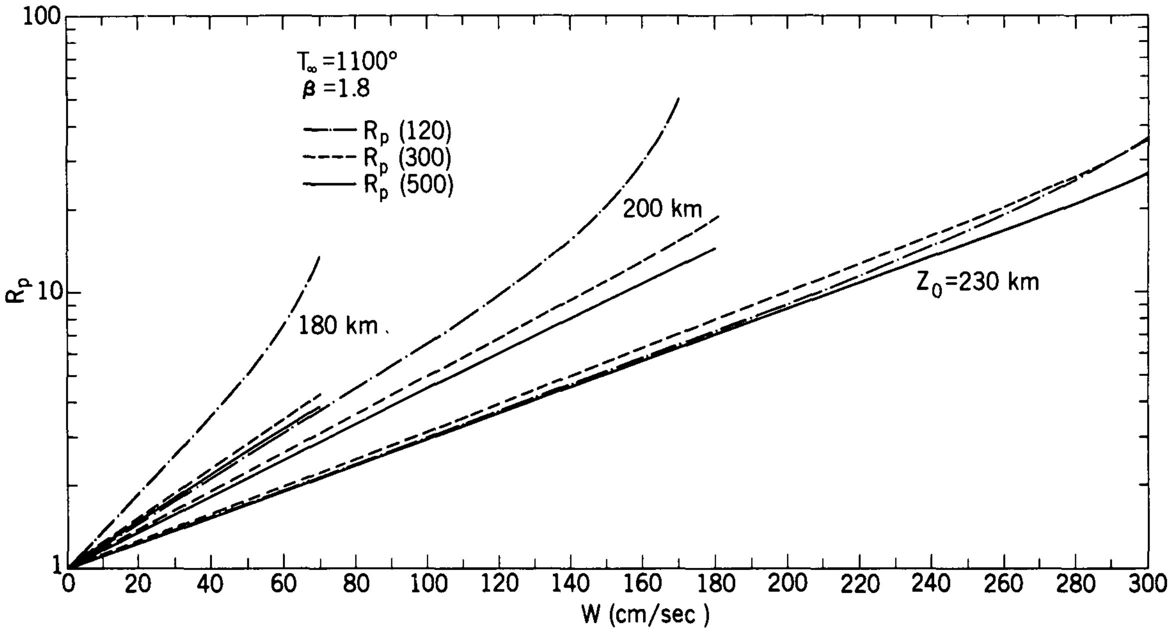

Figure 24. Pole-to-pole ratios, R_p, versus vertical wind speed, w, for T_∞ =1100 and β=1.8.

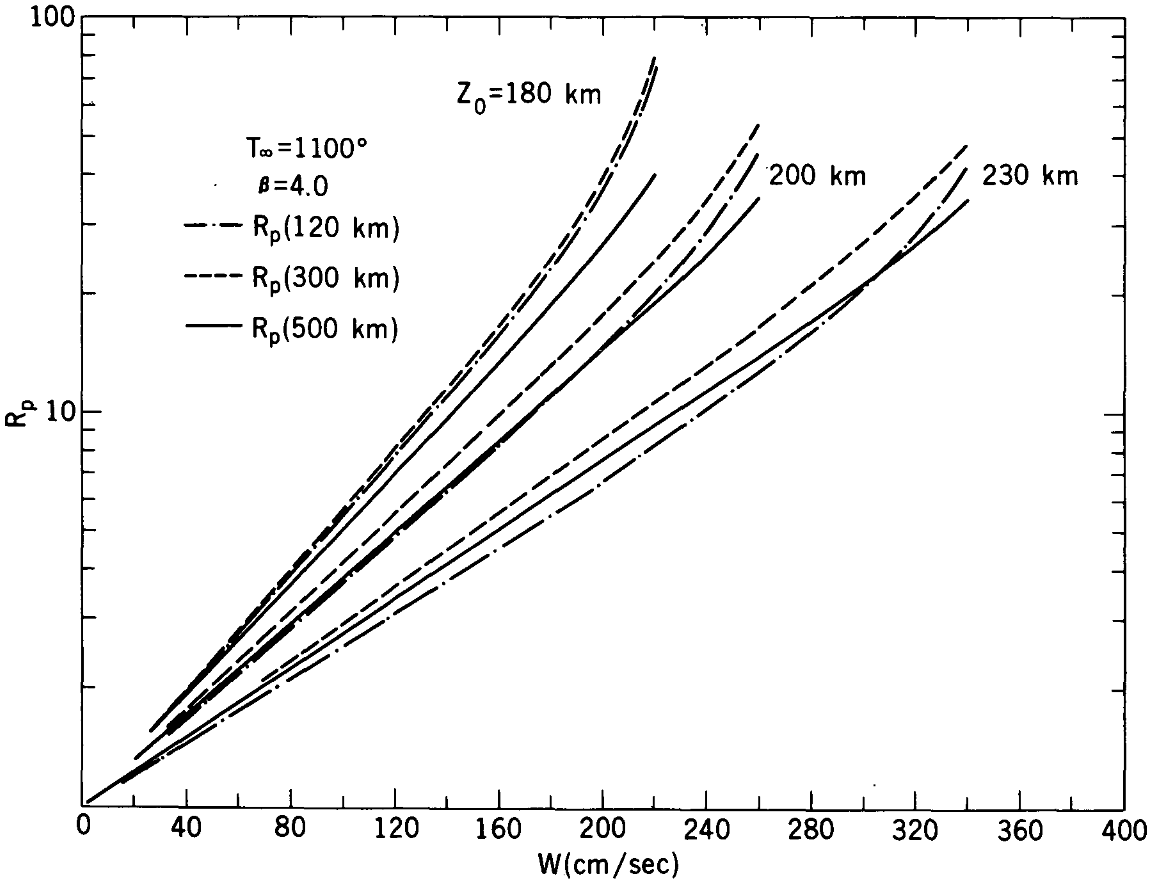

Figure 25. Pole-to-pole ratios, R_p, versus vertical wind speed, w, for T_∞ =1100 and β= 4.0.

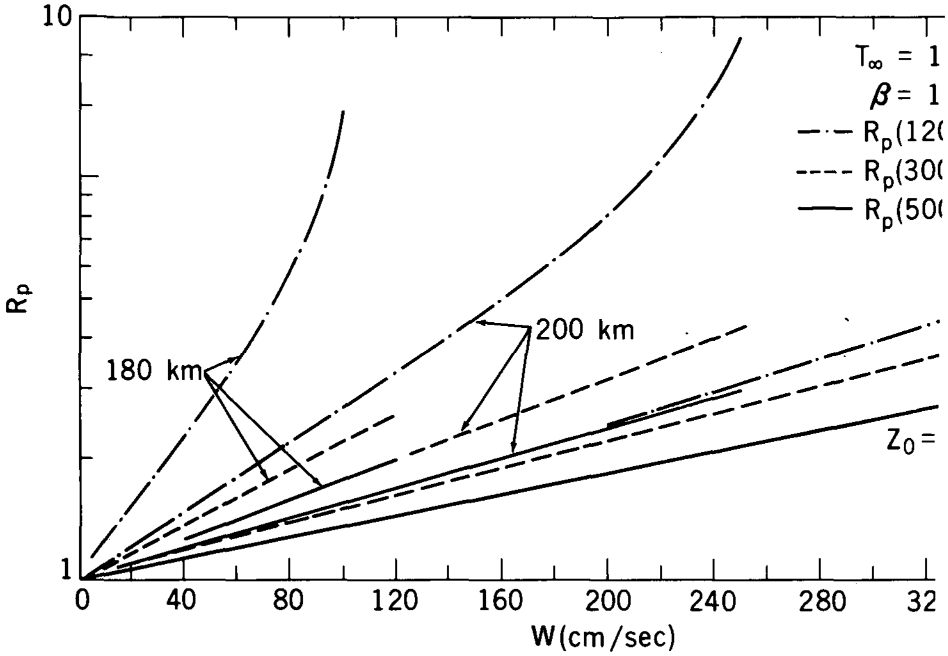

Figure 26. Pole-to-pole ratios, R_p, versus vertical wind speed, w, for T_∞ =1

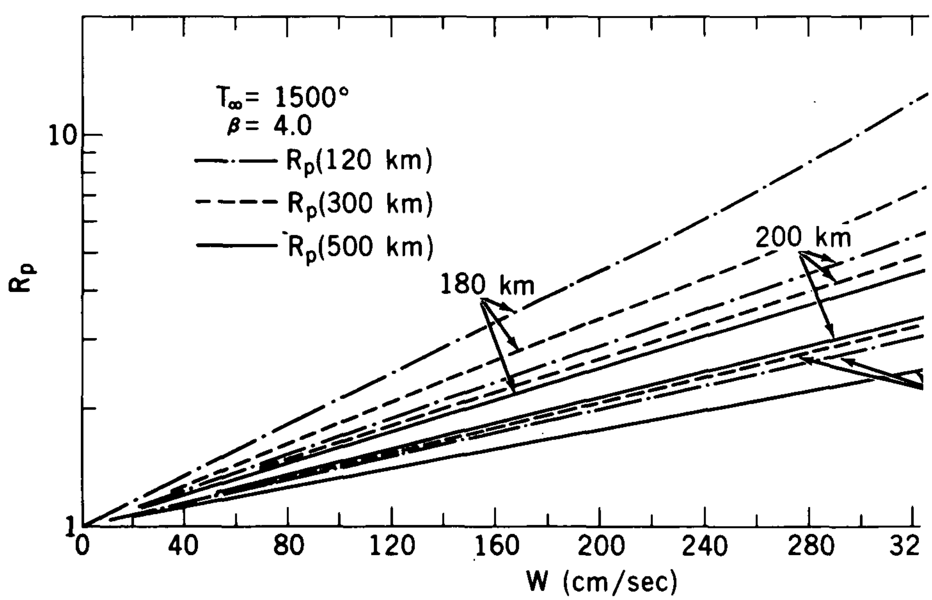

Figure 27. Pole-to-pole ratios, R_p, versus vertical wind speed, w, for T_∞ =

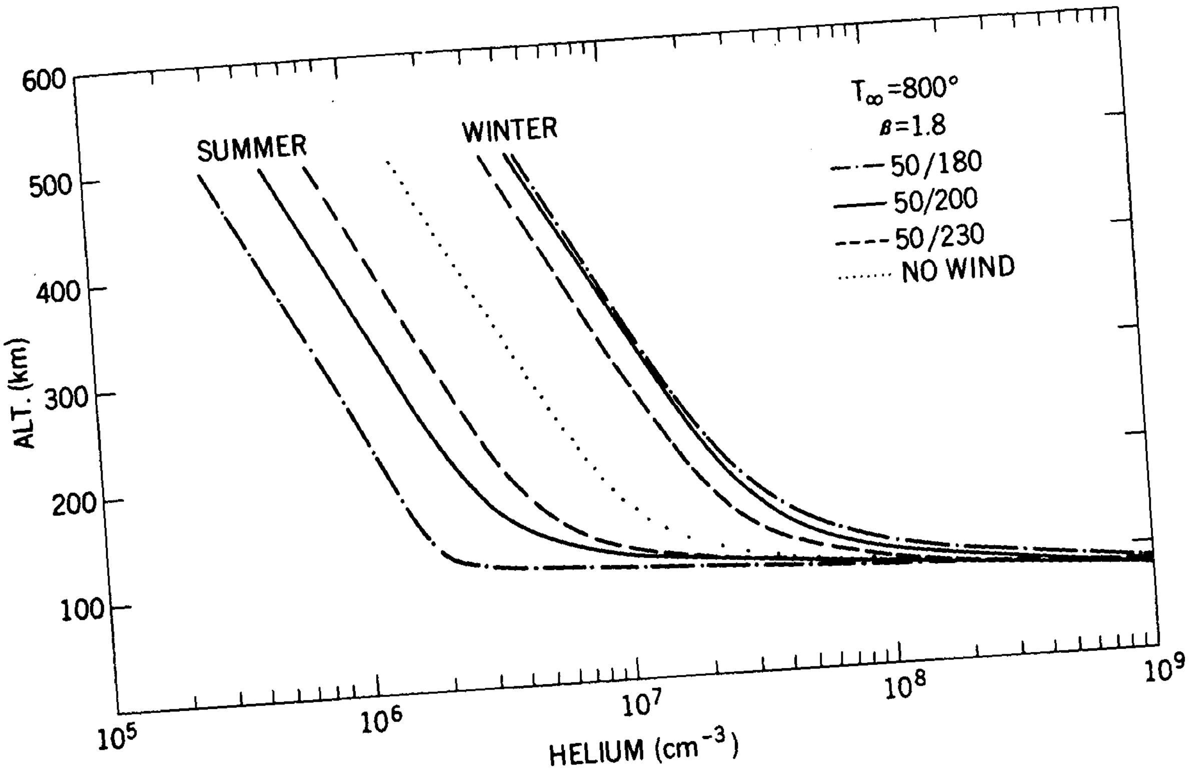

Figure 28. Helium density versus altitude for T_∞ =800° and the wind systems β=1.8, 50/180, 50/200, and 50/230. The static case is also shown.

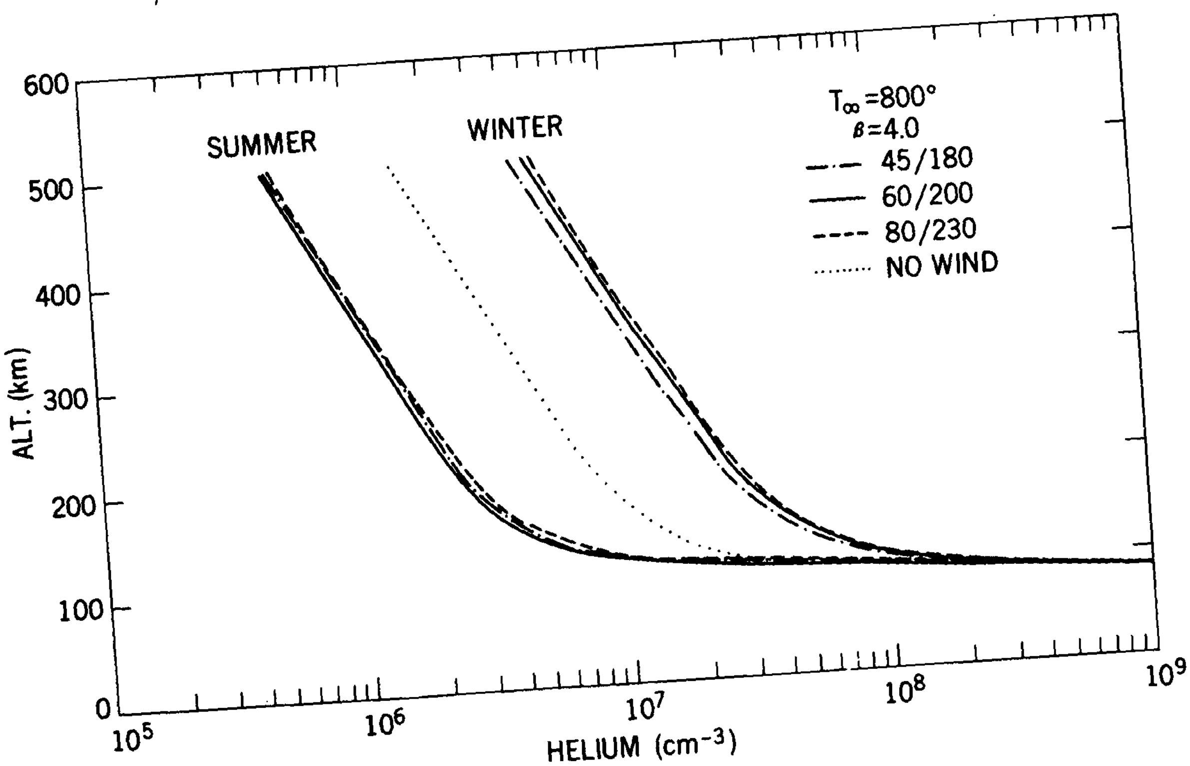

Figure 29. Helium density versus altitude for T_∞ =800° and the wind systems β = 4.0, 45/180, 60/200, and 80/230. These winds produce nearly the same pole-to-pole ratios.

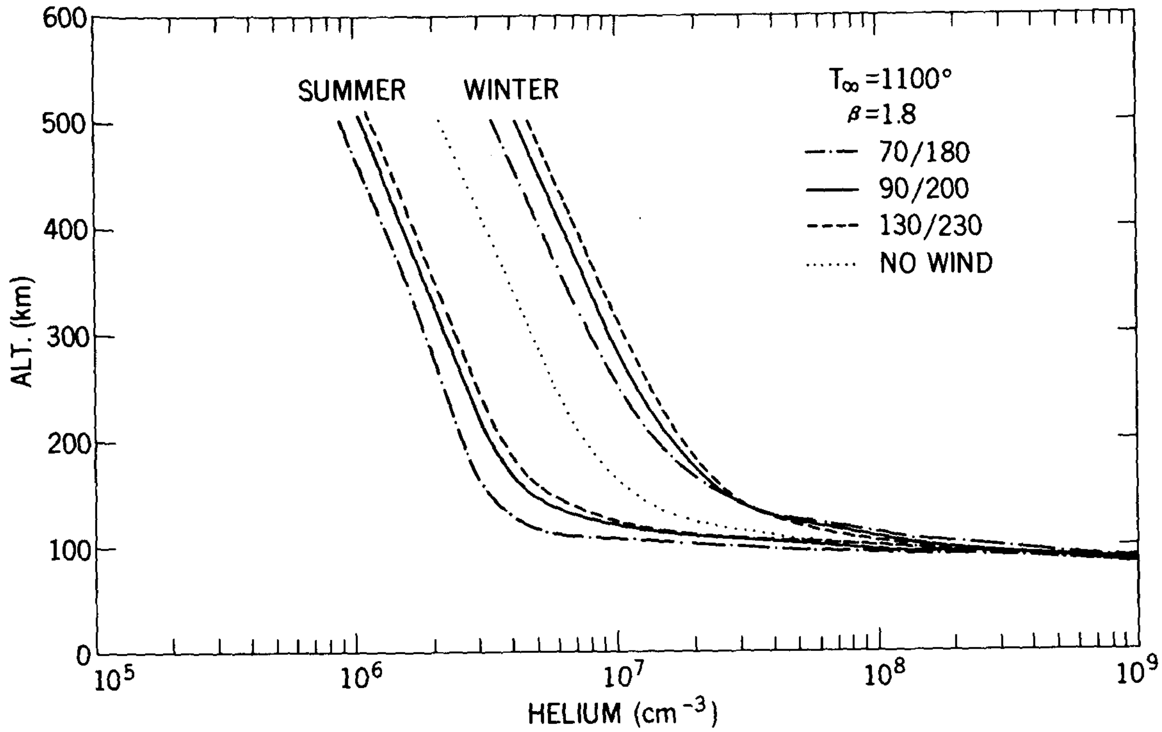

Figure 30. Helium density versus altitude for $T_\infty = 1100°$ and the wind systems $\beta = 1.8$, 70/180, 90/200, 130/230 which produce similar values of R_p (500 km).

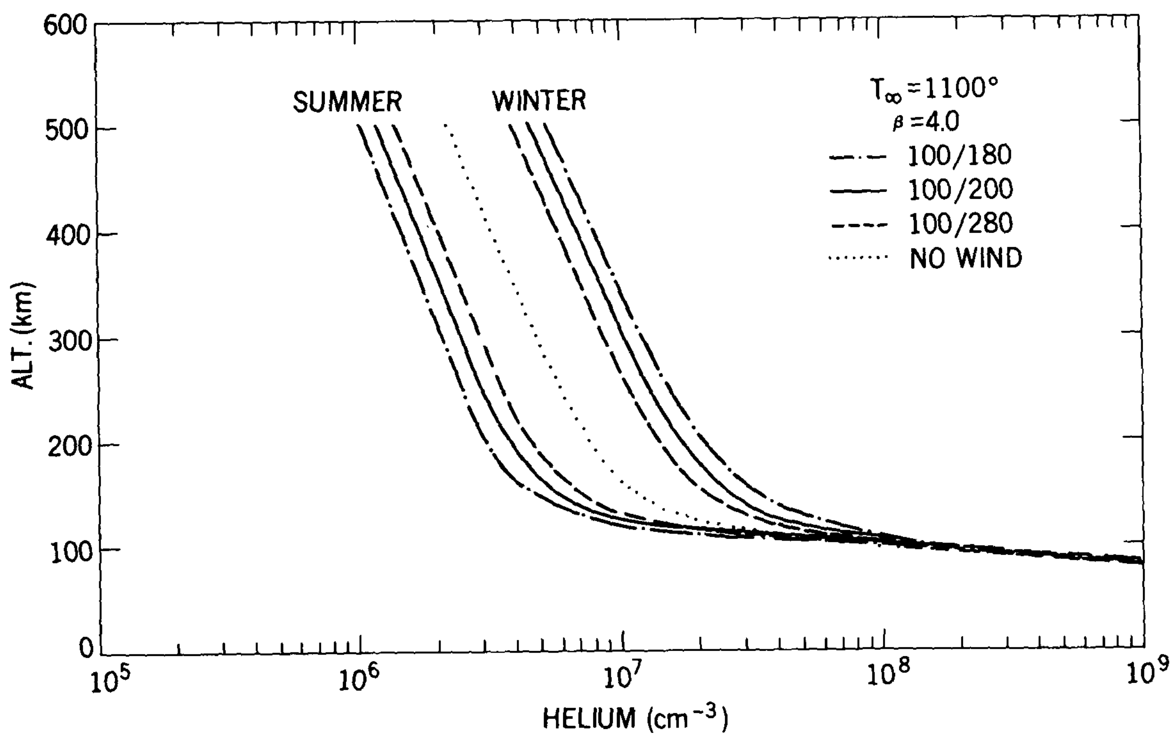

Figure 31. Helium density versus altitude for $T_\infty = 1100°$ and the wind systems $\beta = 4.0$, 100/180, 100/200, and 100/230.

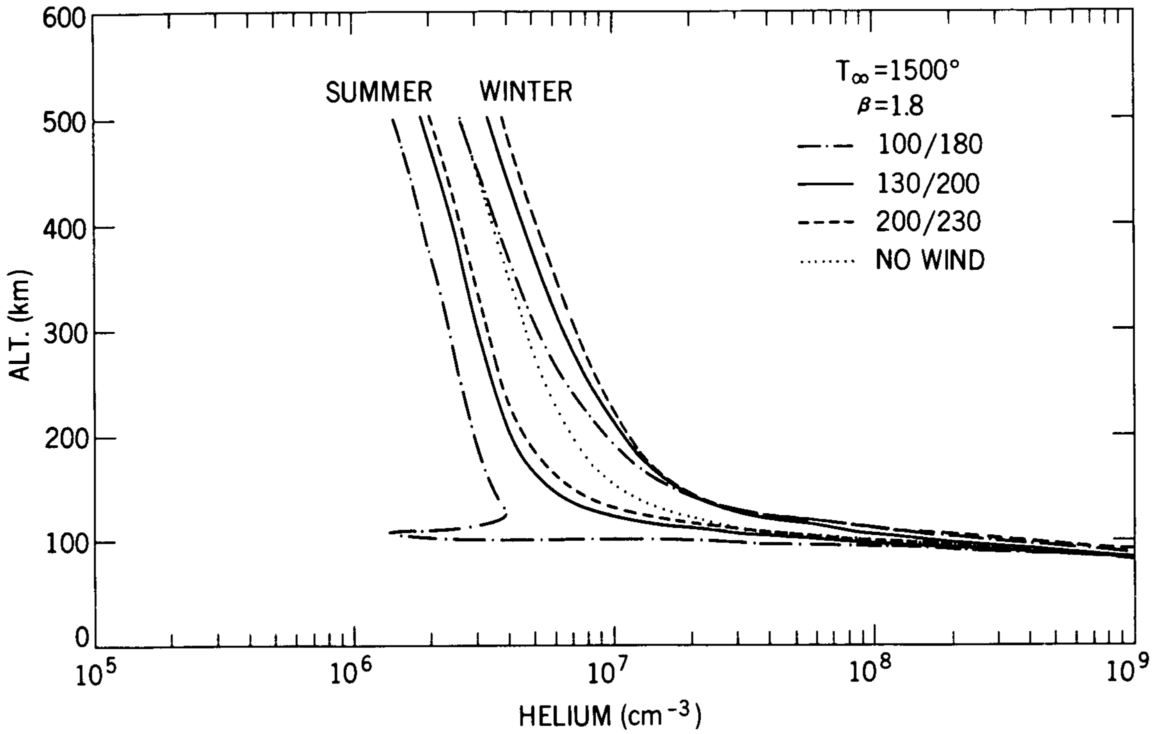

Figure 32. Helium density versus altitude for $T_\infty = 1500°$ and the wind systems $\beta = 1.8$, 100/180, 130/200, and 200/230 which produce similar R_p (500 km).

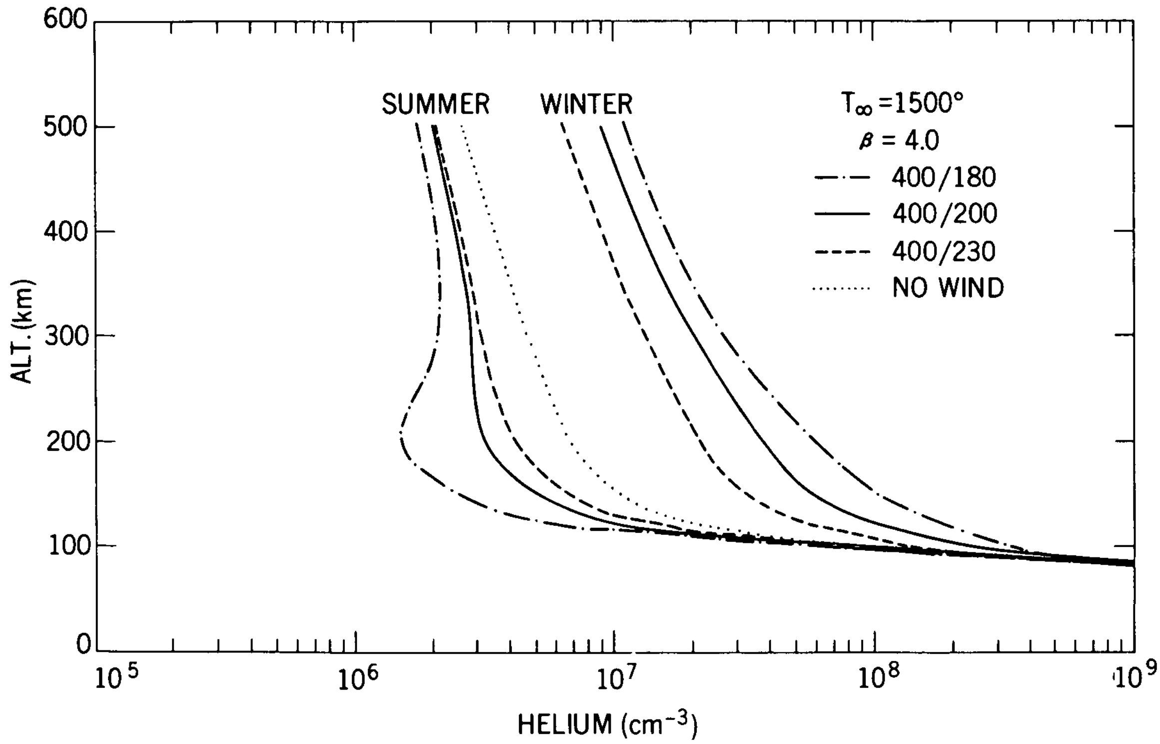

Figure 33. Helium density versus altitude for $T_\infty = 1500°$ and the wind systems $\beta = 4.0$, 400/180, 400/200, and 400/230.

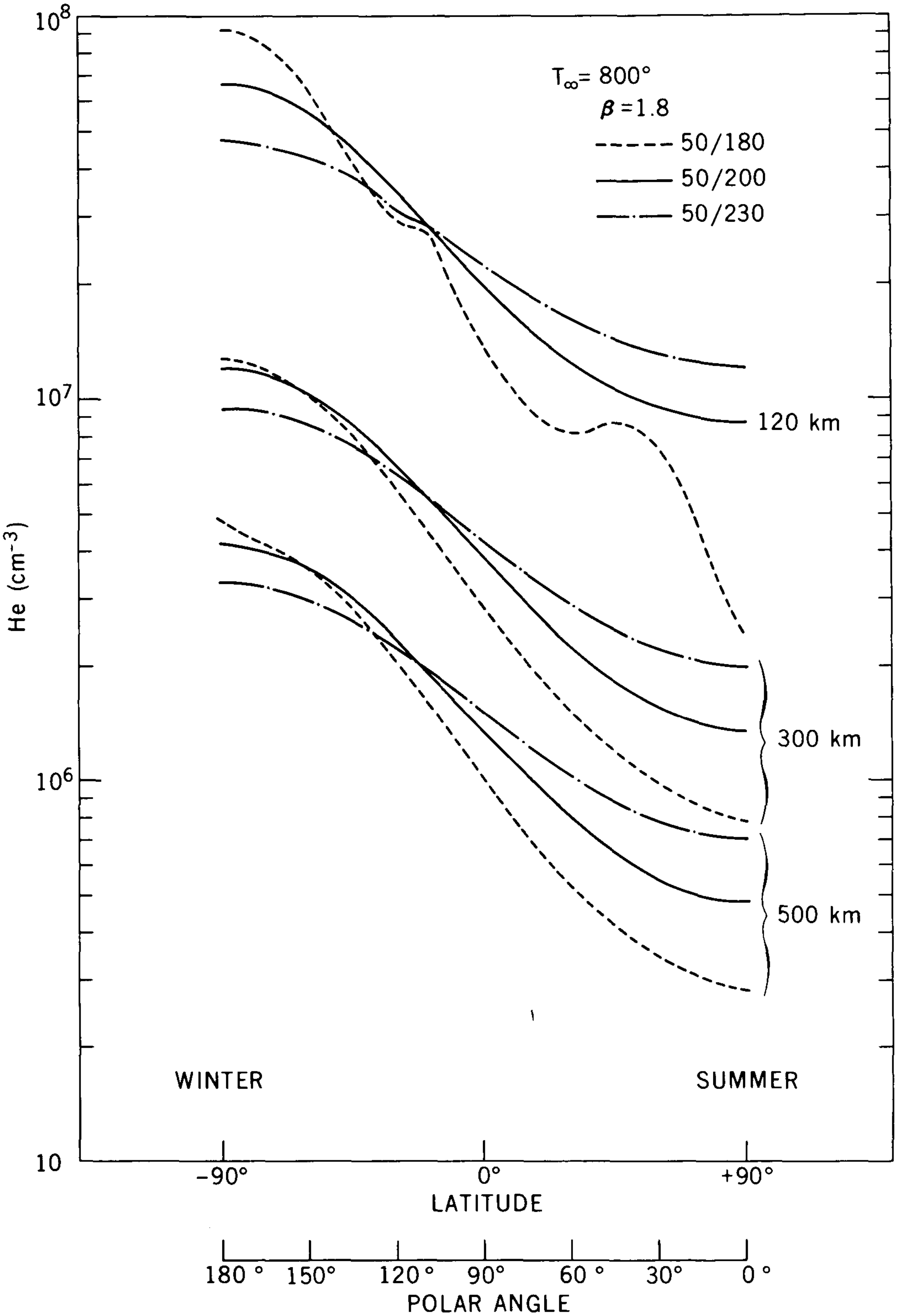

Figure 34. Helium density at 120 km, 300 km and 500 km versus latitude for $T_\infty = 800°$ and the same winds as in Figure 28.

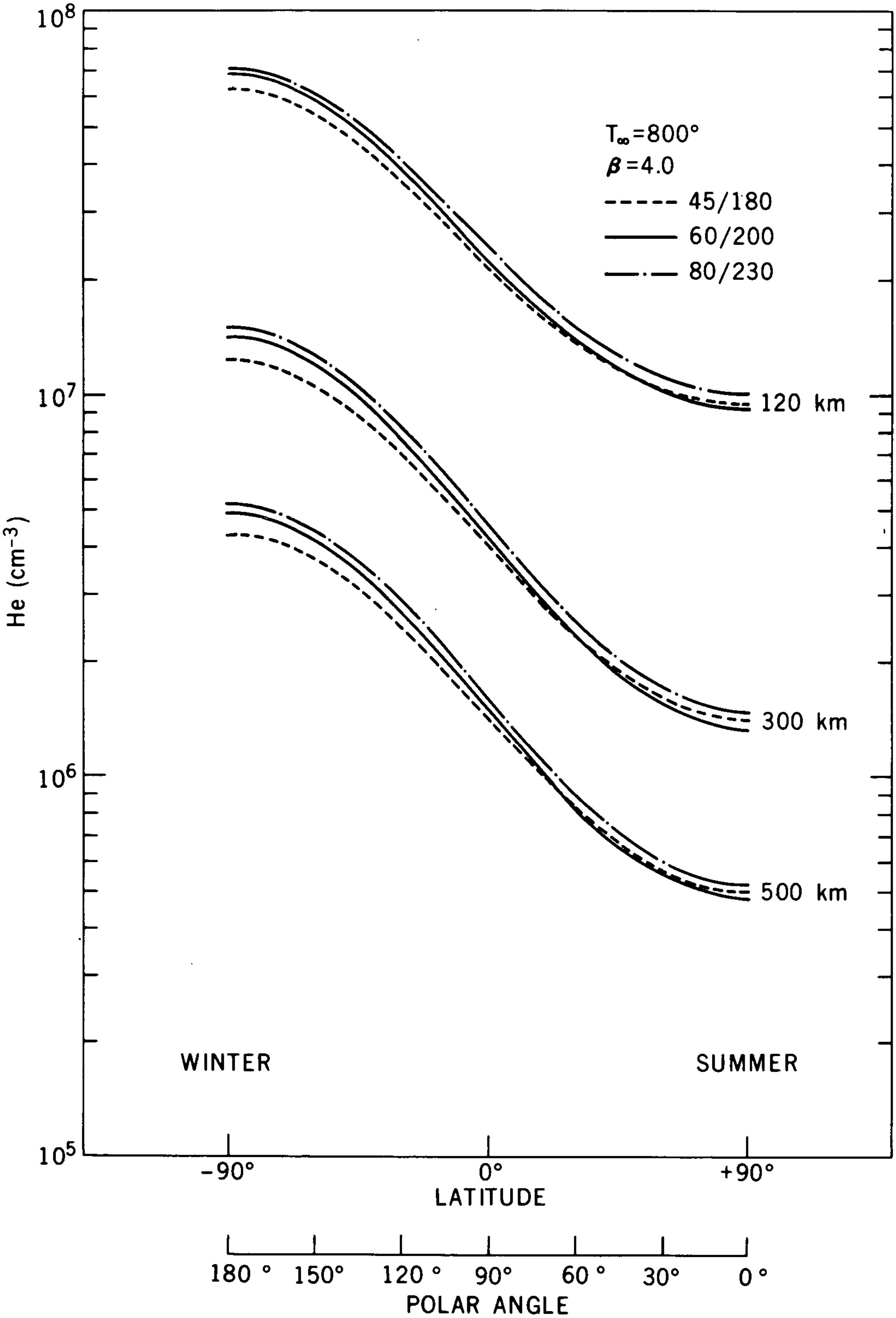

Figure 35. Helium density at 120 km, 300 km and 500 km versus latitude for T_∞ =800° and the winds of Figure 29.

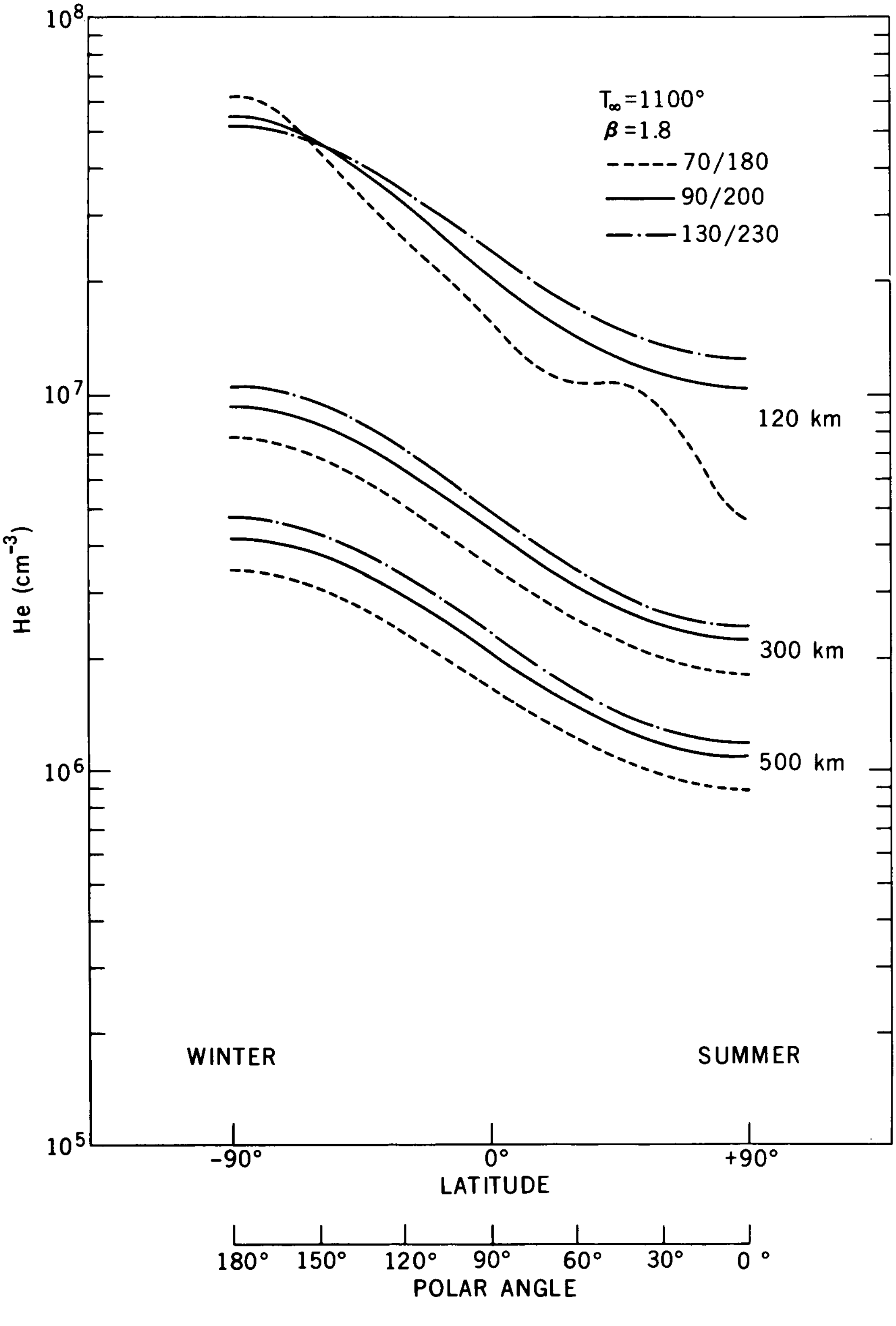

Figure 36. Helium density at 120 km, 300 km and 500 km versus latitude for T_∞ = 1100° and the winds of Figure 30.

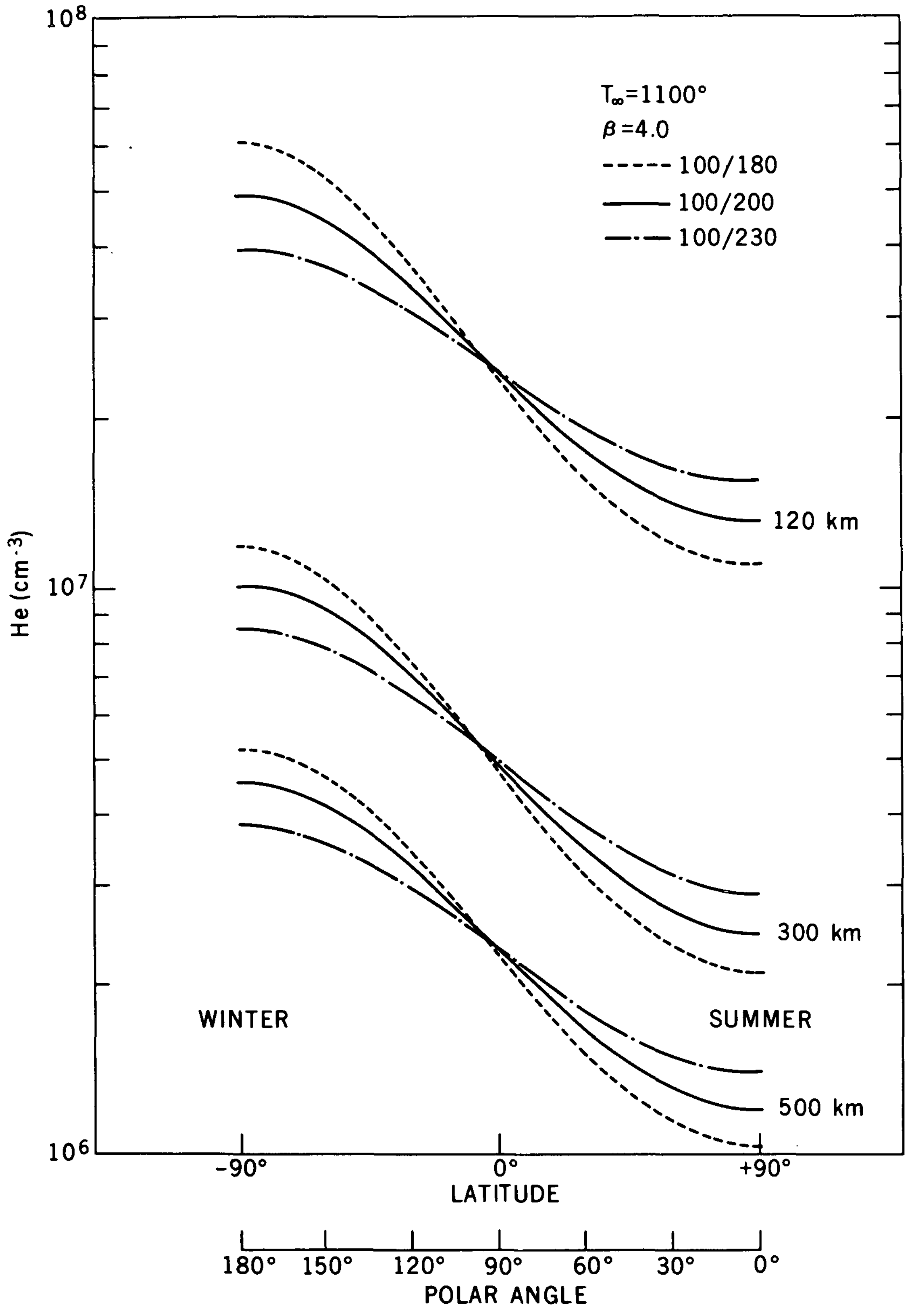

Figure 37. Helium density at 120 km, 300 km and 500 km versus latitude for $T_{\infty} = 1100°$ and the winds of Figure 31.

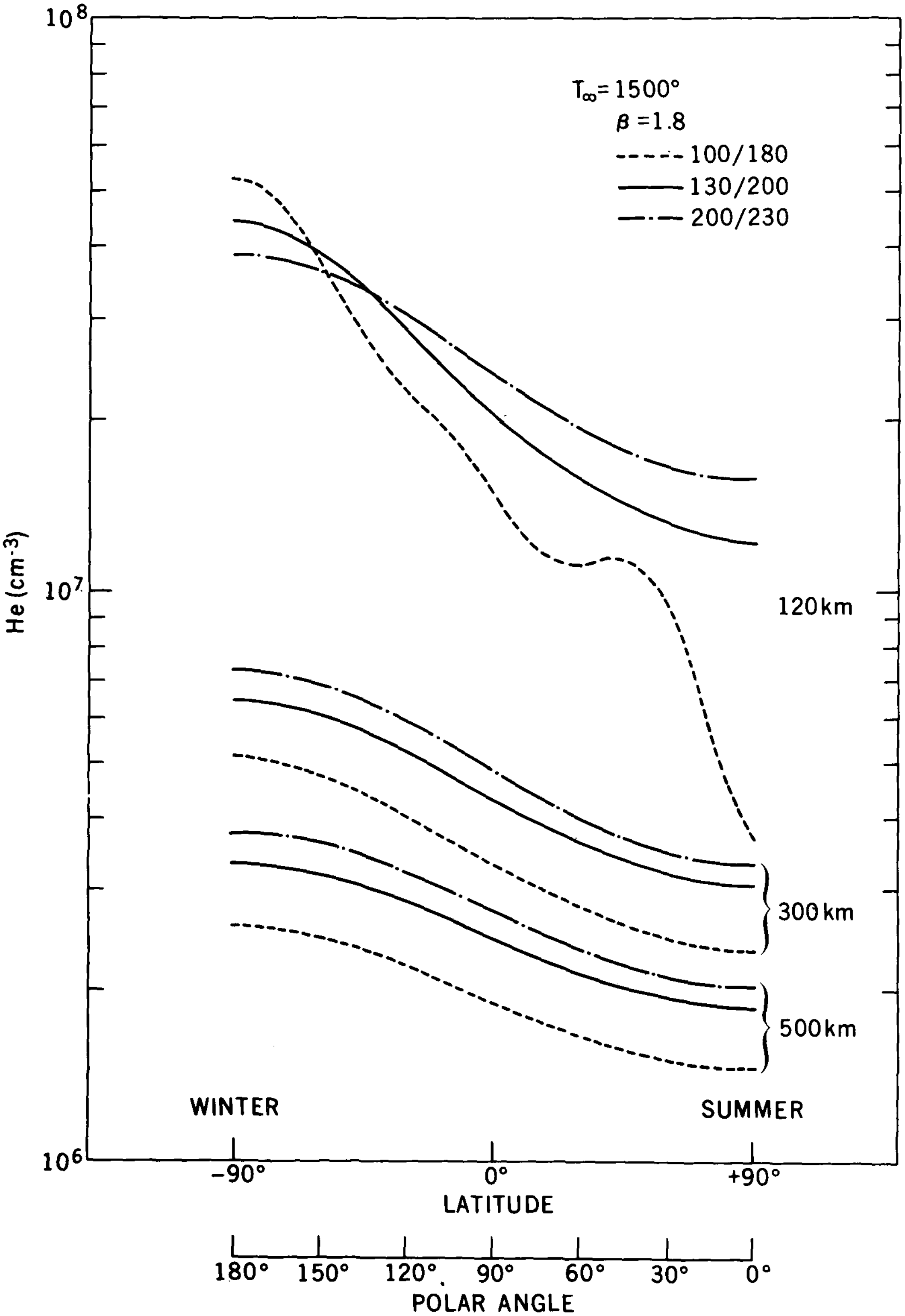

Figure 38. Helium density at 120 km, 300 km, 500 km versus latitude for T_∞ = 1500° and the winds of Figure 32.

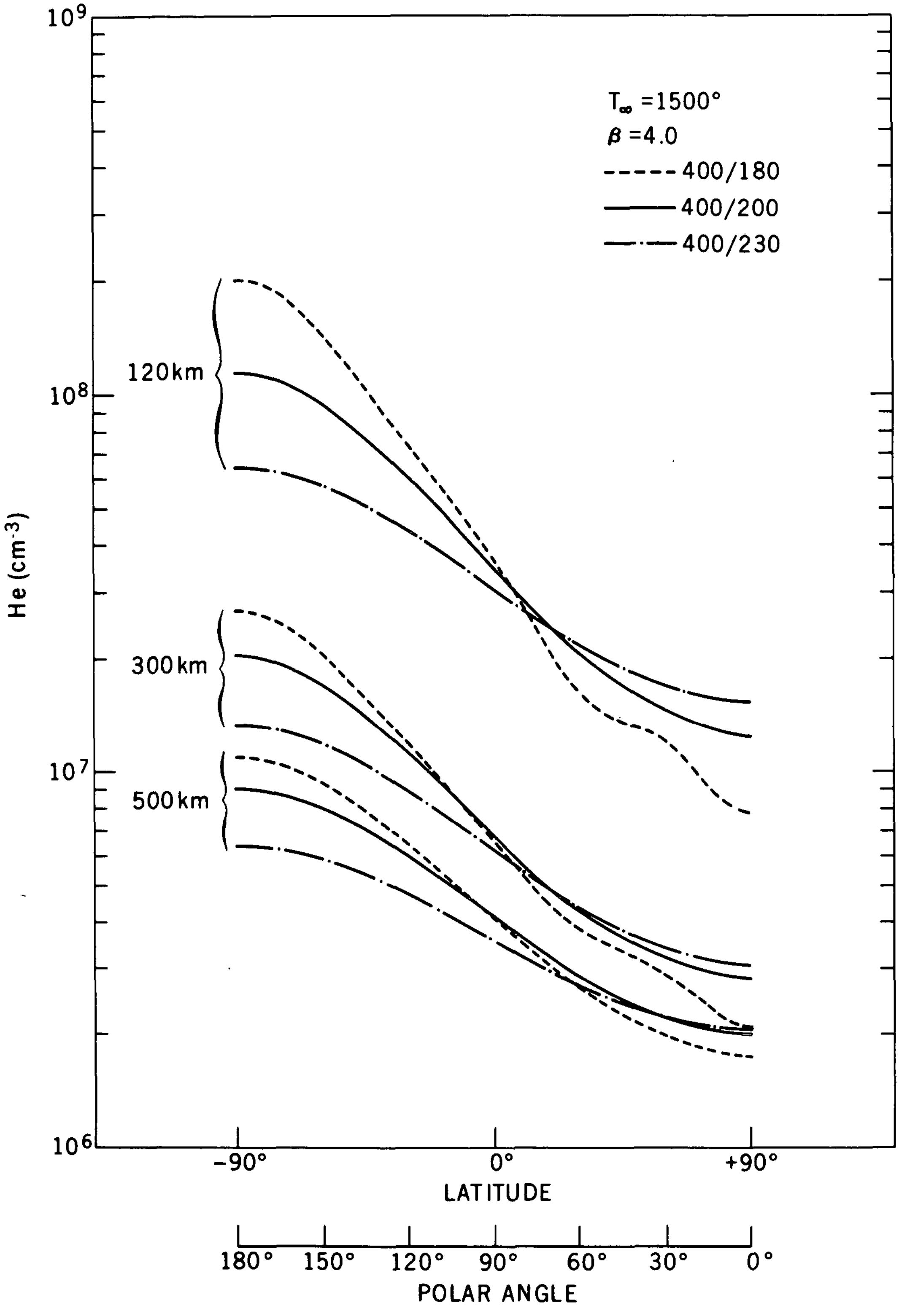

Figure 39. Helium density at 120 km, 300 km, and 500 km versus latitude for T_∞ = 1500° and the winds of Figure 33.

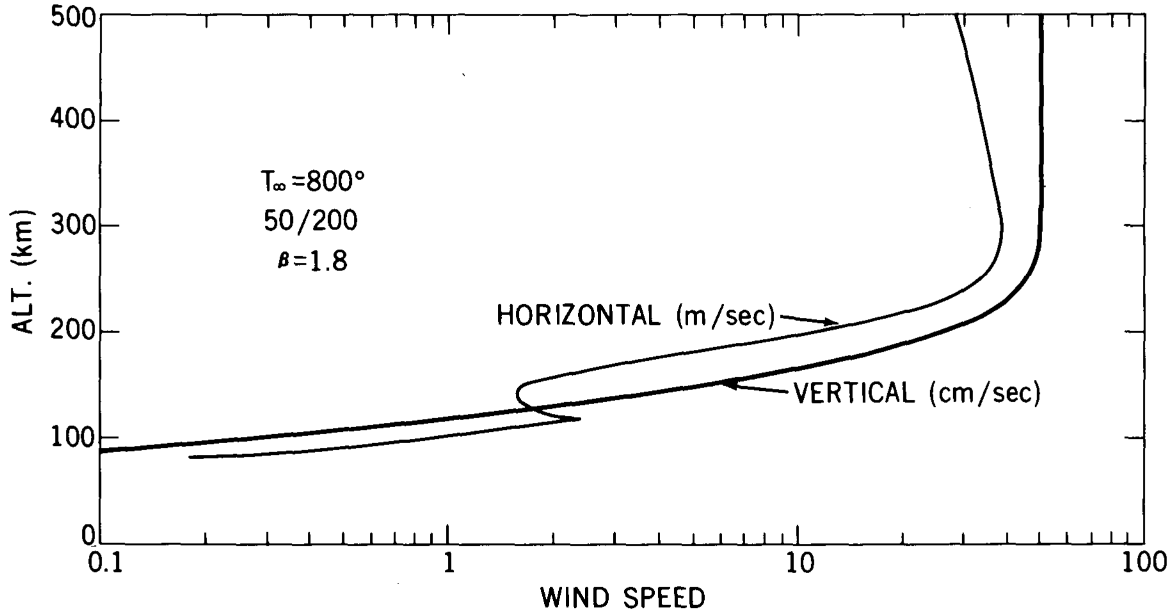

Figure 40. Vertical and horizontal wind profiles for $T_\infty = 800°$, 50/200, $\beta = 1.8$. The values shown represent maximum amplitudes and are multiplied by sin θ for the horizontal component and cos θ for the vertical component, where θ is the polar angle.

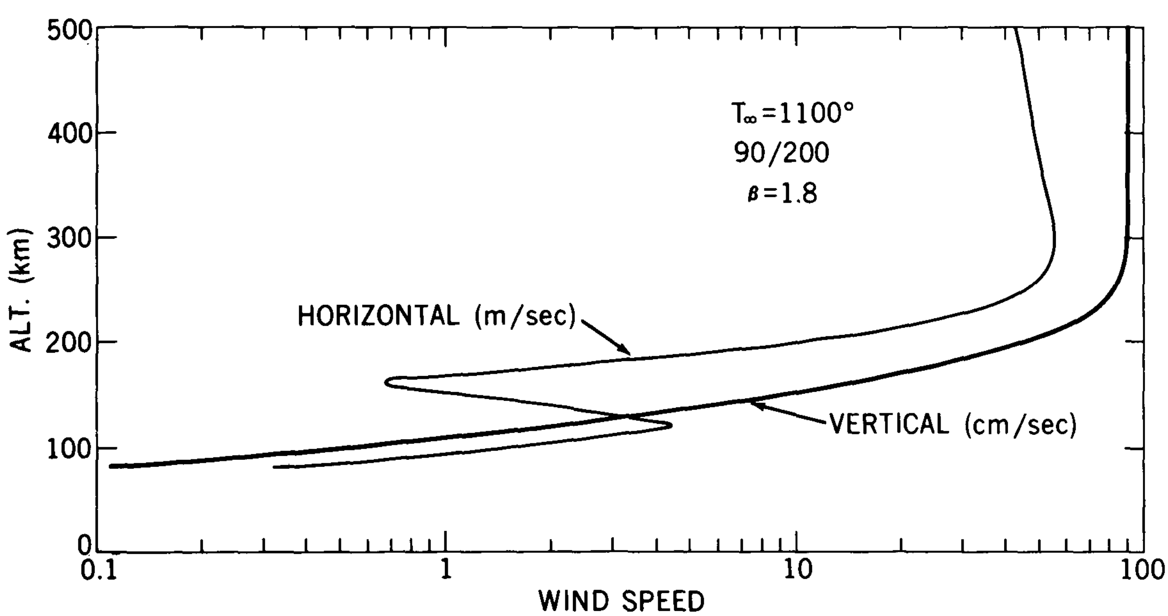

Figure 41. Vertical and horizontal wind profiles for $T_\infty = 1100°$, 90/200, $\beta = 1.8$.

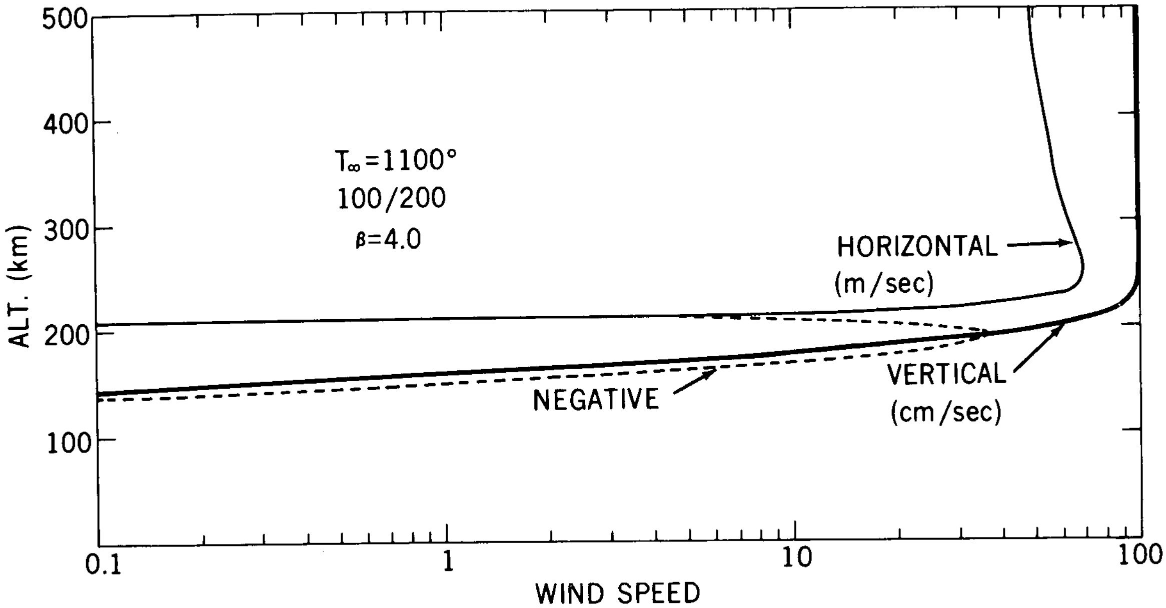

Figure 42. Vertical and horizontal wind profiles for $T_\infty = 1100°$, 100/200, $\beta = 4.0$. The region of horizontal wind labeled "negative" refers to flow from the winter hemisphere toward the summer hemisphere.

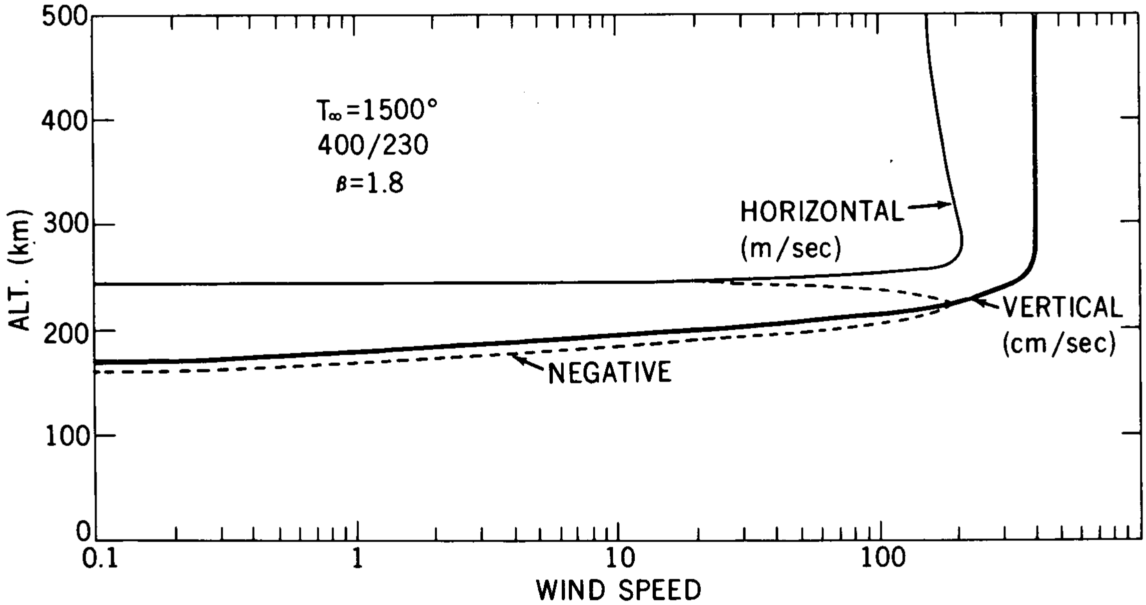

Figure 43. Vertical and horizontal wind profiles for $T_\infty = 1500°$, 400-230, $\beta = 4.0$.

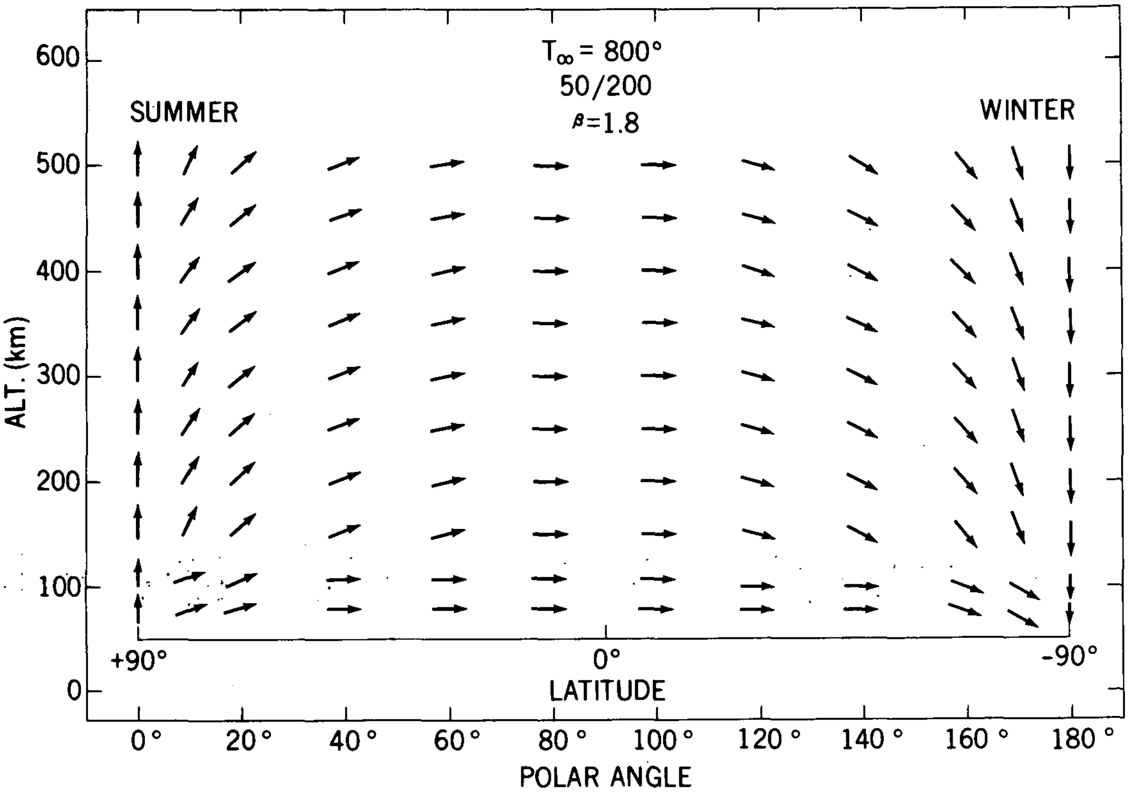

Figure 44. Direction of wind vectors for profiles of Figure 40.

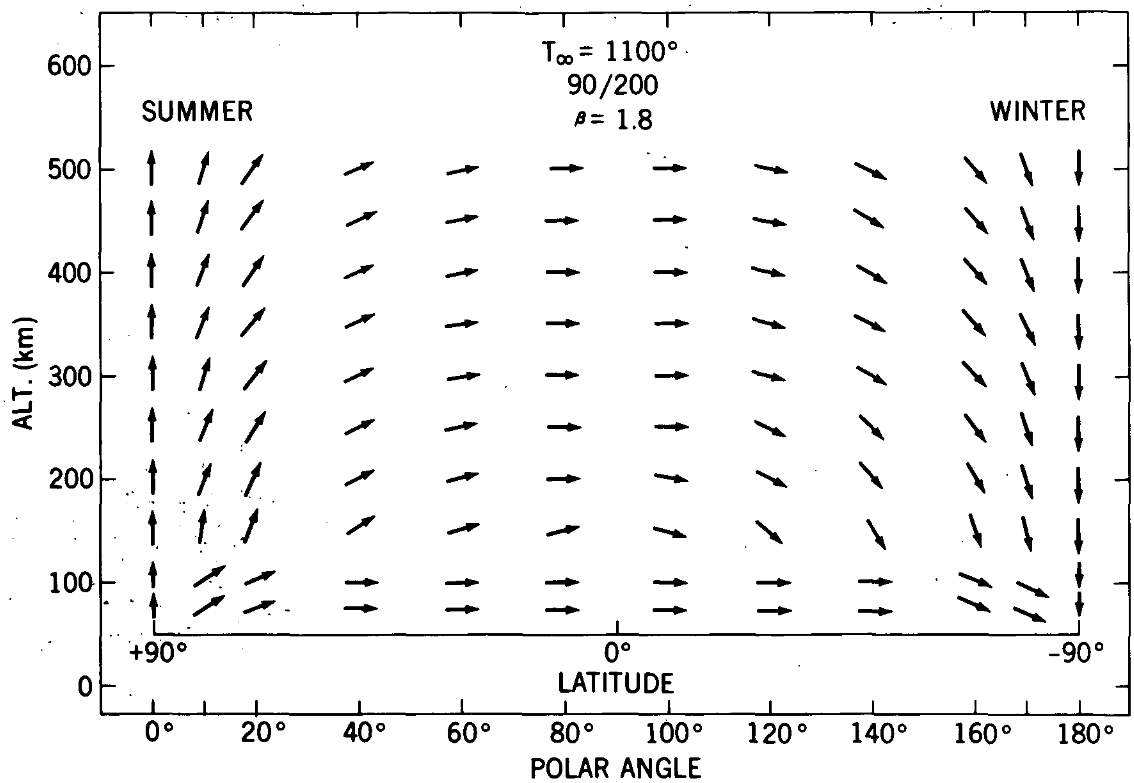

Figure 45. Direction of wind vectors for profiles of Figure 41.

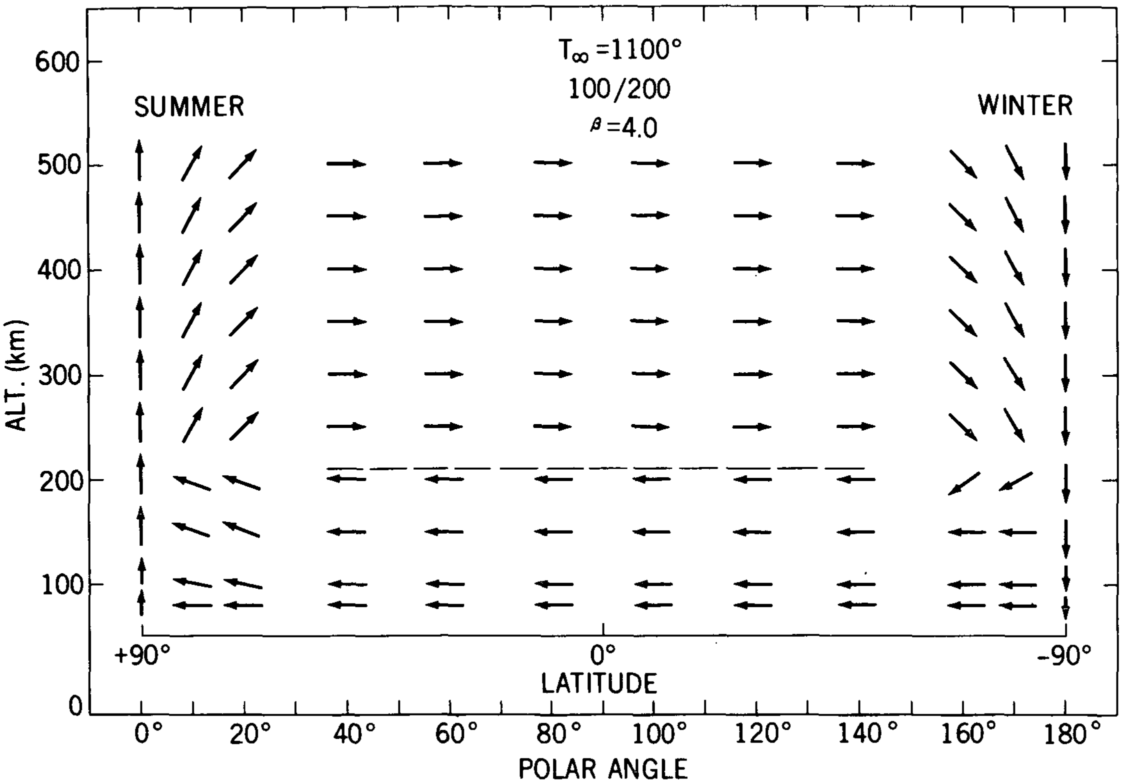

Figure 46. Direction of wind vectors for profiles of Figure 42.

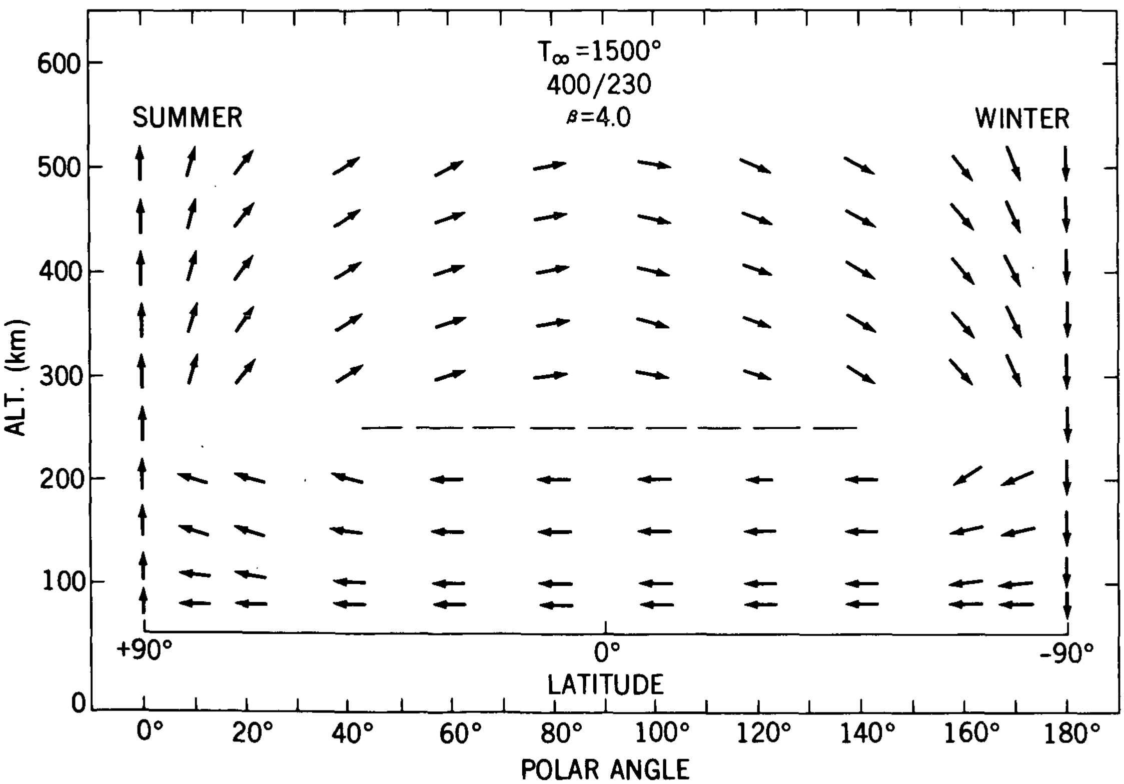

Figure 47. Direction of wind vectors for profiles of Figure 43.

that increasing the altitude of the cell (z_0) or decreasing the wind speed at lower altitudes (increasing β) generally has the effect of raising the high altitude wind speed required for a given pole-to-pole ratio. For low and moderate values of wind speed the variation of the logarithm of R_p with W is seen to be linear. With increasing winds log R_p/W becomes non-linear, with the largest effect occurring at lower altitudes. This reflects once more the smoothing effect of the exospheric return flow at high altitudes, and also indicates that a significant amount of the redistribution effect of the wind occurs in the 100 to 200 km altitude range.

This can be seen most clearly in the variation of helium with altitude, particularly for an exospheric temperature of 1500° and $z_0 = 180$ km. Under these conditions, the summer pole density actually goes through a minimum with increasing altitude: The density is diminished from below by the upward wind and is replenished from the top by the exospheric flux. As the altitude of the circulation cell would most probably rise with increasing exospheric temperature, the occurrence of such a minimum in the density profile is not considered likely; however, this extreme case illustrates the result of the competition between the wind and the exospheric transport in influencing the vertical distribution. This low altitude effect is generally greater for smaller values of β, i.e. when the wind extends to lower altitudes and when the return flow (of the wind field) is below the thermosphere.

The sensitivity of the latitudinal distribution to the altitude of the wind is shown in Figures 48 and 49, where $\alpha(Z_0, T_\infty)$ (the slope of the log R_p vs. w curve in the linear region) is plotted as a function of Z_0 for the three exospheric

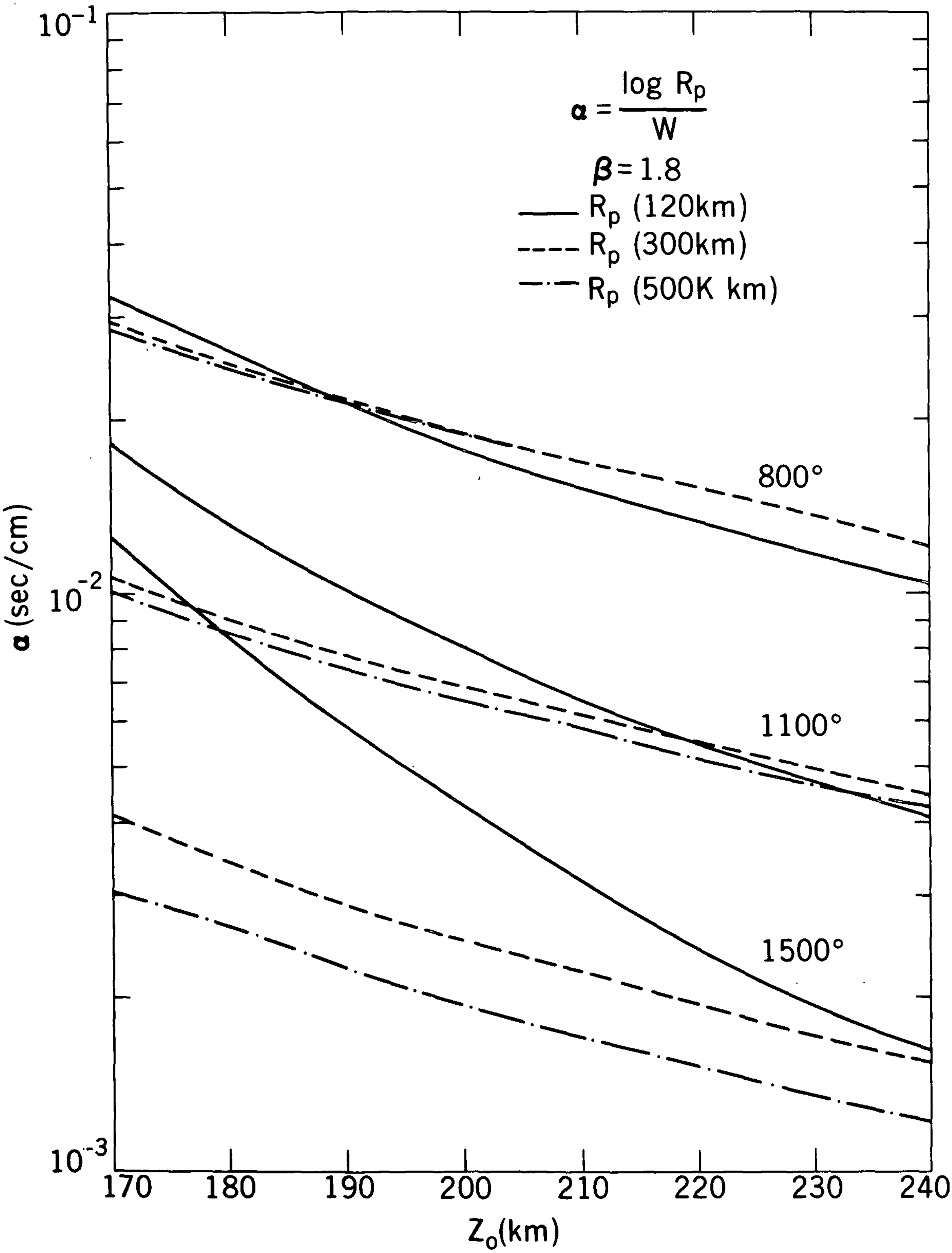

Figure 48. $\alpha = \log R_p/W$ versus Z_0 for $\beta = 1.8$ and low, medium and high solar activity.

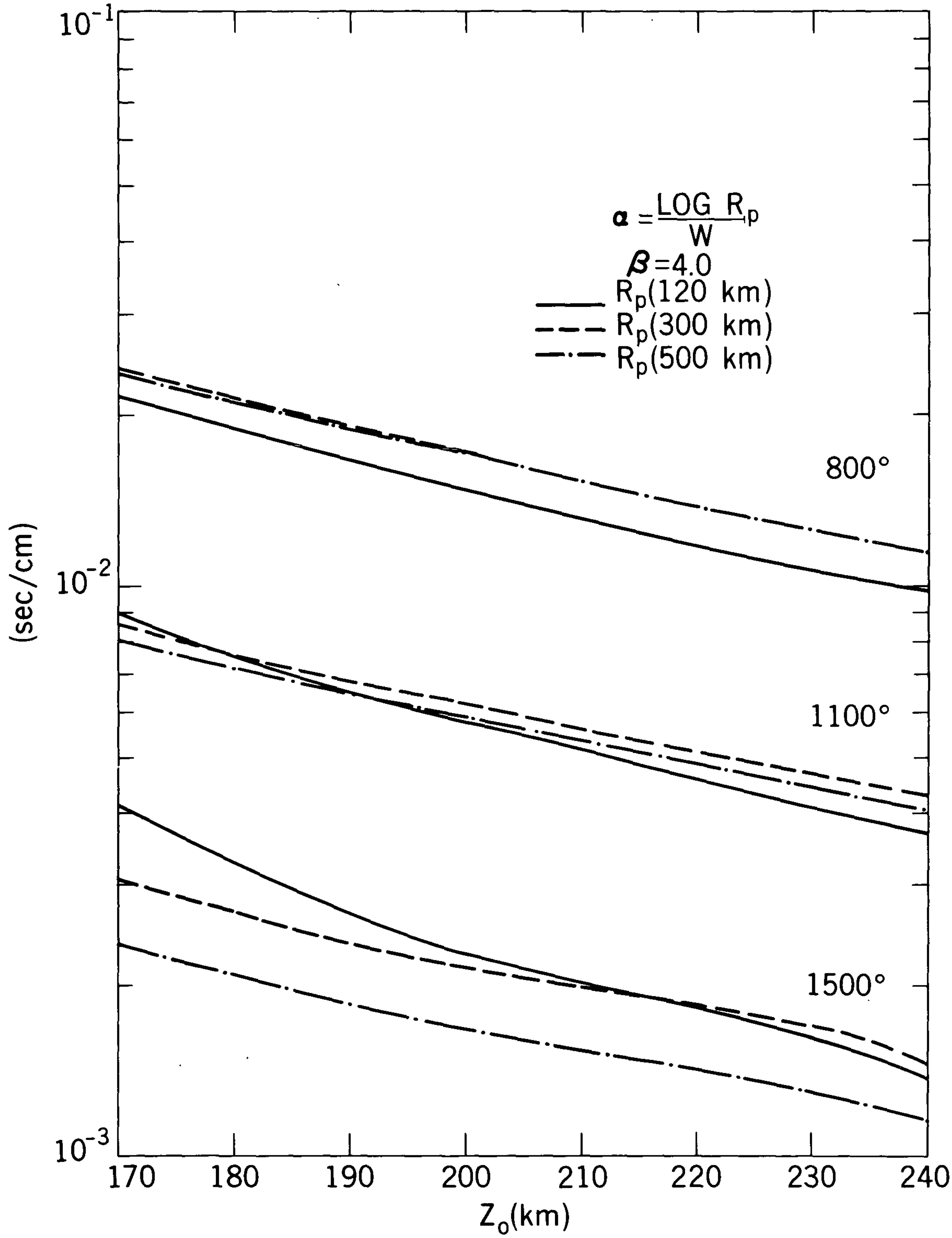

Figure 49. α versus Z_0 for $\beta = 4.0$ and low, medium and high solar activity.

temperatures and $\beta = 1.8$ and 4.0. Again, the low altitude enhancement is evident as the wind height drops, particularly at higher exospheric temperatures. The quantity $\alpha(Z_0, T_\infty)$ is useful also as a parameter for comparing calculated results with observations; given a measure of the pole-to-pole variation (e.g. from satellite measured densities), wind fields consistent with this variation can be calculated from the relation

$$W = \alpha(Z_0, T_\infty) \log R_p.$$

The family of wind fields calculated in this manner for a pole-to-pole ratio of 10 are shown in Figure 50 for $\beta = 1.8$ and 4.0 and the three exospheric temperatures.

The variation of R_p with β for an exospheric temperature of 1100°, W of 100 cm/sec and z_0 of 200 km is given in Figure 51. It can be seen that for β less than 2×10^{-7} the pole-to-pole ratios at all three altitudes increase rapidly, with the greatest increase occurring at 120 km. This increase in R_p is principally due to the large decrease in the helium density in the 100-150 km region near the summer pole, as illustrated previously for a higher exospheric temperature. The enhancement of this effect for low β is evident from the vertical and latitudinal profiles shown in Figures 52 and 53 for $\beta = 1.5$, 2.0 and 4.0×10^{-7}. The reason for the large summer pole decrease is that upward winds in this region lead to an upward flux of helium which must be supported primarily by molecular diffusion from below the turbopause. For large winds in the lower thermosphere (small values of β) this upward flux can be barely supported and the helium density in the 100-150 km region falls drastically. For example, for

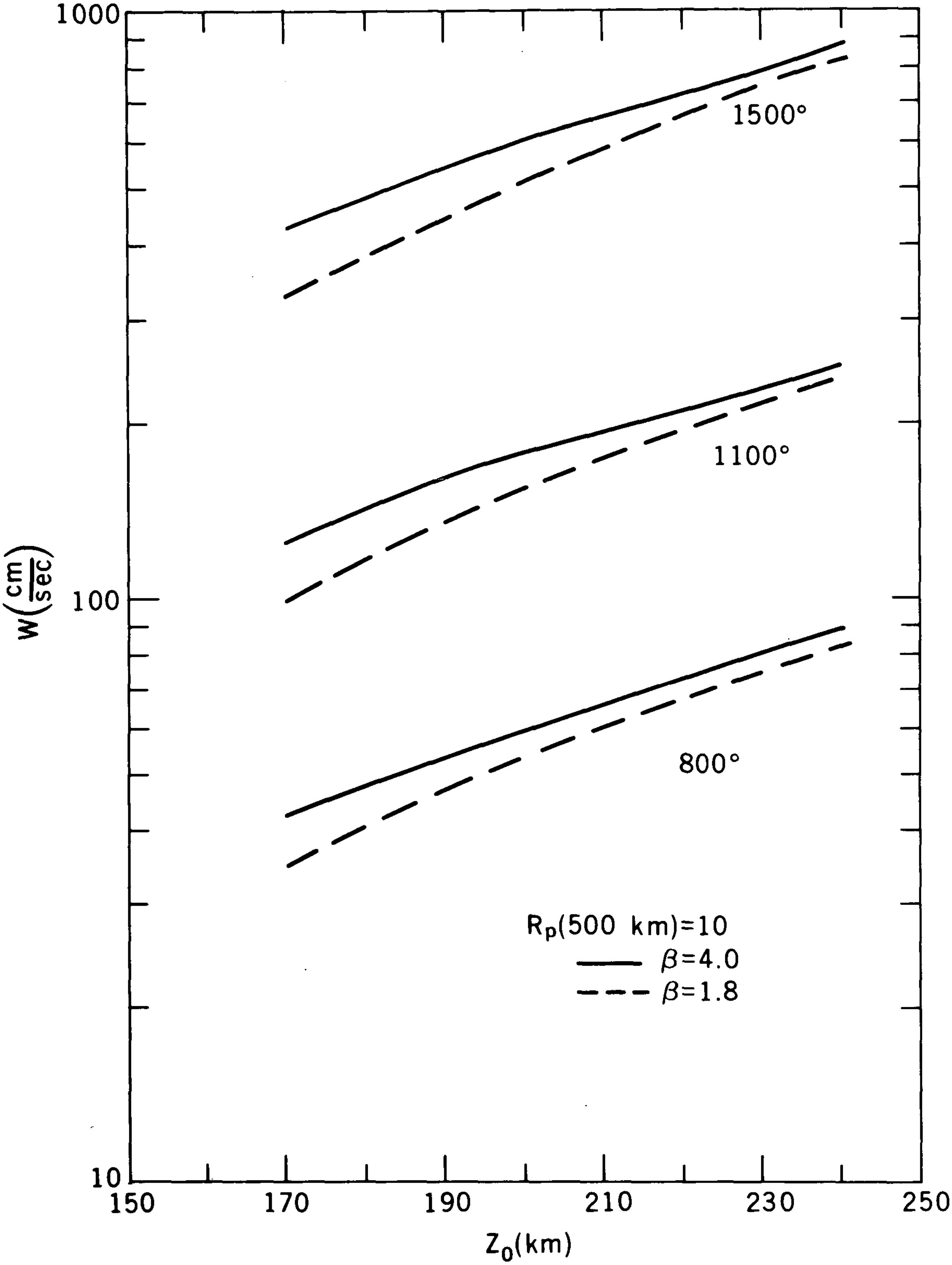

Figure 50. Vertical velocity, W, required to produce R_p (500 km) = 10 as function of Z_0 for β = 1.8 and 4.0.

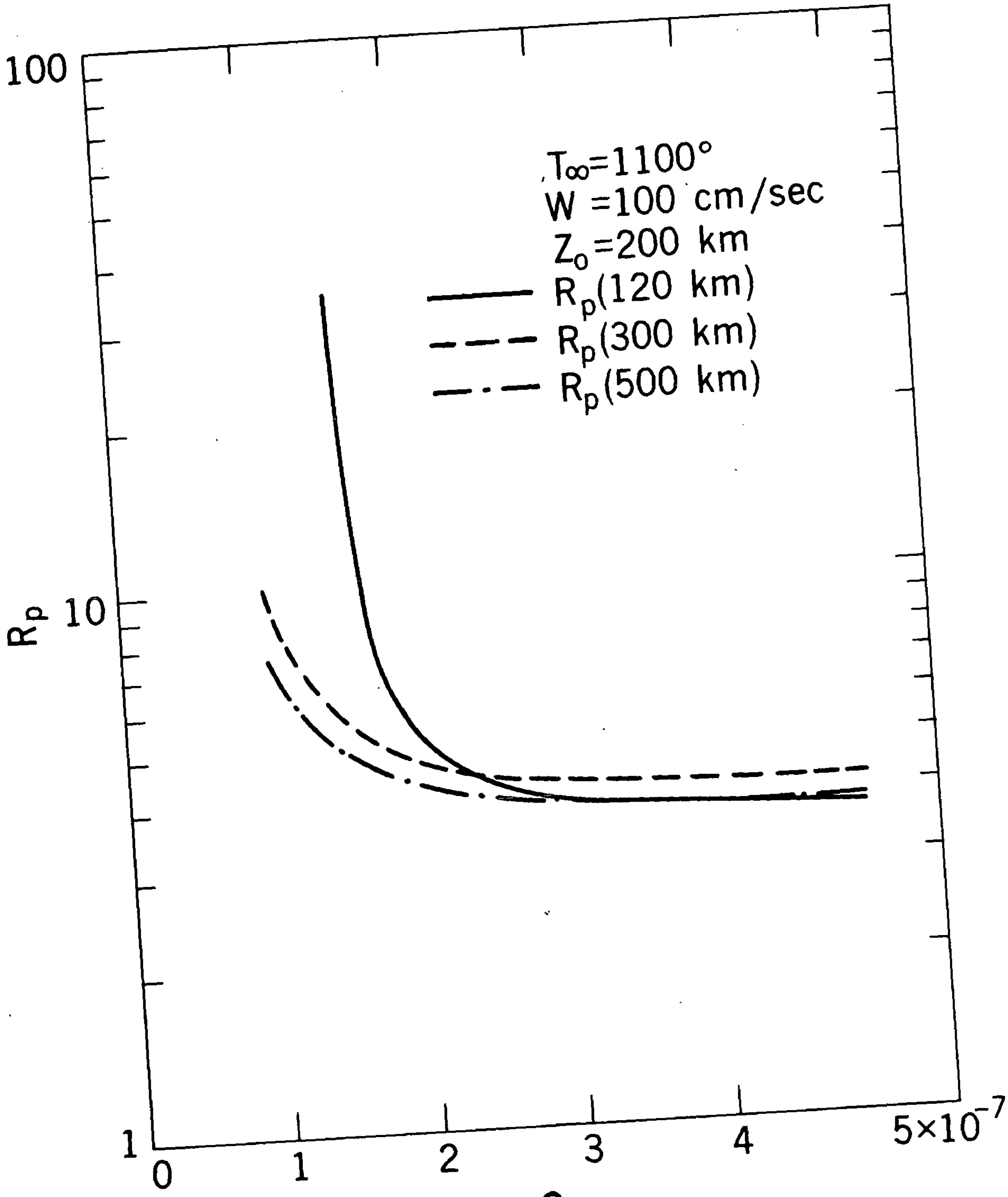

Figure 51. Pole-to-pole ratios, R_p, at 120 km, 300 km and 500 km as functions of β for T_∞ = 1100°, 100/200.

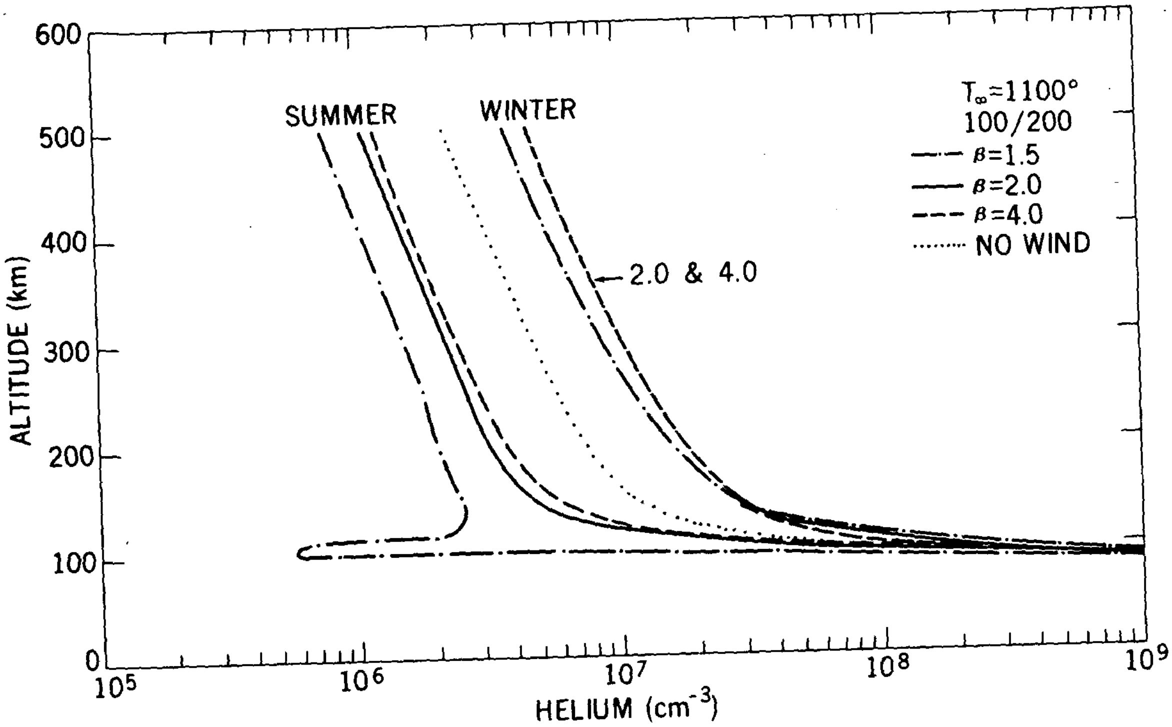

Figure 52. Helium density versus alt for $T_\infty = 1100°$, 100/200 and $\beta = 1.5$, 2.0 and 4.0.

the 100/200, $T_\infty = 1100°$, $\beta = 1.5$ case illustrated, at 100 km altitude the helium density at the summer pole is 6.08×10^6 cm^{-3}, the vertical wind is 1.7 cm/sec, the helium scale height, H, is 32.9 km, the major gas scale height, H^1, is 5.9 km and the molecular diffusion coefficient, D, is 1.32×10^6 cm^2 sec. This leads to an upward helium flux of

$$nv \left(\frac{H}{H^1}\right) = 4.7 \times 10^7/\text{cm}^2\ \text{sec}.$$

The maximum upward flux which can be supplied by molecular diffusion is obtained by setting the eddy diffusion coefficient equal to zero (see Johnson and Gottlieb, 1970):

$$\Phi = Dn \left[-\frac{7}{H}+\frac{1}{H}\right] = 6Dn/H = 1.46 \times 10^7/\text{cm}^2\ \text{sec}.$$

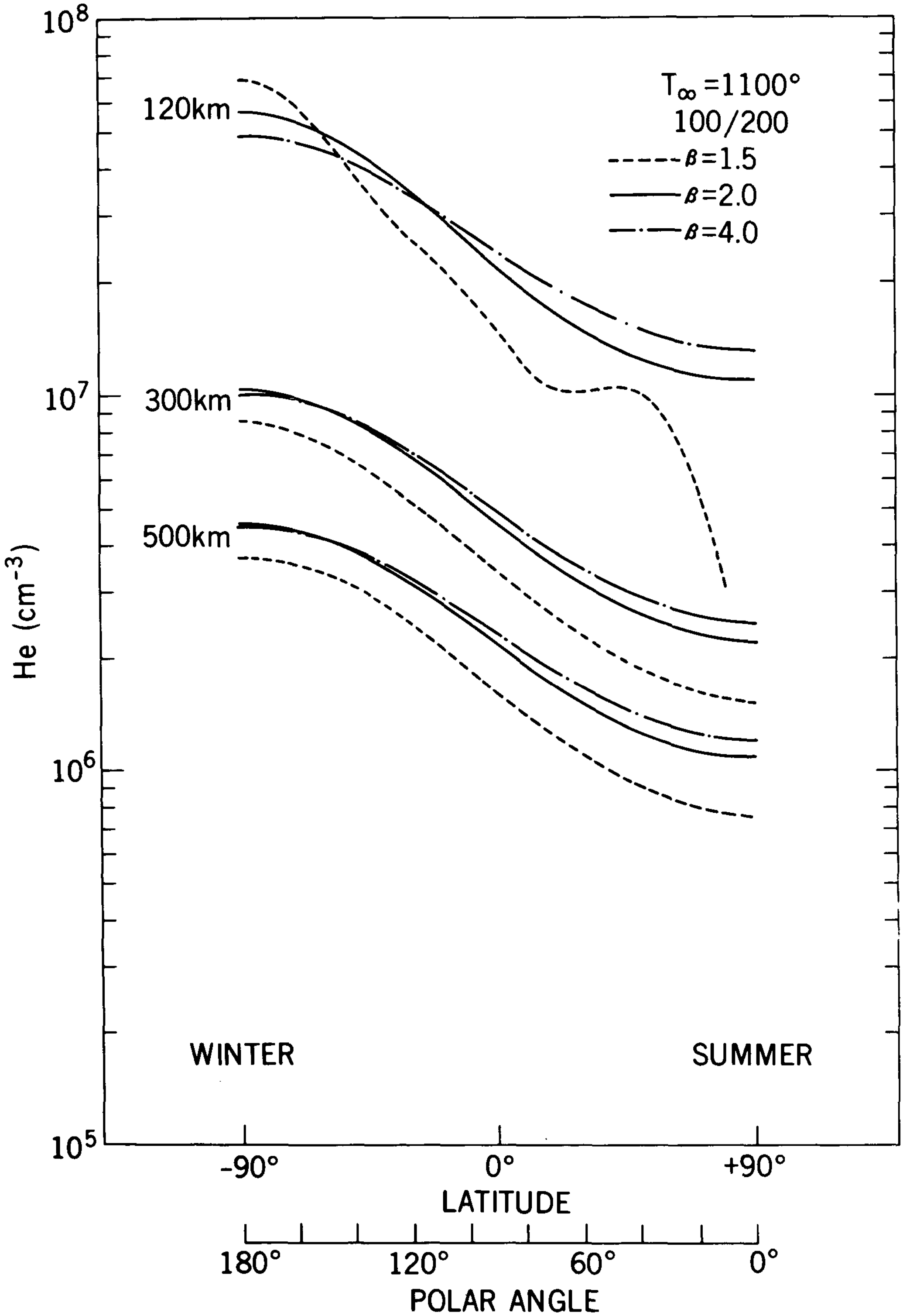

Figure 53. Helium density at 120 km, 300 km and 500 km as function of latitude for T_∞ = 1100°, 100/200 and β = 1.5, 2.0 and 4.0.

The difference between these fluxes must be supplied by transport down from the exosphere, and when this mechanism cannot provide sufficient helium the density falls to very low values. For the $\beta = 1.5$ case in Figure 52 the helium flux is downward above 121 km, reflecting the replenishment resulting from exospheric transport. The sharp decrease between 90 and 120 km is due to the limitation on flow imposed near the turbopause: (Under these conditions the calculated densities become essentially meaningless. These densities result from differences between large numbers, where machine roundoff errors and numerical integration errors combine to invalidate the result).

There is little cahnge in R_p at any altitude when β is increased above 3. These high β wind systems are significant only at the higher altitudes and are characterized by a relatively strong return flow in the middle thermosphere. The variation of R_p with β shown in Figure 51 is typical of the wind systems studied, varying only in detail for different values of W, Z_0 and T_∞.

C. Comparison with Observations

1. Satellite Data: Latitudinal Profiles

Figure 1 gives the latitudinal distribution of helium near solstice as measured by the mass spectrometer flown on OGO-6 and normalized by the Jacchia (1965) model atmosphere to eliminate the effect of varying altitude during the measurement (Reber, et al., 1971). A different method of eliminating the altitude effect is now being employed which has the advantage of greatly reducing the sensitivity to the atmospheric model used. This technique utilizes only the exospheric temperature (from Jacchia, 1965) and the scale height corresponding to this temperature to extrapolate the component density to a common altitude.

For helium the measurements generally lie between 400 km and 600 km altitude, so reducing the data to 500 km requires an extrapolation over less than half a scale height. Data corresponding to the same measurements as those in Figure 1, but reduced to 500 km are shown in Figure 54; this format will be used for the bulk of the comparisons with the calculated distributions.

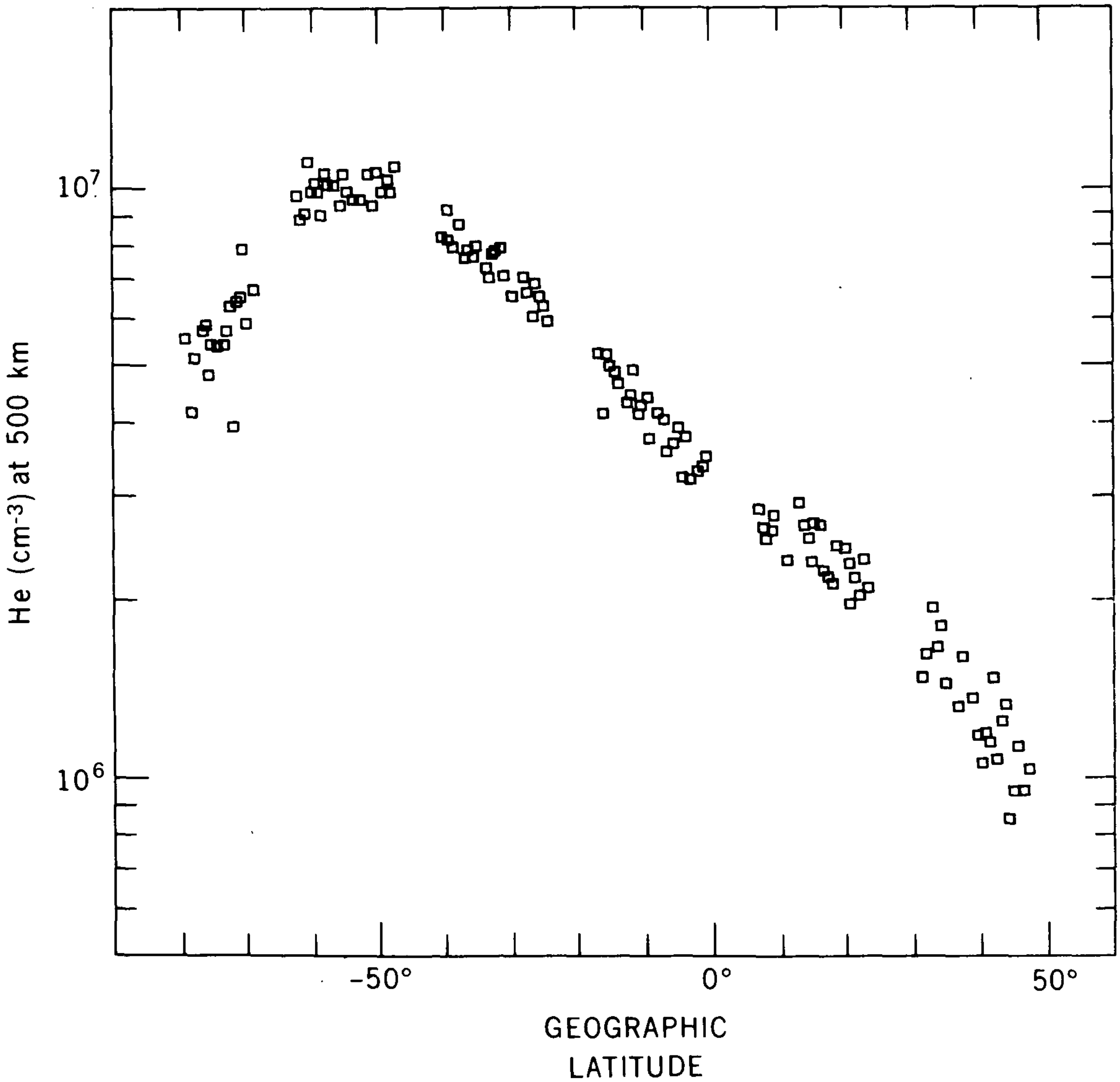

Figure 54. Helium density measured from OGO-6 satellite extrapolated to an altitude of 500 km versus geographic latitude. These data correspond to those shown in Figure 1 taken 7 June 1969 on orbit 24.

The solstice data referenced above indicate a density peak in the winter hemisphere which varies from -50° to -70° geographic latitude. This is not consistent with the results of the calculations presented so far, which indicate a cosine-like latitudinal variation, effectively mirroring the simple wind field assumed. Subsequent analysis of data from the same experiment (during times when perigee was near the poles) implies the existence of a persistent heat source in both polar regions, even during periods of relatively low geomagnetic activity (Hedin, et. al., 1970; Reber and Hedin, 1971). This postulated heat source is deduced from localized enhancements in the density of molecular nitrogen (consistent with a temperature increase), accompanied by depletions in the density of helium (consistent with a rising column of air). The result of this polar heating is superimposed on any large scale circulation system and it effectively reduces the helium density in its region of influence. Thus, the direct comparison of the calculated helium distributions with the OGO data should be made with by this polar phenomenon in mind.

The comparison of data from two OGO-6 orbits with the calculated results from two wind systems, chosen to match the measurements, is shown in Figure 55. The error bars on the measurements reflect the scatter in the data, while the difference in location of the density peak between the two orbits is clearly seen. The wind cells which are characterized by different altitudes, amplitudes and β's, effectively reproduce the measurements between 70° latitude in the winter hemisphere to 50° in the summer. The pole-to-pole ratio at 500 km associated with these wind systems is approximately 18; the full family of wind fields which yield the same R_p is shown in Figure 56 for $\beta = 1.8$ and 4.0, and Z_0 between 170 and 200 km.

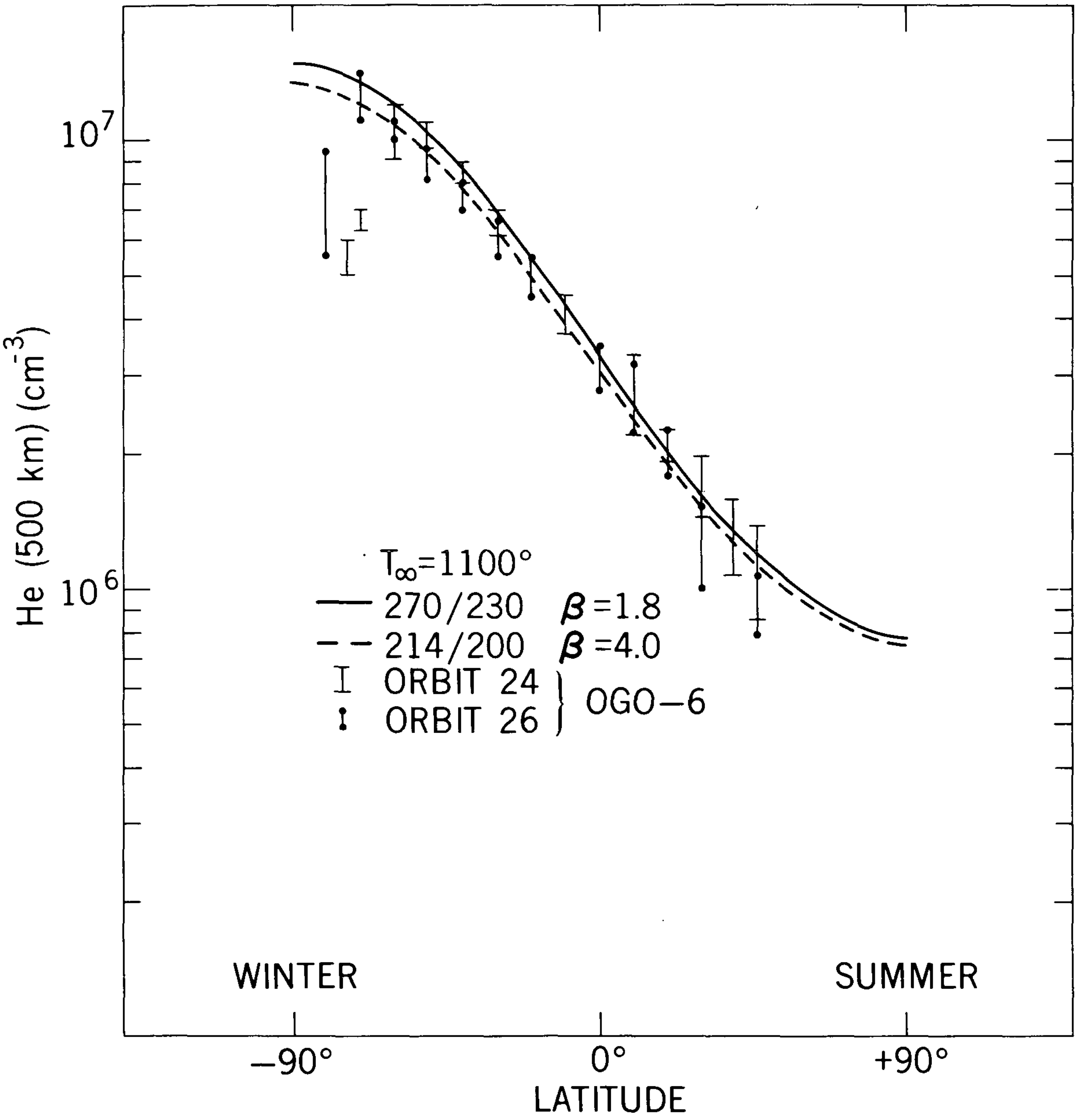

Figure 55. Data from orbits 24 and 26 of OGO-6 extrapolated to 500 km and calculated results using the wind fields 270/230, β = 1.8 and 214/200, β = 4.0. An exospheric temperature of 1100° was used in the calculation corresponding to the average daily temperature for the time of the measurements.

As Z_0 increases, the distinction between the two values of β decreases, so that for Z_0 greater than 230 km there is less than a 7% difference in the high altitude wind speed necessary to generate the given value of R_p. Reference to Figure 11 indicates that as Z_0 increases the value of β necessary to induce a

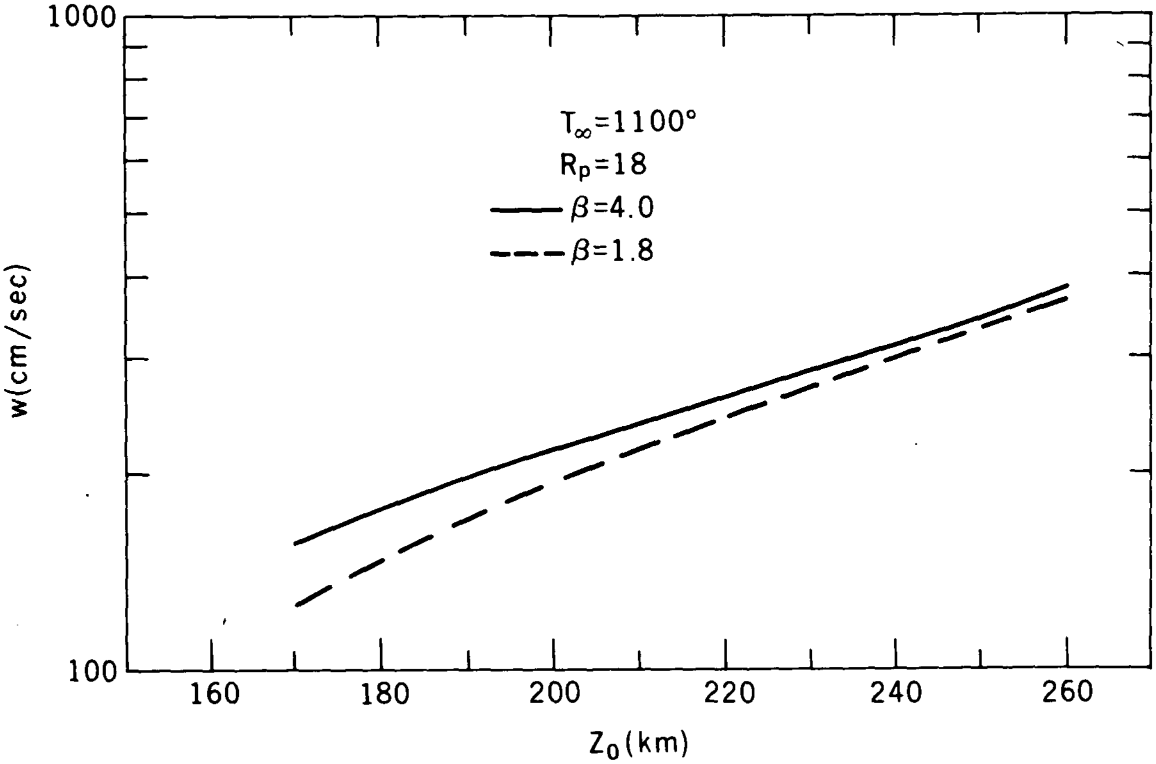

Figure 56. Vertical wind speed required, as a function of Z_0, to produce pole-to-pole ratio of 18 for helium at 500 km. This value of R_p best fits the data from the OGO-6 mass spectrometer.

return flow in the thermosphere decreases, with the result that both the wind systems shown in Figure 55 share the common feature of a fairly intense lower thermospheric return flow. Conversely, lowering Z_0 and β while maintaining a given value of R_p at 500 km has been shown to result in an extreme decrease in helium density near the summer pole in the 100-200 km altitude region, as well as to decrease the altitude of the return flow to below 80 km. Since rocket measurements do not indicate such low values for helium in the summer hemisphere, it is strongly suggested that the vertical wind profile be consistent with a return flow in the thermosphere. Figures 57 and 58 give the vertical profiles of the horizontal and vertical components of the wind systems used for the calculations shown in Figure 55. It is seen that the maximum horizontal velocity at

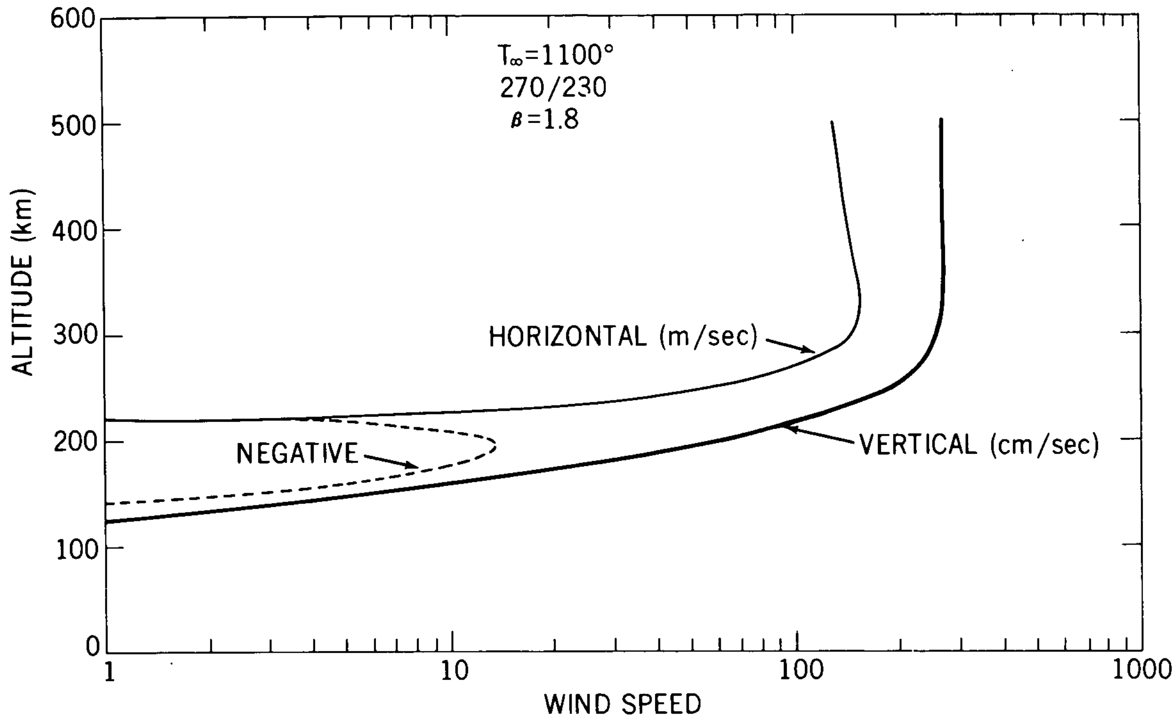

Figure 57. Vertical and horizontal wind profiles for 270/230, $\beta = 1.8$, $T_\infty = 1100°$. The region labeled negative refers to flow from the winter to the summer hemisphere.

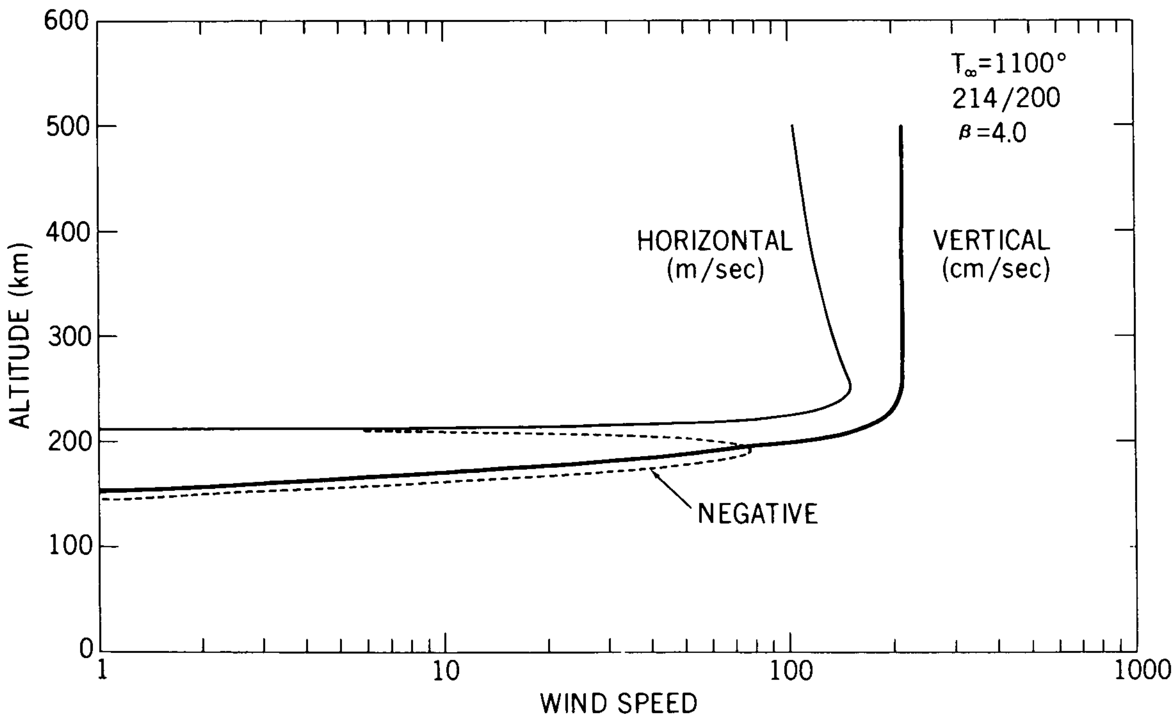

Figure 58. Vertical and horizontal wind profiles for 214/200, $\beta = 4.0$, $T_\infty = 1100°$.

the equator is about 150 m/sec for both systems; their main differences lie in the intensity of the return flow near 200 km and the vertical velocities below 180 km.

The latitudinal variation at 500 km for $R_p = 18$, $\beta = 1.8$ and 4.0 is shown in Figure 59 and 60 for a number of wind cell amplitudes and altitudes. It will be noticed that increasing Z_0 increases the absolute value of the helium density, with a 10 km change in Z_0 resulting in a 10% to 25% change in density. Assuming that the eddy diffusion coefficient is as determined from equinox data, the absolute helium density provides a constraint on the allowable wind systems to explain the solstice measurements. Thus, not all the wind cells parameterized in Figure 56 for R_p (500 km) = 18 are equally consistent with the data.

Enhancing the effect of the vertical wind in the 100 km altitude region, either by decreasing Z_0 or decreasing β (as shown in Figure 61), results in lower helium densities. Winds in this region can be thought of as turbulence, and the reaction to a wind cell is similar to that of increasing the eddy diffusion coefficient: they both decrease the density of a light gas in the thermosphere. That this is running counter to the overall result of a wind cell whose effect is confined to the upper thermosphere can be seen by considering that the helium density at 500 km for the "no wind" case is 2.2×10^6. This value is exceeded at the equator by as much as a factor of three for the wind cells considered here. The "pumping" action taking place – transporting helium up into the thermosphere by the wind system – may be seen by reference to Figures 62 and 63, the latitudinal and vertical profiles of helium associated with a circulation cell when only the amplitude of the wind is varied. Increasing the wind speed

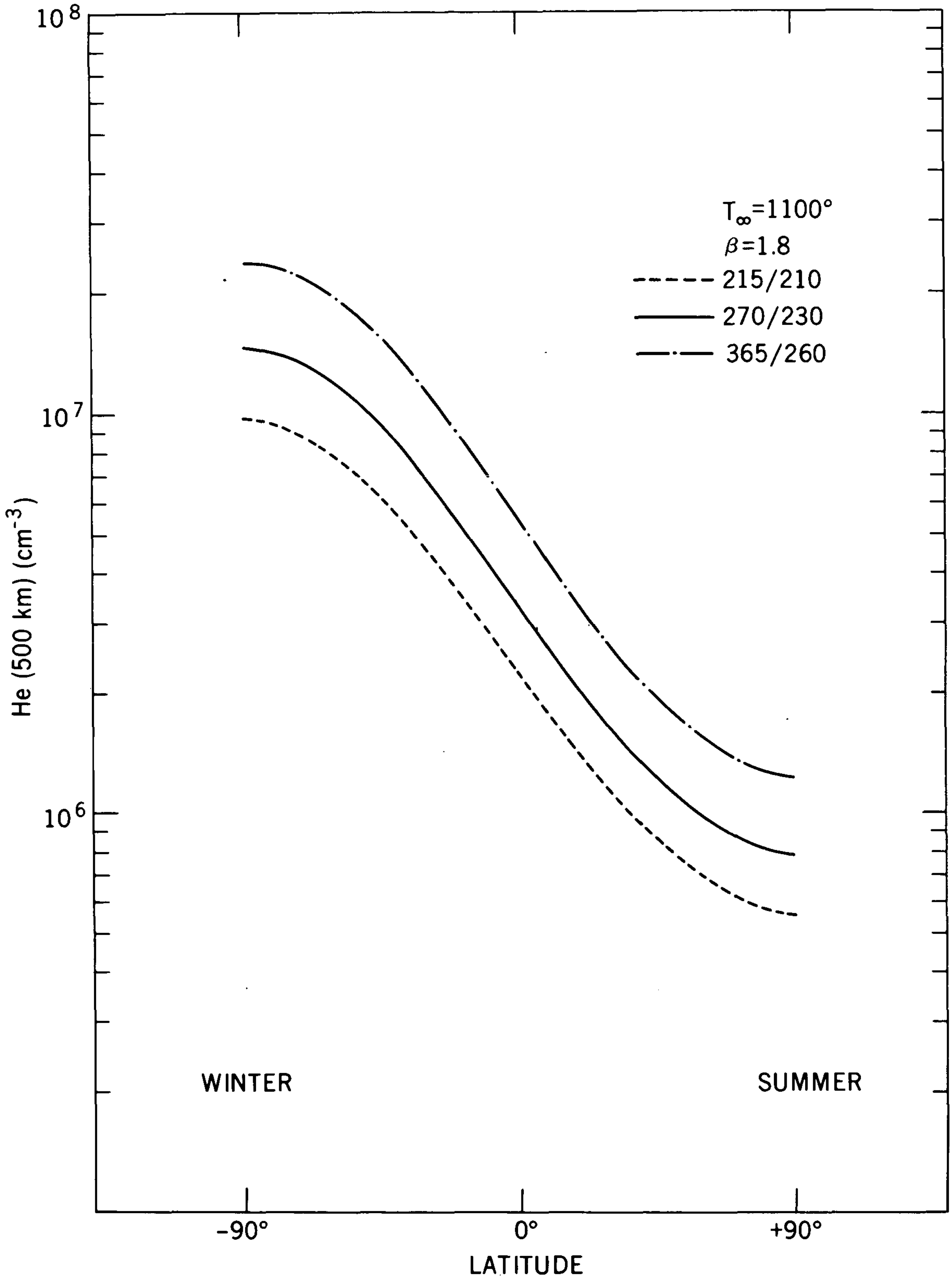

Figure 59. Helium density at 500 km versus latitude for $T_\infty = 1100°$, $\beta = 1.8$ and 215/210, 270/230, and 365/260. These wind systems all produce nearly the same R_p (500 km), but the absolute values differ by more than a factor of two.

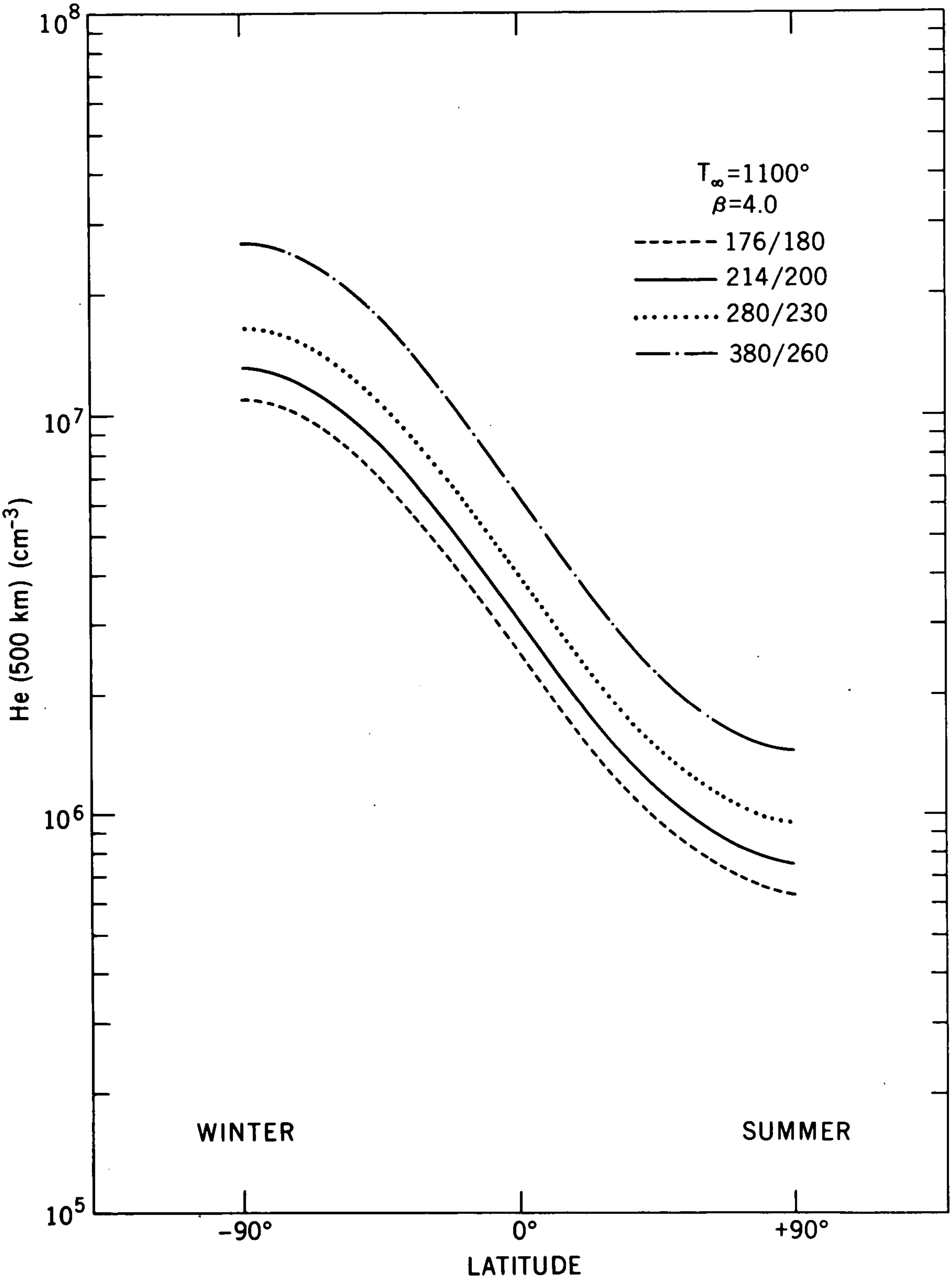

Figure 60. Helium density at 500 km versus latitude for $T_\infty = 1100°$, $\beta = 4.0$ and 176/180, 214/200, 280/230, and 380/260.

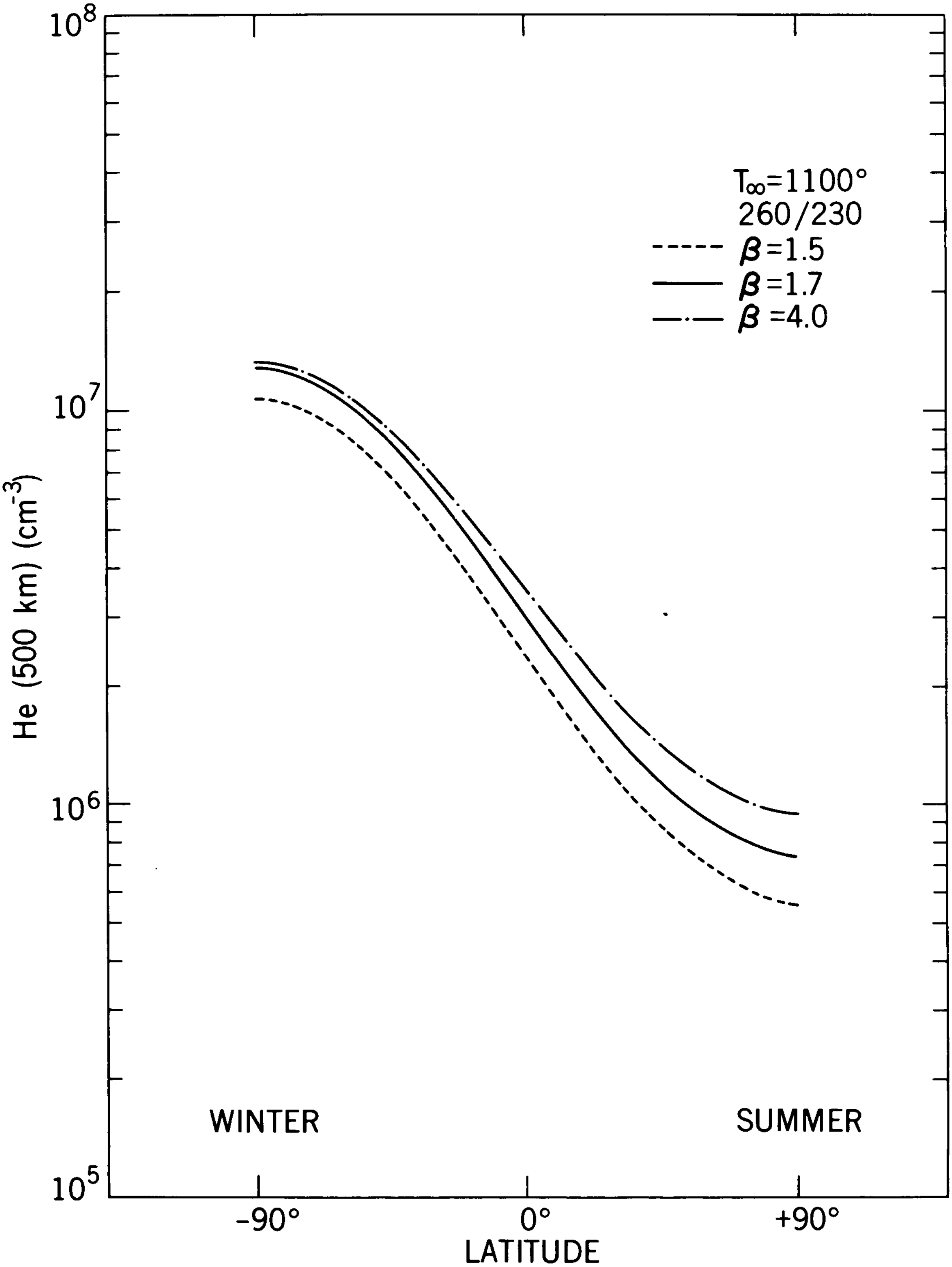

Figure 61. Helium density at 500 km versus latitude for $T_\infty = 1100°$, 260/230, and $\beta = 1.5$, 1.7, and 4.0.

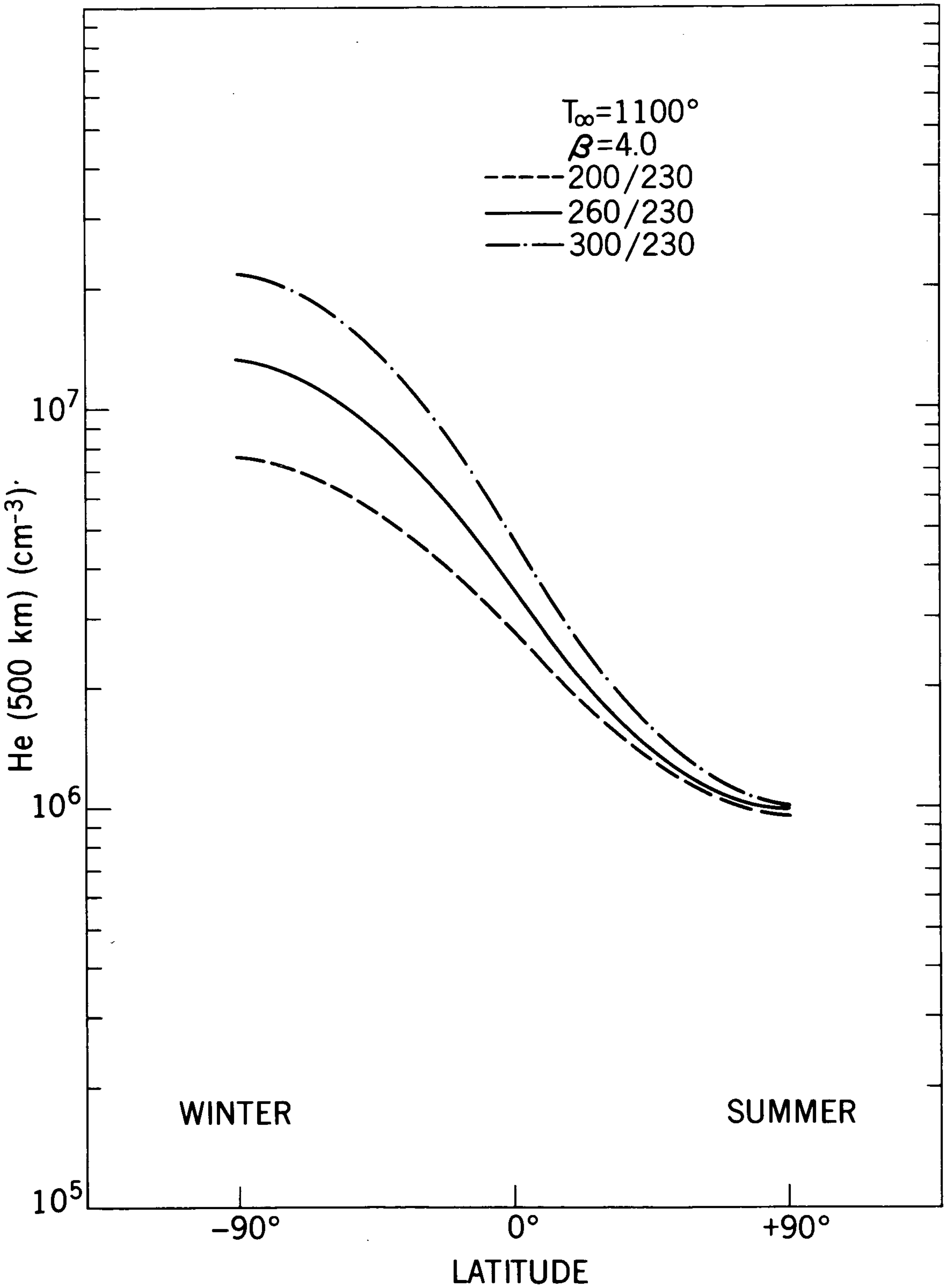

Figure 62. Helium density at 500 km versus latitude for T_∞ = 1100°, β = 4.0, and 200/230, 260/230, and 300/230.

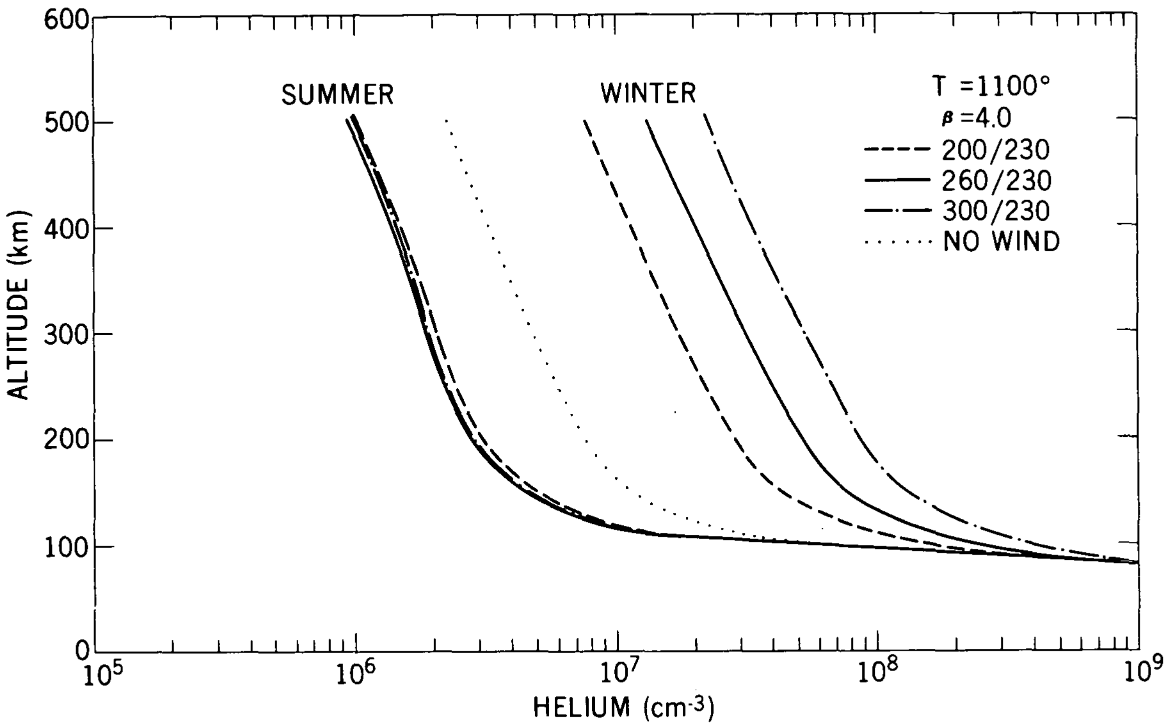

Figure 63. Helium density as a function of altitude for the same conditions as Figure 62.

primarily increases the density in the winter hemisphere while the density in the summer hemisphere is relatively unchanged. The diffusion limitation exhibits itself in both hemispheres: the vertical profiles at the summer pole are nearly identical up to 150 km, while at the winter pole there is a "piling up" of helium which is transported in by the wind and cannot readily diffuse down below 150 km.

1. Rocket Data: Vertical Profiles

One of the two main conclusions from the many determinations of helium density by rocket-borne mass spectrometers is that the lower thermosphere exhibits a similar seasonal variation to that observed at higher altitudes from satellites. The other, perhaps more significant, result is that helium often is not in static diffusive equilibrium with the major gases in the altitude region from 120 to 250 km. On the contrary, in nearly all the measurements reported to date by the group at the University of Minnesota (e.g. Hedin and Nier, 1966; Krankowski, et al., 1968) and one by Goddard Space Flight Center (Cooley and Reber, 1969) the altitude profile of helium has indicated a lower scale height, H_{He}, than would be consistent with the temperature deduced from the scale heights of the other gases. The single exception is the winter measurement at Fort Churchill reported by Hartmann, et. al. (1968; see also Müller and Hartmann, 1969) which indicated a high density and a nearly static scale height. A number of the Minnesota results have been summarized and interpreted by Kasprzak (1969) as due to an upward flux of helium, perhaps initiated by lateral transport in the exosphere (McAfee, 1967). Reber (1968) suggested that the relatively long diffusion times in the lower thermosphere coupled with a temperature change or variation in turbopause level might be responsible for the low scale heights. None of the mechanisms proposed, however, indicate why the flux is predominantly upwards, or equivalently, why the scale heights are generally lower than expected.

Reference to Figures 64 through 68 indicates the behavior of the scale height of helium under the influence of a variety of wind cells. Figure 64 shows the summer profiles up to 500 km for β from 1.5 to 4.0 compared with the static profile; it is seen that all the scale heights approach the static value at high altitude, even though there is as much as a factor of two difference between 200 and 300 km. Figures 65 and 66 emphasize the lower thermosphere summer and winter profiles for the same family of wind systems, while Figures 67 and 68 give similar profiles for a set of wind systems (both for β = 4.0) which produces

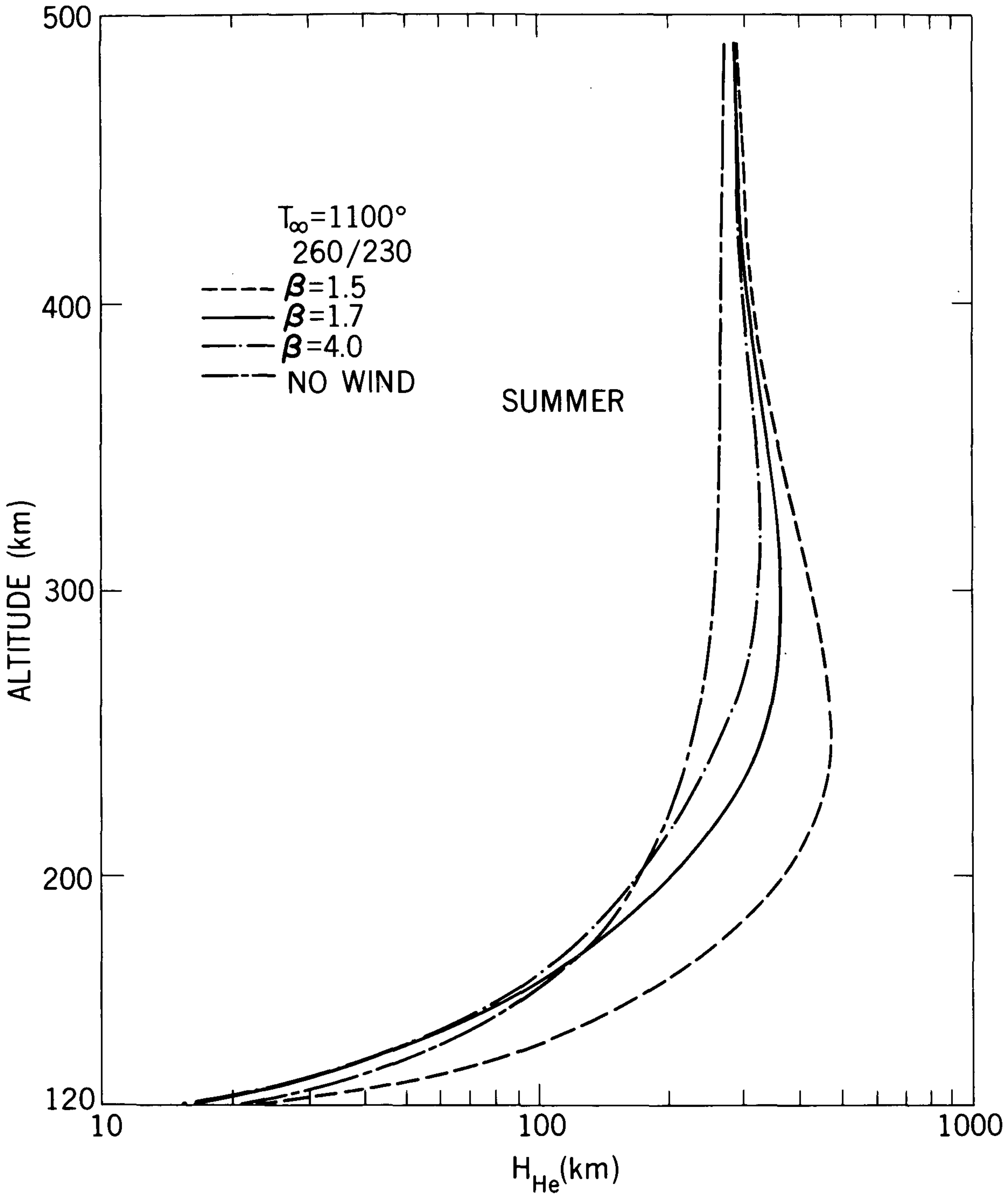

Figure 64. Helium scale height, H_{He}, as a function of altitude at the summer pole for $T_\infty = 1100°$. The winds represented are 260/230, $\beta = 1.5$, 1.7 and 4.0; also shown is the scale height in the case of no wind.

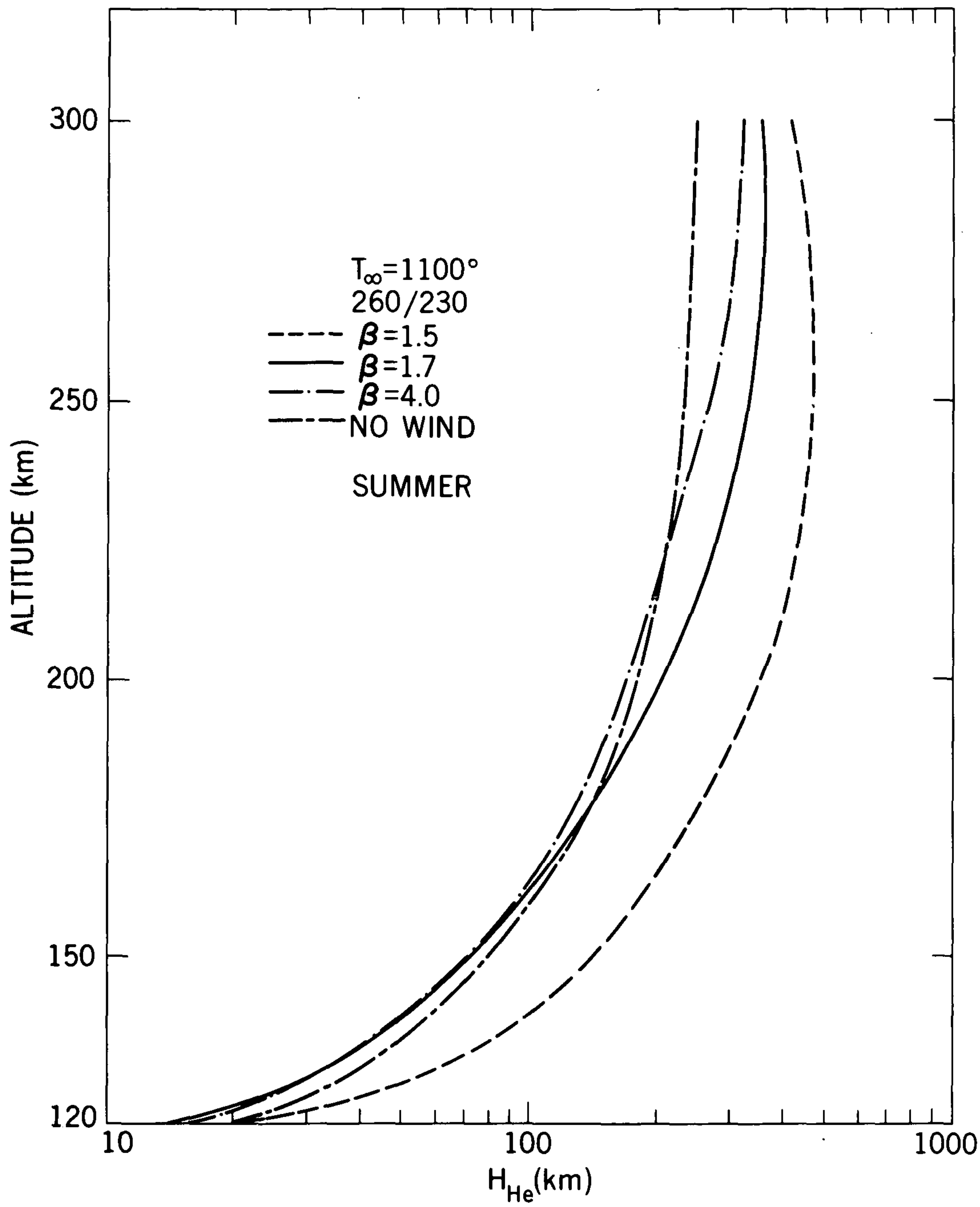

Figure 65. Same as Figure 62 with emphasis on the region below 300 km.

pole-to-pole latitudinal ratios consistent with satellite measurements, but which have different altitudes and amplitudes.

The dynamic summer profiles exhibit a lower scale height than the static scale height for $\beta \geq 1.7$ and altitudes less than 170 km. As the value of β is increased (raising the effective altitude of the cell), the altitude of lower scale

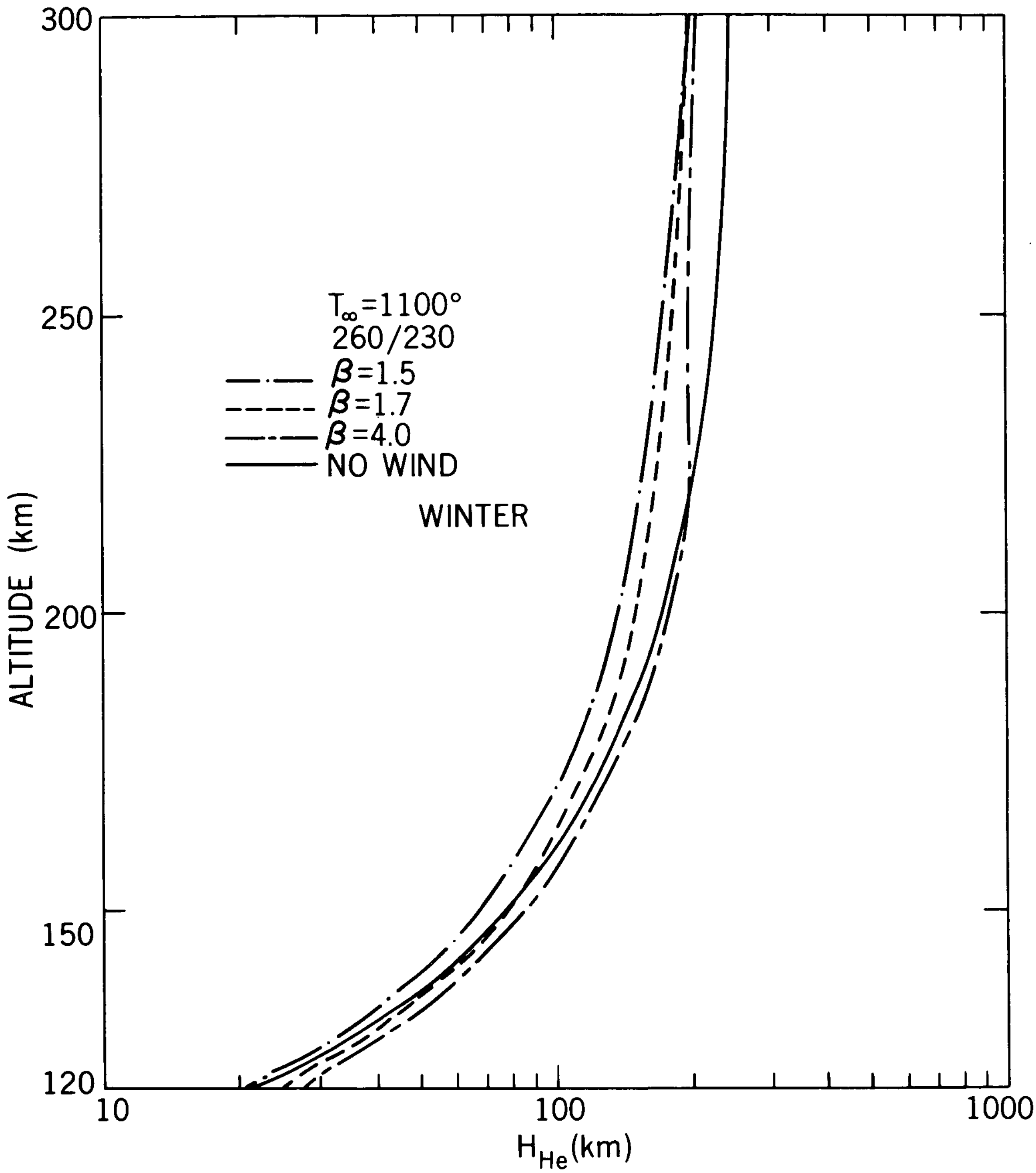

Figure 66. The winter pole scaleheights corresponding to the wind systems of Figures 62 and 63.

height is also raised. For lower altitude cells (and for altitudes above about 200 km) the downward flux from the exosphere dominates the distribution and the dynamic scale heights are greater than their static counterpart. For β = 1.5 the dynamic scale height is less than the static up to 120 km, indicating the region of dominance for this particular cell.

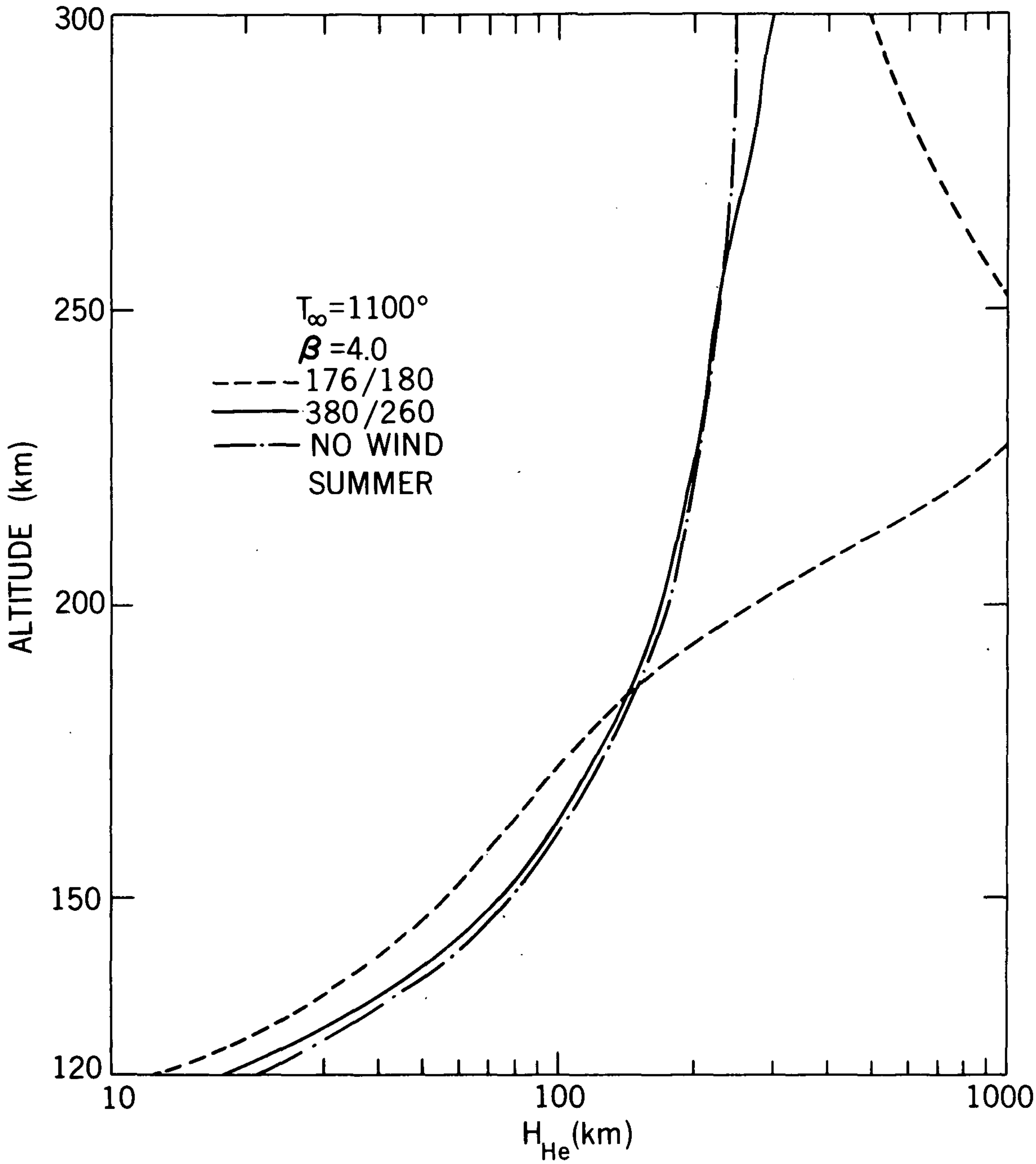

Figure 67. Helium summer pole scale heights for T_∞ = 1100°, β = 4.0, 176/180 and 380/260, emphasizing the result of lowering the dominant altitude of the wind field.

The wintertime profiles show that essentially the opposite situation prevails in a region of subsidence. Here, the cells effective to lower altitudes produce scale heights lower than static in the lower thermosphere, while higher altitude cells generate higher scale heights. At the upper altitudes all the

C2

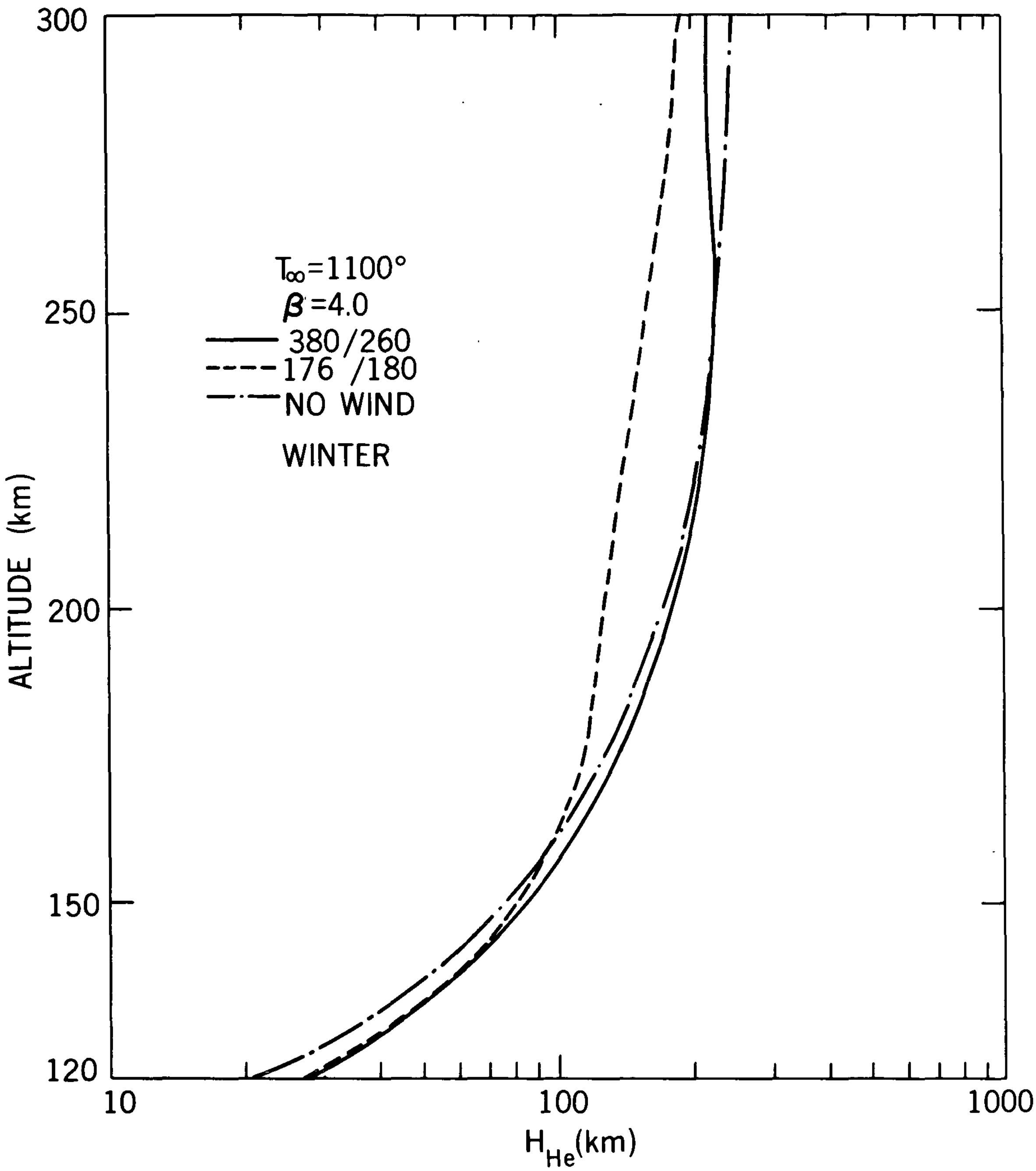

Figure 68. Helium winter pole scale heights for the conditions of Figure 65.

dynamic scale heights fall short of the static values due, once more, to the upward flux to the exosphere. This behavior is shown accentuated in Figure 69 where the scale height due to a very low altitude cell ($\beta = 1.8$, $Z_0 = 170$ km) is compared to those from higher altitude cells and to the static scale height. In

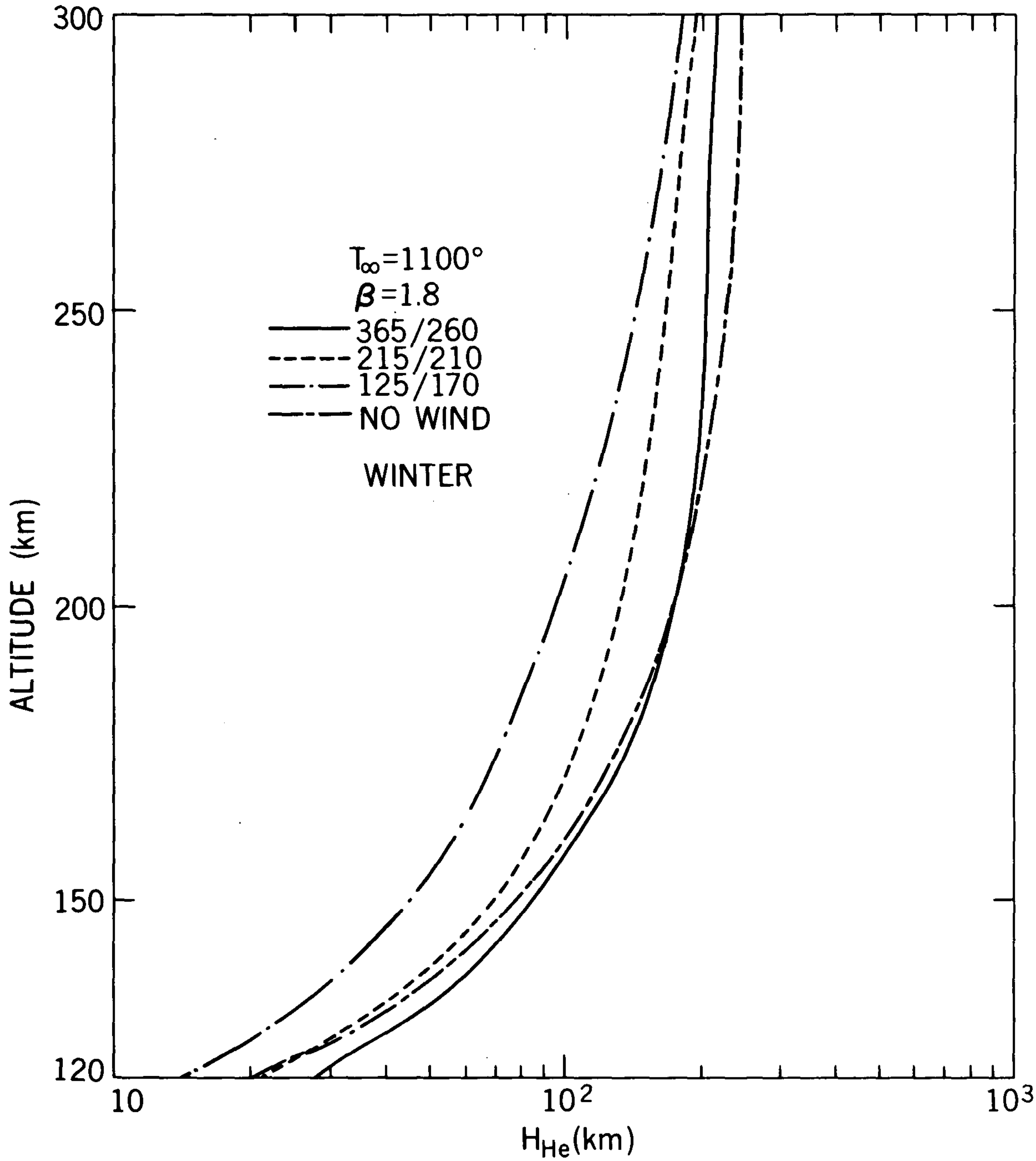

Figure 69. Helium winter pole scale heights for T_∞ = 1100°, β = 1.8, 365/260, 215/210, and 125/170.

this case H_{He} is nearly a factor of two lower than static in the altitude region from which most of the rocket data are obtained. Thus, while virtually any of the winter wind profiles considered generate helium profiles consistent with rocket measurements, these same measurements require a summer wind system which is more effective in the lower thermosphere. It is most likely that the simple, symmetric wind system considered here is not adequate, and also that there are other cells (e.g. diurnal) existing in conjunction with the seasonal cells, each independently influencing the helium distribution.

D. Time Development of Response

The evolution of the helium response to a wind system that is suddenly "turned on" was studied using time increments of three hours, twelve hours and two days. This was found necessary as use of large increments caused oscillations in the early phases of the response, while use of small increments required excessive computer time. The combined results are shown in Figures 70 through 73 for exospheric temperatures of 800°, 1100°, and 1500° using $\beta = 1.8$, and 1100° for $\beta = 4.0$. Here the helium densities at the winter and summer poles are given as functions of time for altitudes of 120, 300 and 500 km. It can be seen that there is an initial response which varies from about fifteen days for an 800° exosphere down to three days at 1500°, followed by a relatively long term density variation. In the case of all three temperatures, the latter manifests itself as a gentle increase (less than 0.6%/day) at both poles and all altitudes. It is also apparent that the wind is more effective in evoking a response at the higher altitudes as the initial phase is significantly longer at 120 km for all three temperatures, indicating that the variation is being propagated downwards.

The exact cause of the long term portion of the response is not clear, but it is apparently related to the exospheric transport (through the induced "pumping" effect discussed previously) and the relatively long time required for helium to

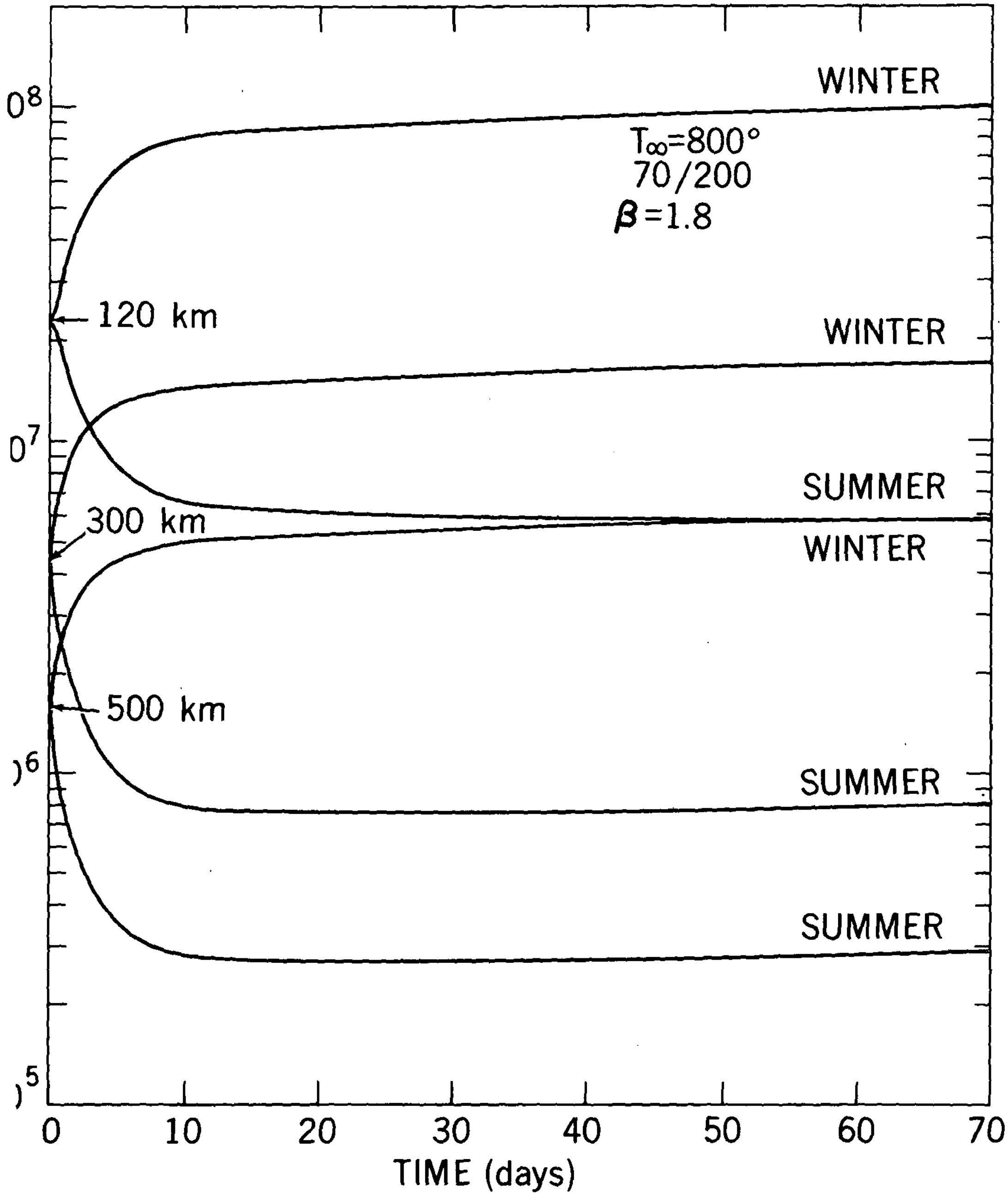

ure 70. Time development of the summer and winter pole helium distributions at 120, 300 and 500 km for low solar conditions; the 70/120, $\beta \approx 1.8$ wind is "turned on" at $t = 0$.

se up through the lower thermosphere. This phase of the response is ically less important than the initial phase, however, as it would most y be masked by shorter term variations in exospheric temperatures due to ıetic activity and the 27-day solar cycle.

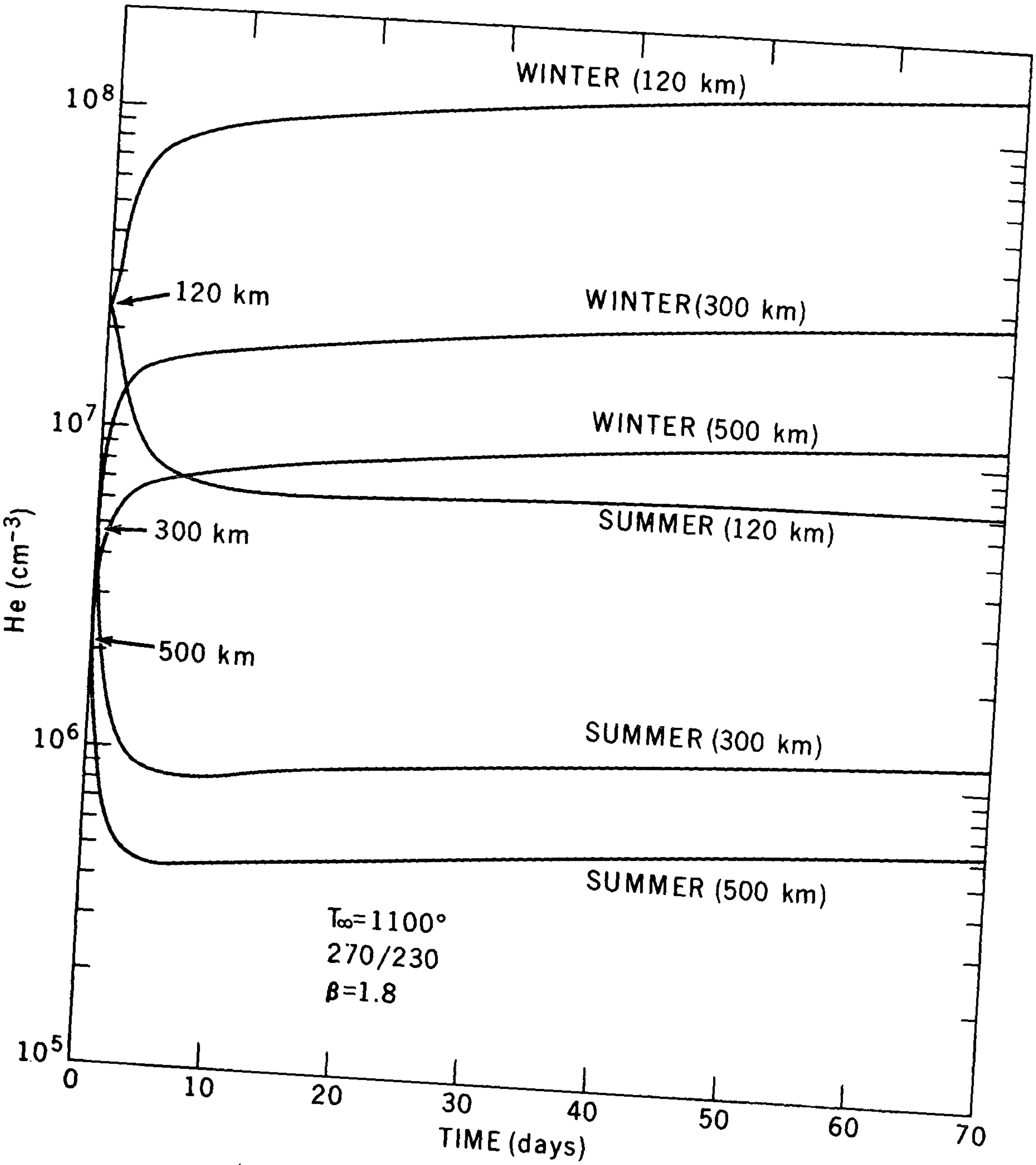

Figure 71. Time development of the summer and winter pole helium distributions for medium solar conditions; the wind field is 270/230, β = 1.8.

The primary response, particularly for average solar conditions is interesting in that it indicates the possibility of a factor of two charge at one pole in a time period of half a day. Interpreting this as a longitudinal (rather than latitudinal) phenomenon, this would imply the potential for a night time

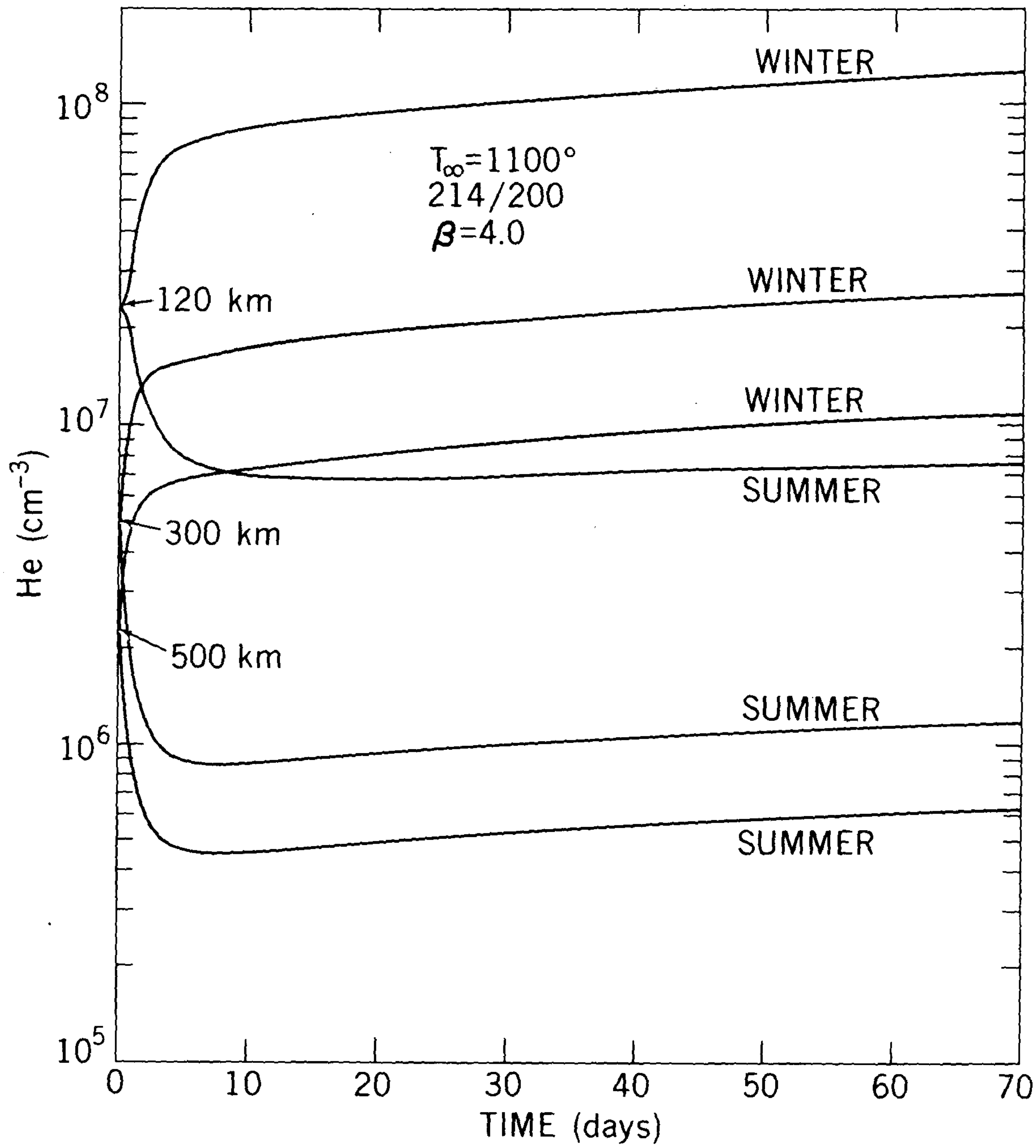

Figure 72. Time development of the helium response for medium solar conditions and a 214/200, β = 4.0 wind field.

enhancement of a factor of four over the density at the sub-solar point. The amplitude drops below this for both high and low solar cycle conditions; however, the temperature differential at high solar cycle would tend to produce a similar variation due to exospheric transport (McAfee, 1965), so the net effect might be

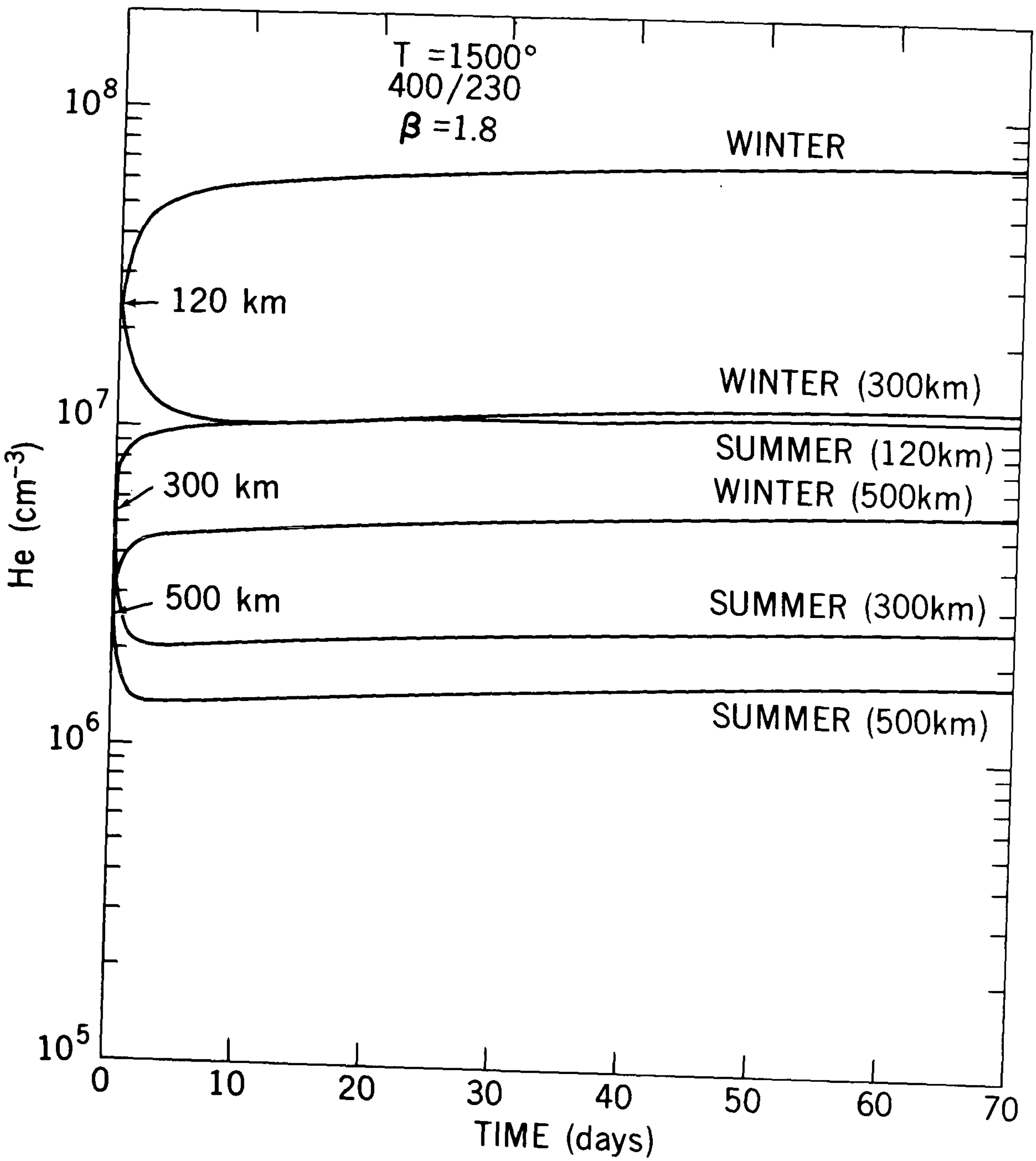

Figure 73. Time development of helium response for high solar conditions and a 400/230, $\beta = 1.8$ wind field.

equal to or larger than that at mid-solar cycle. At low solar conditions, it appears likely that less than a factor of two day-night variation could be maintained at high altitudes due to this mechanism.

E. Other Minor Species: Argon

Of the minor gases of interest after helium, argon is the most useful to study as it is also inert and it has been measured by rocket and satellite borne mass spectrometers. Also, its mass of 40 is greater than the mean mass in the lower thermosphere, so in accord with Equation 5 its response to a wind system should be opposite that of helium. In addition, due to its high mass (relative to helium) the effect of exospheric transport should be negligible.

The latitudinal variation of argon at 300 km (where it can, in principle, be measured by satellite-borne mass spectrometers) is shown in Figure 74 for the 214/200, $\beta = 4.0$ and 270/230, $\beta = 1.8$ wind systems which provided good agreement with helium measurements at 500 km (see Figure 55). The effect of the high relative mass can be seen immediately, with the densities near the summer pole higher than the winter densities by nearly a factor of four; the distributions corresponding to the two systems also compare well with each other, with less than a 4% density difference at any latitude. As the effective altitude of the vertical wind is raised, by raising β (Figure 75) or by increasing Z_0 (Figure 76), the effect on argon is to decrease the amplitude of the latitudinal variation in a nearly symmetric manner. It will be recalled that the same variation in wind field caused a general increase of the helium density at 500 km, while maintaining the pole-to-pole ratio relatively constant (see Figures 60 and 61). Thus, when simultaneous latitudinal profiles of argon and helium are available, one can in principle narrow down the family of wind fields consistent with the two distributions.

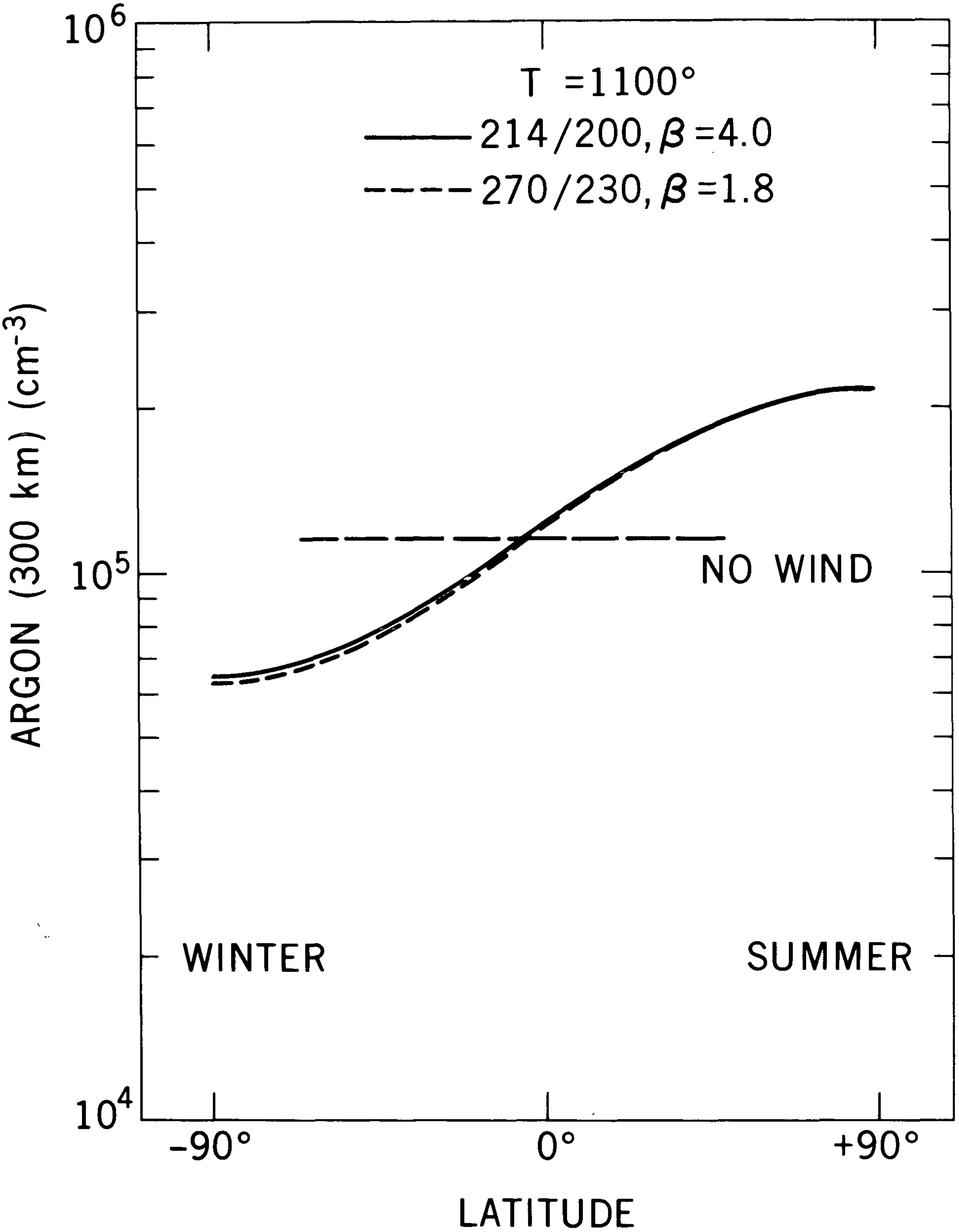

Figure 74. Argon density at 300 km versus latitude for T_∞ = 1100°, 214/200, β = 4.0 and 270/230, β = 1.8 winds. These winds give the best fit to the OGO-6 data for helium.

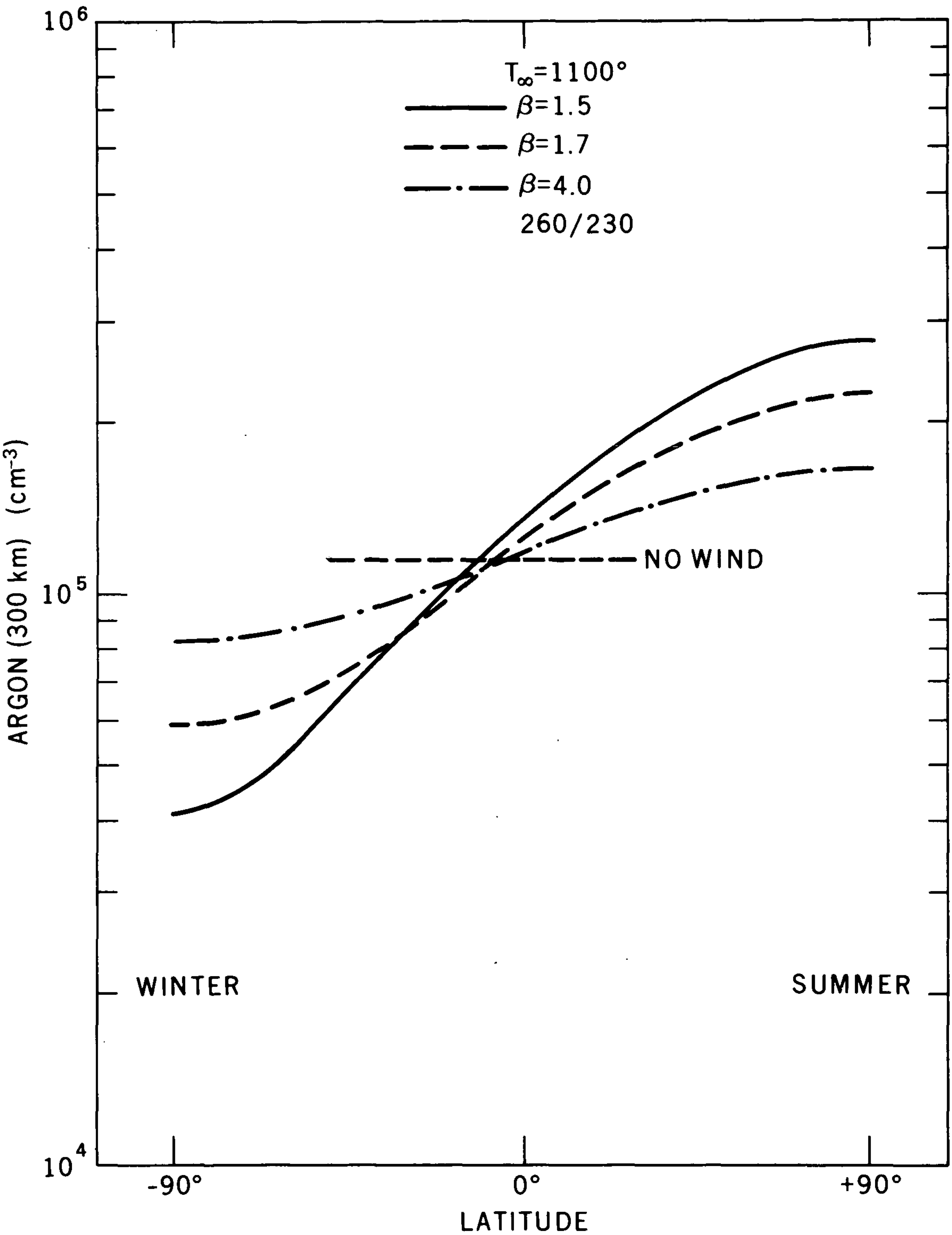

Figure 75. Argon density at 300 km versus latitude for T_∞ = 1100°, 260/230 and β = 1.5, 1.7 and 4.0.

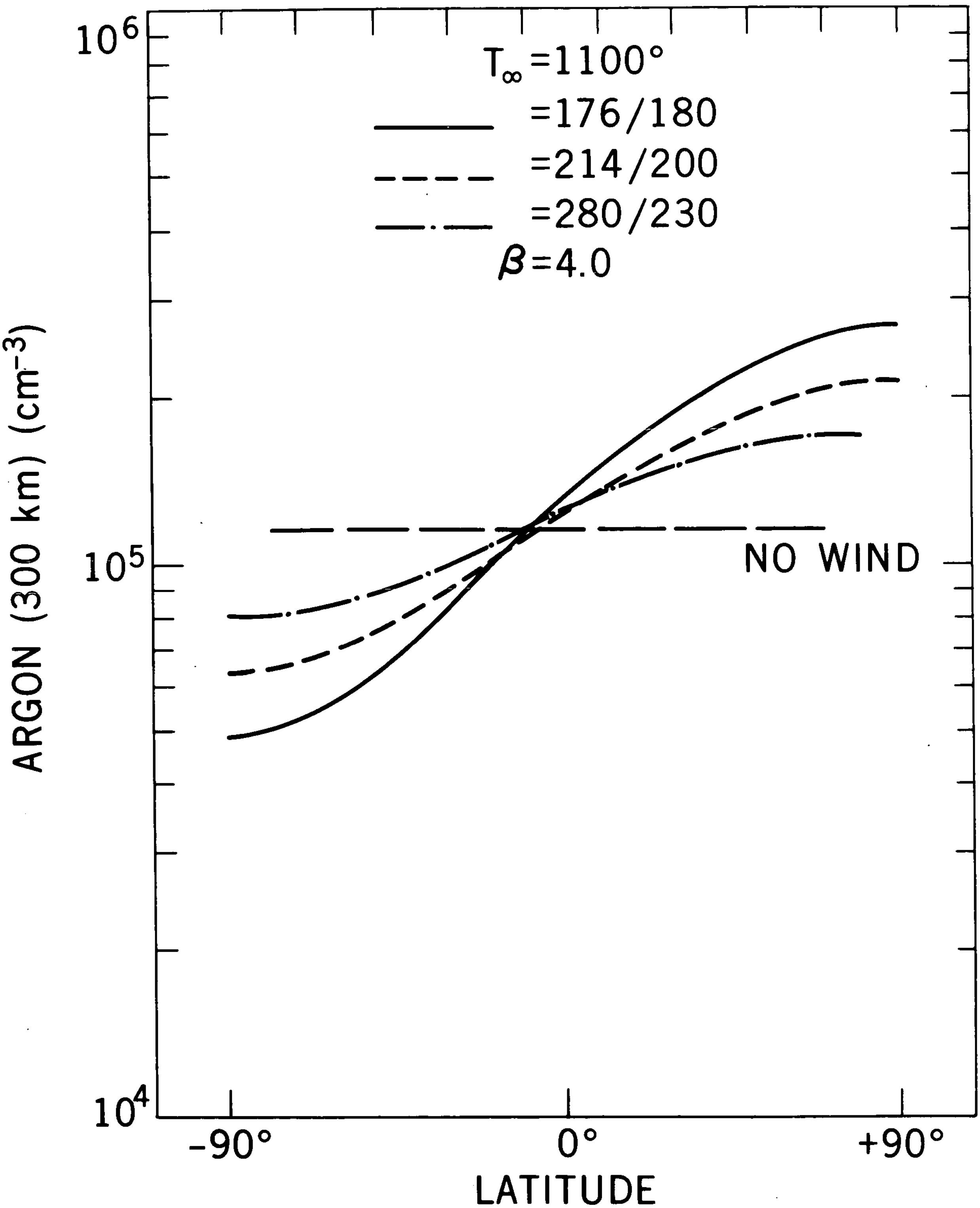

Figure 76. Argon density at 300 km versus latitude for $T_\infty = 1100°$, $\beta = 4.0$, 176/180, 214/200, and 280/230.

The insensitivity to exospheric transport can be seen in Figure 77 which shows vertical profiles for an exospheric temperature of 1500° and vertical wind speeds of 4 m/sec. Under the same conditions (see Figure 33), helium displays a distinct depression in the summer hemisphere near 200 km, with the higher altitude density enhanced by exospheric flow.

IV. CONCLUSIONS

A large scale meridional circulation system in the thermosphere (upwelling in the summer hemisphere, flowing toward and descending in the winter hemisphere) was shown to be sufficient to generate the observed enhancement of helium in the winter upper atmosphere. The increase of exospheric transport with temperature results in a smaller latitudinal variation at high solar activity

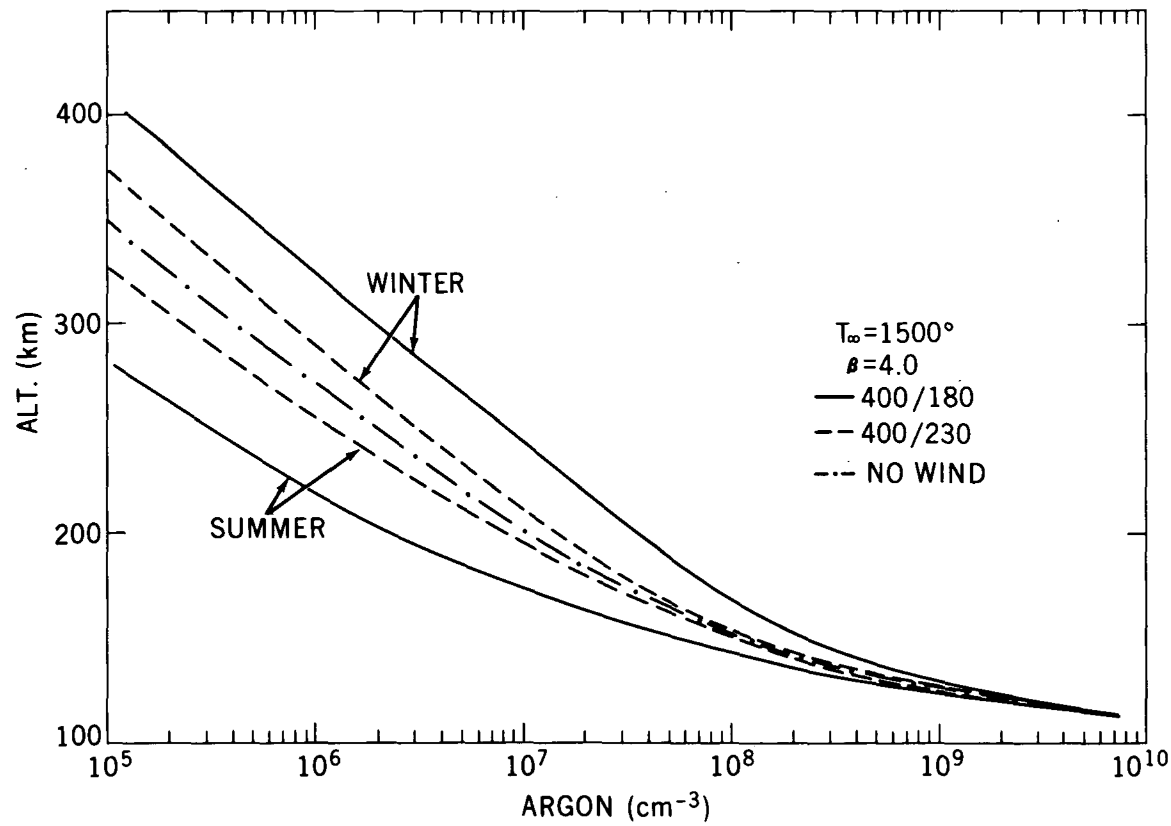

Figure 77. Argon density versus altitude for $T_\infty = 1500°$, $\beta = 4.0$, 400/180 and 400/230.

than at low activity, due to the large smoothing effect of the return flow. Horizontal diffusion in the thermosphere, however, is negligible as a smoothing agent compared to exospheric flow. On the basis of satellite-type measurements of helium alone it is impossible to distinguish between a variety of wind fields as the causative mechanism; however, wind fields consistent with the helium distribution measured by OGO-6 are characterized by vertical velocities of two to three meters per second above 200 km and horizontal velocities at the equator of one to two hundred meters per second. These are within a factor of two of the amplitudes proposed by Johnson and Gottlieb (1970) to explain the temperature in the winter thermosphere, but are 100 km higher in altitude.

Argon is affected in the opposite way from helium, being enhanced in the summer hemisphere and depleted in the winter; there is negigible effect here from exospheric transport. The calculated vertical helium profiles indicate departure from a static-diffusion profile in much the same manner as observed by rocket measurements. In order to be more consistent with observations, however, it would be necessary to disregard the simple, symmetric circulation cells used here and adopt a wind field which is effective to lower altitudes in the winter hemisphere than in the summer. By use of latitudinal data on helium and argon, in conjunction with vertical profiles of helium, it should prove possible to narrow down the number of potential wind fields causing the distributions. Disregarding photochemical effects, atomic oxygen should exhibit the same behavior as helium, but with a lower amplitude. However, since it is more temperature sensitive than helium, the wind and temperature effects tend to be self cancelling. Thus, the net effect in oxygen might well be the absence of an expected enhancement in the summer hemisphere at higher altitudes. This type of response has already been noted in the high latitude neutral gas data from OGO-6 following magnetic storms (Taeusch, et. al., 1971), where the N_2 density rises, the helium falls and the oxygen remains relatively constant.

The time response of the helium density to a wind field indicates a significant variation in less than half a day. This leads to the likelihood of a factor of two to four density enhancement at night. This, as well as the other effects discussed here, clearly indicate the need for the inclusion of dynamics in describing and studying any but the simplest of upper atmosphere phenomena.

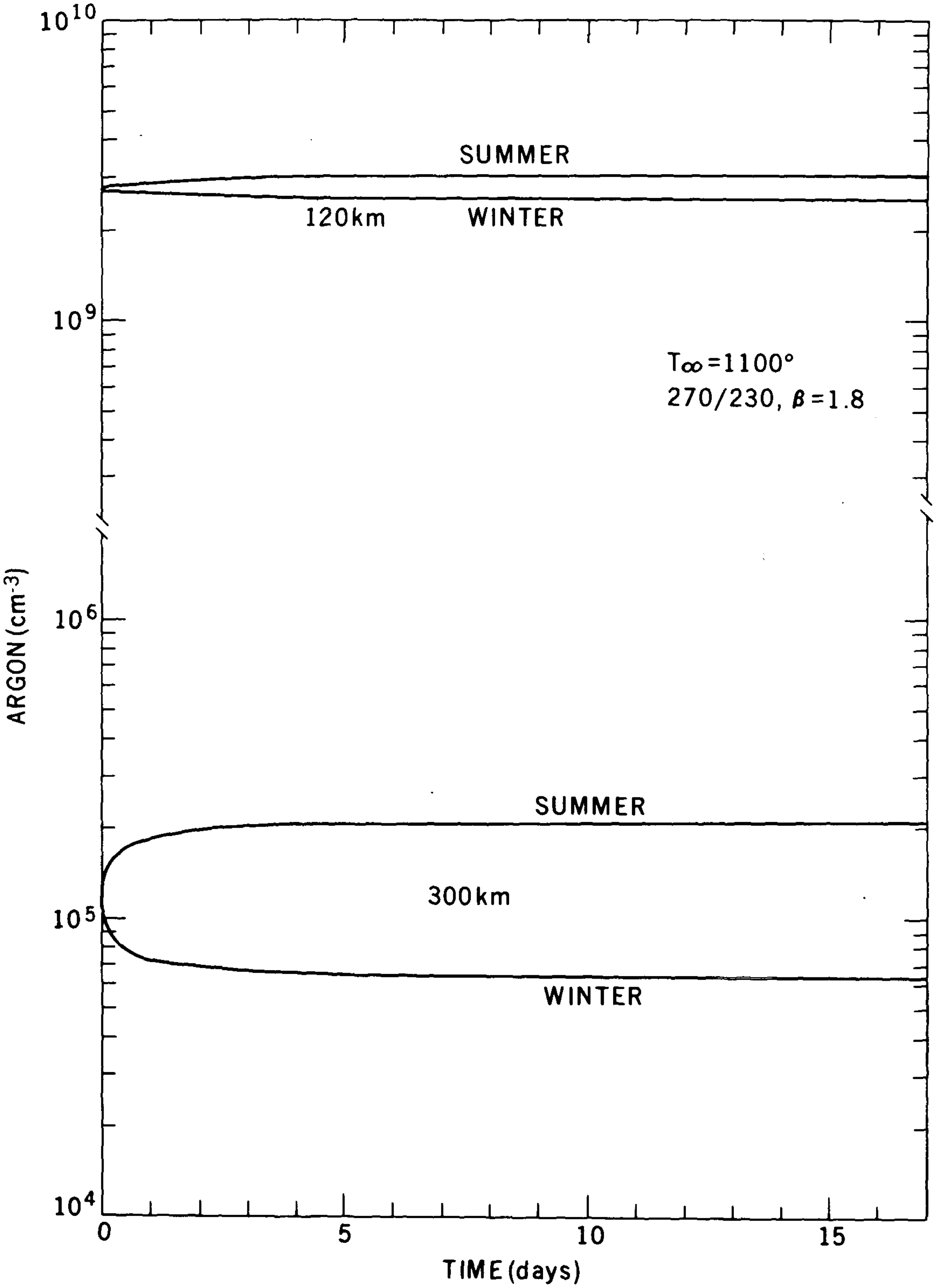

Figure 78. Time development of argon response to a 270/230, $\beta = 1.8$ wind for medium solar conditions.

REFERENCES

Bailey, G. J., R. J. Moffett, and H. Risbeth, Solution of the coupled ion and neutral air equations of the mid latitude ionospheric F2-layer, J. Atmos. Terrestrial Phys., 31, 1969, 253.

Challinor, R. A., The apparent rotation of the upper atmosphere, Planet. Space Sci., 16, 1968, 557.

Challinor, R. A., Neutral Air Winds in the Ionospheric F-Region for an Asymmetric Global Pressure System, Planet. Space Sci., 17, 1969, 1097.

Chapman, S. and R. S. Lindzen, Atmospheric Tides, D. Reidel Publ. Co., Dordrecht-Holland, 1970.

COSPAR International Reference Atmosphere, 1965, North Holland Publishing Company, Amsterdam, 1965.

Colegrove, F. D., W. B. Hanson and F. S. Johnson, Eddy diffusion and oxygen transport in the lower thermosphere, J. Geophys. Rev., 70, 19, 1965.

Colegrove, F. D., F. S. Johnson and W. B. Hanson, Atmospheric Composition in the Lower Thermosphere, J. Geophys. Res., 71, 9, 1966, 2227.

Cooley, J. E. and C. A. Reber, Neutral atmosphere composition measurement between 133 and 533 kilometers from the geoprobe rocket mass spectrometer, Goddard Space Flight Center, X-621-69-260, 1969.

Crank, J. and P. Nicholson, A practical method for numerical evaluation of solutions of partial differential equations of the heat conduction type, Proc. Cambridge Phil. Soc. 43, 50-67, 1947.

Dickinson, R. E. and J. E. Geisler, Vertical motion field in the middle thermosphere from satellite drag densities, Monthly Weather Rev., 96, 9, 1968.

Dickinson, R. E., C. P. Lagos and R. E. Newell, Dynamics of the neutral gas in the thermosphere for small Rossby number motions, J. Geophys. Res. 73, 13, 1968.

Geisler, J. E., Atmospheric winds in the middle latitude F-region, J. Atmos. Terrestrial Physics, 28, 1966, 703.

Geisler, J. E., A numerical study of the wind system in the middle thermosphere, J. Atmos. and Terrestrial Phys., 29, 1967, 1469.

Hartmann, G., K. Mauersberger, and D. Müller, Evaluation of the turbopause level from measurements of the helium and argon content of the lower thermosphere above Fort Churchill, Space Res. VIII, North Holland Publ. Comp., Amsterdam, 1968.

Hedin, A. E. and A. O. Nier, Diffusive separation in the upper atmosphere, J. Geophys. Res., 70, 1965, 1273.

Hedin, A. E. and A. O. Nier, A determination of the neutral composition, number density, and temperature of the upper atmosphere from 120 to 200 kilometers with rocket-borne mass spectrometers, J. Geophys. Res., 71, 4121, 1966.

Hedin, A. E., C. A. Reber and R. Horowitz, Apparent daily variation of atmospheric densities near the South Pole, Trans. Am. Geophys. Union, 51, 11, 1970.

Hodges, R. R. and F. S. Johnson, Lateral transport in planetary exospheres, J. Geophys. Res., 73, 23, 1968.

Jacchia, L. G., Static diffusion models of the upper atmosphere with empirical temperature profiles, Smithsonian Astrophys. Obs., Spec. Rpt. 170, 1964.

Johnson, F. S. and B. Gottlieb, Composition changes in the lower thermosphere, Space Res. IX, North-Holland Publ. Corp., Amsterdam, 1969.

Johnson, F. S. and B. Gottlieb, Eddy mixing and circulation at ionospheric levels, Planet. Space Sci., 18, 1970, 1707.

Kasprzak, W. T., Evidence for a helium flux in the lower thermosphere, J. Geophys. Res. 74, 3, 1969.

Kasprzak, W. T., D. Krankowski and A. O. Nier, A study of day-night variations in the neutral composition of the lower thermosphere, J. Geophys. Res., 73, 1968, 6765.

Keating, G. M. and E. J. Prior, The winter helium bulge, Space Res. VIII, North Holland Publ. Comp., Amsterdam, 1968.

King, J. W., H. Kohl and R. Pratt, The effect of atmospheric winds on the height of the F2-layer peak at middle and high latitudes, J. Atmos. Terres. Phys., 29, 1529, 1967.

King, J. W., H. Kohl, D. M. Preece, and C. Seabrook, An explanation of phenomena occurring in the high-latitude ionosphere at certain universal times, J. Atmos. Terres. Phys., 30, 11, 1968.

Kockarts, G. and M. Nicolet, Aeronomical Problem of Neutral Helium and Hydrogen, Annales de Geophysic, 18, 1962, 269.

Kockarts, G., Distribution of hydrogen and helium in the upper atmosphere, paper presented at Conf. on Theoretical Model Ionospheres, Penn. State Univ., June 1971.

Kohl, H. and J. W. King, Atmospheric winds between 100 and 700 km and their effects on the ionosphere, J. Atmos. Terres. Phys., 29, 1045, 1967.

Krankowski, D., W. T. Kasprzak and A. O. Nier, Mass spectrometric studies of the composition of the lower thermosphere during summer 1967, J. Geophys. Res., 73, 7291, 1968.

Lettau, H., Diffusion in the Upper Thermosphere, in Compendium of Meteorology, ed. by T. F. Malone, American Meteorological Society, N.Y., 1951.

Lindzen, R. S., Crude estimate for the zonal velocity associated with the diurnal temperature oscillation in the thermosphere, J. Geophys. Res., 71, 865, 1966.

Lindzen, R. S., Reconsideration of diurnal velocity oscillation in the thermosphere, J. Geophys. Res., 72, 1591, 1967.

Lindzen, R. S. and H. L. Kus, A reliable method for the numerical integration of a large class of ordinary and partial differential equations, Monthly Weather Rev., 97, 10, 1969.

Magnus, W. and F. Oberhettinger, Formulus and therorems for the functions of mathematical physics, Chelsea Pub. Comp., New York, 1954

Mange, P., Diffusion in the Thermosphere, Annales de Geophysique, 17, 1961, 277.

Mayr, H. G. and H. Volland, Semiannual variations in the neutral composition, Trans. Am. Geophys. Union, 52, 1971.

McAfee, J. R., The effect of lateral flow on exospheric densities, SRCC Rep. #12, Univ. of Pittsburgh, Pittsburgh, Penna.

McAfee, J. R., Lateral flow in the exosphere, Planet. Space Sci., 15, 1967, 599.

Müller, D. and G. Hartmann, A mass spectrometric investigation of the lower thermosphere above Fort Churchill with special emphasis on the helium content, J. Geophys. Res., 74, 1287, 1969.

Reber, C. A. and M. Nicolet, Investigation of the Major Constituents of the April-May 1963 Heterosphere by the Explorer 17 Satellite, Planet. Space Sci., 13, 1965, 617.

Reber, C. A., J. E. Cooley and D. N. Harpold, Upper atmosphere hydrogen and helium measurements from the Explorer 32 Satellite, Space Res. VIII, North Holland Publ. Comp., Amsterdam, 1968.

Reber, C. A., Helium distribution and dynamics in the lower thermosphere, Trans. Am. Geophys. Union, 49, 1, 1968.

Reber, C. A., H. G. Mayr and P. B. Hays, Thermospheric wind effects on the global distribution of helium, Trans. Am. Geophys. Union, 51, 4, 1970

Reber, C. A., D. N. Harpold, R. Horowitz and A. E. Hedin, Horizontal distribution of helium in the earth's upper atmosphere, J. Geophys. Res., 76, 1845, 1971.

Reber, C. A. and A. E. Hedin, The distribution of neutral gases in the northern fall polar atmosphere, Trans. Am. Geophys. Union., 52, 4, 1971.

Risbeth, H., R. J. Moffett, and G. J. Bailey, Continuity of air motion in the mid-latitude thermosphere, J. Atmos. Terrestrial Physics, 31, 1969, 1035.

Taeusch, D. R., G. R. Carignan and C. A. Reber, Neutral composition variation above 400 km during a magnetic storm, J. Geophys. Res., 7, 197.

Volland, H., A theory of thermosphere dynamics-I; diurnal and solar cycle variation, Planet Space Sci., 17, 1581, 1969.

Volland, H. and H. G. Mayr, A theory of the diurnal variations of the thermosphere, Ann. Geophys. 26, 907, 1970.

PRECEDING PAGE BLANK NOT FILMED

APPENDIX A

COUPLED MOMENTUM AND CONTINUITY EQUATIONS FOR A MINOR GAS

The continuity equation for a single gas is written as

$$\frac{\partial n}{\partial t} + \vec{\nabla} \cdot (n \vec{v}) = 0$$

where n is the gas density in molecules (or atoms) per cubic centimeter and $\vec{v}$ is the flow velocity of the gas. In spherical coordinates, with no longitudinal dependence, this becomes

$$\frac{\partial}{\partial r}(n v_r) + \frac{2 n v_r}{r} + \frac{1}{r \sin\theta} \frac{\partial}{\partial \theta}(n v_\theta \sin\theta) = \frac{\partial n}{\partial t}, \qquad \text{(A.1)}$$

where θ and r are the polar angle (latitudinal) and radial variables, and the subscripts refer to the respective velocity components. The momentum equation for a neutral atmospheric component experiencing negligible acceleration, can be written

$$\nabla \vec{p}_n - n m \vec{g} + m n \nu \, [\vec{v} - \vec{V}] = 0,$$

where

p_n = partial pressure of species with density n,

$\vec{g}$ = local acceleration of gravity,

m = molecular mass (gms) of species n,

ν = momentum transfer collision frequency for gas n in background gas, and

$\vec{V}$ = flow velocity of background gas.

Using the ideal gas law, $p_n = nkT$, this becomes

$$n\,[\vec{v} - \vec{V}] = \frac{1}{m\,\nu}\,[n\,m\,\vec{g} - \overrightarrow{\nabla p_n}]$$

or

$$n\,[\vec{v} - \vec{V}] = -\frac{kTn}{m\,\nu}\left[\frac{1}{p_n}\,\nabla\,\vec{p}_n - \frac{m\,\vec{g}}{k\,T}\right]$$

where

k = Boltzmann constant

and T = local temperature.

The radial component of the momentum equation then becomes

$$n\,[v_r - V_r] = -\,D\left[\frac{\partial n}{\partial r} + \frac{n\,(1+\alpha)}{T}\,\frac{\partial T}{\partial r} + \frac{n}{H}\right] \qquad \text{(A.2)}$$

where

$H = \dfrac{kT}{mg}$, the local scale height for the species with mass m,

$D = \dfrac{kT}{m\nu}$, the molecular diffusion coefficient,

and α is the thermal diffusion factor (Chapman and Cowling, 1939; Kockarts and Nicolet, 1963; Colegrove, et. al., 1966). Similarly, the latitudinal component becomes

$$n\,[v_\theta - V_\theta] = -\frac{D}{r}\left[\frac{\partial n}{\partial \theta} + \frac{n\,(1+\alpha)}{T}\,\frac{\partial T}{\partial \theta}\right] \qquad \text{(A.3)}$$

Lettau (1951) has rigorously modified the atmospheric diffusion equation to include the effects of eddy diffusion. Colegrove, et. al. (1965) arrive at the same expression for the vertical concentration gradient as Lettau by considering the flux for a given component to be composed of a molecular diffusion term and an eddy diffusion term. Following this approach, the radial momentum equation becomes

$$n\,[v_r - V_r] = -D\left[\frac{\partial n}{\partial r} + \frac{n\,(1+\alpha)}{T}\,\frac{\partial T}{\partial r} + \frac{n}{H}\right] - K\left[\frac{\partial n}{\partial r} + \frac{n}{T}\,\frac{\partial T}{\partial r} + \frac{n}{H'}\right] \quad \text{(A.2')}$$

where K is the eddy diffusion coefficient and H' is the scale height associated with the mean molecular mass. No corresponding eddy mixing term is added to the latitudinal flux equation as no horizontal temperature gradient is assumed, and the horizontal density gradient for the minor gas is assumed to be small in the region where eddy mixing is appreciable. (Since the addition of this term would decrease any horizontal gradients, the results of the calculation when it is neglected justify the latter assumption.)

Adding $-\partial/\partial r\,(n\,V_r)$ to both sides of (A.1), the continuity equation becomes

$$\frac{\partial}{\partial r}\,n\,(v_r - V_r) = -\frac{2\,n\,v_r}{r} - \frac{1}{r\sin\theta}\,\frac{\partial}{\partial\theta}\,(n\,v_\theta\,\sin\theta) - \frac{\partial}{\partial r}\,(n v_r) + \frac{\partial n}{\partial t}. \quad \text{(A.1')}$$

adding

$$-\frac{1}{r\sin\theta}\,\frac{\partial}{\partial\theta}\,(n\,V_\theta\,\sin\theta)$$

to both sides of (A.1') and making use of (A.3):

$$\frac{\partial}{\partial r}\,n\,(v_r - V_r) - \frac{1}{r\sin\theta}\,\frac{\partial}{\partial\theta}\,(n\,V_\theta\,\sin\theta) - \frac{2\,n\,v_r}{r} - n\,\frac{\partial V_r}{\partial r} - V_r\,\frac{\partial n}{\partial r}$$

$$+\frac{1}{r\sin\theta}\,\frac{\partial}{\partial\theta}\left[\frac{D}{r}\sin\theta\left(\frac{\partial n}{\partial\theta} + \frac{n\,(1+\alpha)}{T}\,\frac{\partial T}{\partial\theta}\right)\right] = \frac{\partial n}{\partial t}. \quad \text{(A.4)}$$

The continuity equation for the major background gas with number density N is

$$\frac{\partial}{\partial r}(N V_r) + \frac{2 N V_r}{r} + \frac{1}{r \sin\theta}\frac{\partial}{\partial \theta}(N V_\theta \sin\theta) = \frac{\partial N}{\partial t}.$$

Assuming no change with time or latitude for the major species

$$\left(\frac{\partial N}{\partial t} = \frac{\partial N}{\partial \theta} = 0\right),$$

this can be written

$$-\frac{1}{r \sin\theta}\frac{\partial}{\partial \theta}(V_\theta \sin\theta) = \frac{1}{N}\frac{\partial}{\partial r}(N V_r) + \frac{2 V_r}{r} + \frac{V_\theta}{N r}\frac{\partial N}{\partial \theta}. \tag{A.5}$$

Using the identity

$$\frac{1}{r \sin\theta}\frac{\partial}{\partial \theta}(n V_\theta \sin\theta) = \frac{n}{r \sin\theta}\frac{\partial}{\partial \theta}(V_\theta \sin\theta) + \frac{V_\theta}{r}\frac{\partial n}{\partial \theta}$$

substitution of (A.5) into (A.4) yields

$$\begin{aligned}\frac{\partial}{\partial r} n (v_r - V_r) + \frac{n}{N}\frac{\partial}{\partial r}(N V_r) + \frac{2 n V_r}{r} + \frac{n V_\theta}{N r}\frac{\partial N}{\partial \theta} - \frac{V_\theta}{r}\frac{\partial n}{\partial \theta} - \frac{2 n v_r}{r}& \\ - n \frac{\partial V_r}{\partial r} - V_r \frac{\partial N}{\partial r} + \frac{1}{r^2 \sin\theta}\frac{\partial}{\partial \theta}\left[D \sin\theta \left(\frac{\partial n}{\partial \theta} + \frac{n(1+\alpha)}{T}\frac{\partial T}{\partial \theta}\right)\right] = \frac{\partial n}{\partial t}.&\end{aligned} \tag{A.6}$$

Replacing $n (v_r - V_r)$ by use of (A.2') and rearranging gives

$$\begin{aligned}\frac{\partial n}{\partial t} = \frac{\partial}{\partial r}&\left\{D\left[\frac{\partial n}{\partial r} + \frac{n(1+\alpha)}{T}\frac{\partial T}{\partial r} + \frac{n}{H}\right] + K\left[\frac{\partial n}{\partial r} + \frac{n}{T}\frac{\partial T}{\partial r} + \frac{n}{H'}\right]\right\} \\ &+ \frac{2}{r}\left\{D\left[\frac{\partial n}{\partial r} + \frac{n(1+\alpha)}{T}\frac{\partial T}{\partial r} + \frac{n}{H}\right] + K\left[\frac{\partial n}{\partial r} + \frac{n}{T}\frac{\partial T}{\partial r} + \frac{n}{H'}\right]\right\} \\ &+ V_r\left[\frac{n}{N}\frac{\partial N}{\partial r} - \frac{\partial n}{\partial r}\right] + V_\theta \frac{1}{r}\left[\frac{n}{N}\frac{\partial N}{\partial \theta} - \frac{\partial n}{\partial \theta}\right] \\ &+ \frac{1}{r^2 \sin\theta}\frac{\partial}{\partial \theta}\left[D \sin\theta\left(\frac{\partial n}{\partial \theta} + \frac{n(1+\alpha)}{T}\frac{\partial T}{\partial \theta}\right)\right].\end{aligned} \tag{A.7}$$

This is the continuity equation for a minor gas, modified by motion in the background gas, which appears as Equation (4) in Chapter II.

APPENDIX B

MODEL ATMOSPHERE

The model atmosphere used in the calculations was based in the COSPAR International Reference Atmosphere (CIRA, 1965) for the altitude range 80 to 120 kilometers and the Jacchia (1965) model as modified by Walker (1965) for altitudes above 120 km. The CIRA model is presented as a tabulation and utilizes a number of straight line temperature profiles. In the calculation of horizontal winds, the expression for B (r) contains a term proportional to the scale height of the major species, which in turn, is related to the temperature gradient:

$$\frac{\partial N}{\partial r} + \frac{N}{T}\frac{\partial T}{\partial r} + \frac{N}{H'} = 0.$$

It was found that the horizontal wind so calculated went through a number of discontinuities at the intersections of the straight line temperature profiles, so the tabulated temperature profile was modified slightly to eliminate the discontinuities in slope. The CIRA and the modified temperature profiles are shown in Figure 79; the effect on the calculation of $B_\ell(r)$ for both profiles is shown in Figure 80 for a typical wind system. The smoothed temperature is given in Table B1 and the complete tabulation, including the densities and mean mass up to 120 km, is given in one of the block data subroutines listed in Appendix E.

Above 120 km the model is analytic and presents the temperature, T, and component number densities, n_i, as functions of altitude, z:

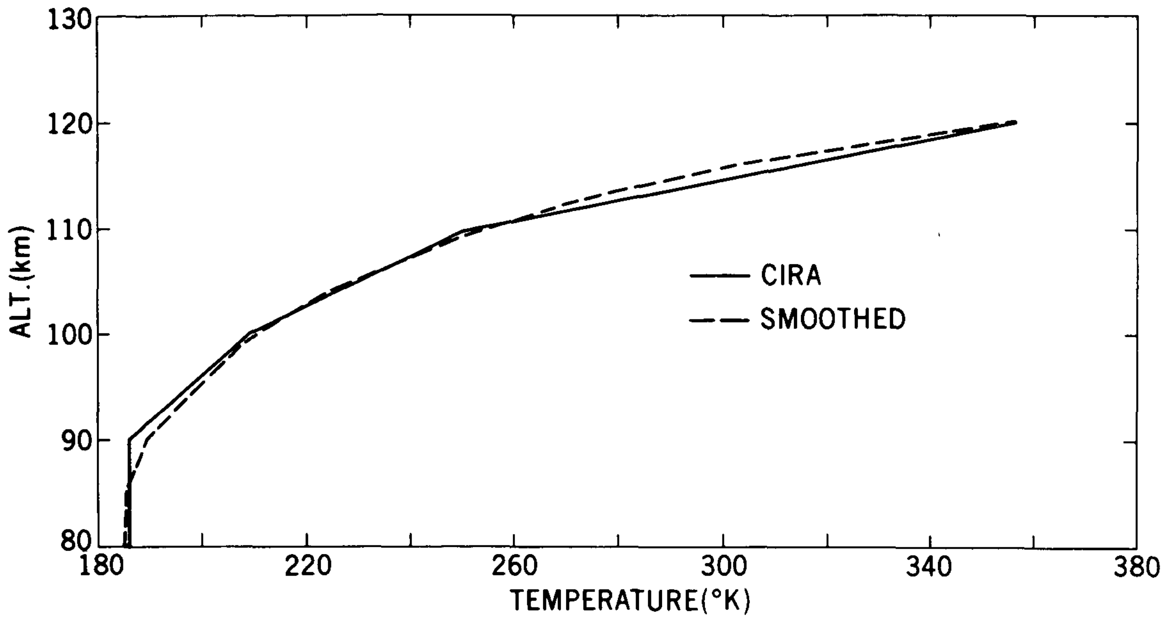

Figure 79. CIRA, 1965 temperature profile compared with the smoothed profile used for the present work.

$$T(z) = T_\infty - (T_\infty - T_{120}) \exp(-\sigma \xi) \tag{B.1}$$

and

$$n_i(z) = n_i(120) \left[\frac{1 - a}{1 - a \exp(-\sigma \xi)} \right]^{1+\alpha+\gamma} \exp(-\sigma \gamma \xi), \tag{B.2}$$

where

T_∞ = exospheric temperature,

T_{120} = temperature at 120 km,

$\sigma = S + 0.00015$,

$S = 0.0291 \exp(-X^2/2)$,

$\xi = (Z - 120)(R + 120)/R + Z$ = geopotential altitude,

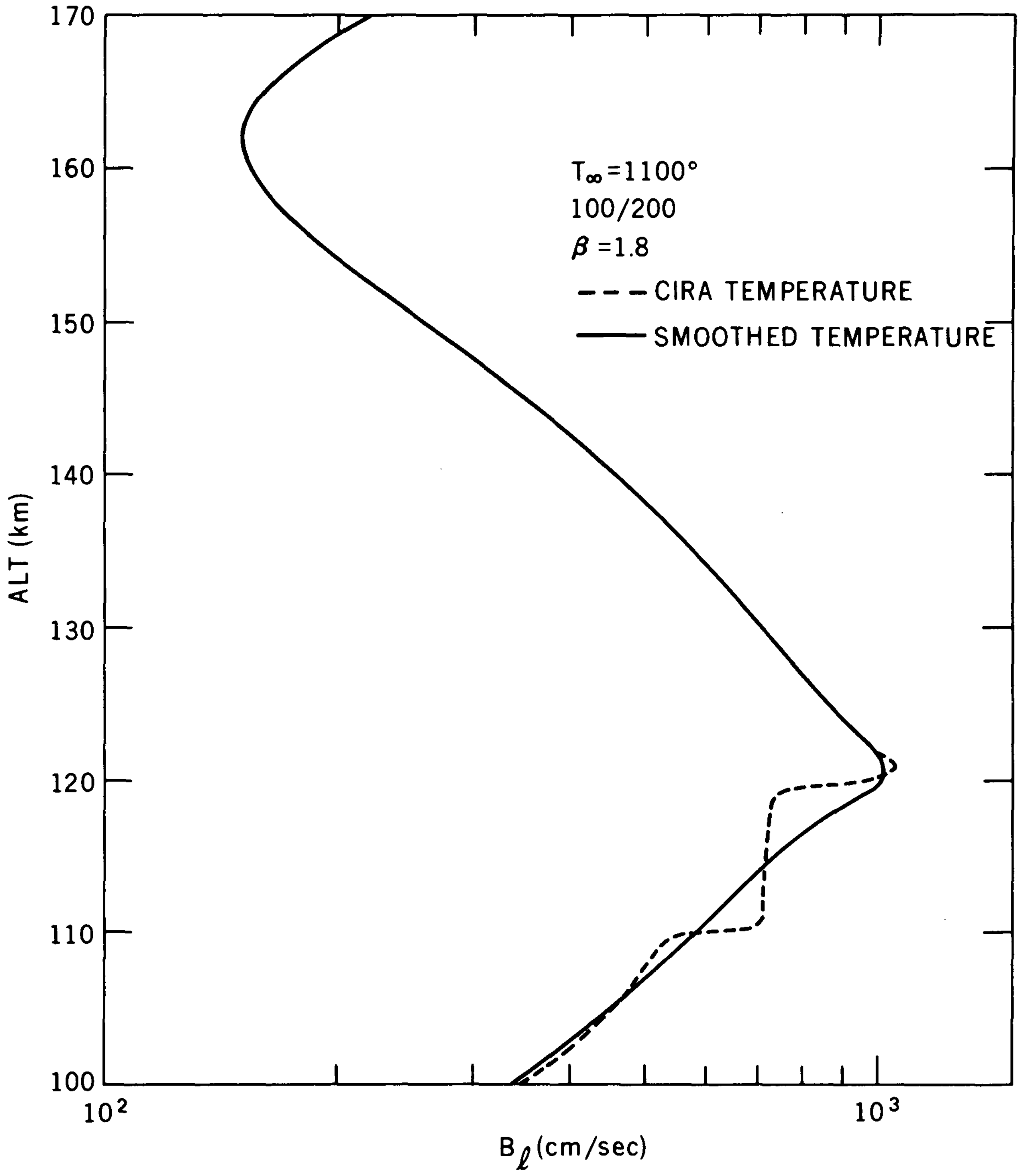

Figure 80. Effect on B_ℓ (twice horizontal wind component) of smoothing CIRA 1965 temperature profile.

Table B-1

Altitude (km)	CIRA	Smoothed CIRA	Altitude (km)	CIRA	Smoothed CIRA
80	186.0		101	212.2	212.6
81	186.0	184.6	102	215.7	216.0
82	186.0	184.6	103	220.0	219.6
83	186.0	184.7	104	224.6	223.4
84	185.9	185.0	105	229.0	227.6
85	185.9	185.3	106	233.4	232.1
86	185.9	185.8	107	237.9	236.9
87	185.9	186.5	108	242.3	242.0
88	185.9	187.3	109	246.8	247.6
89	185.8	188.3	110	251.1	253.5
90	185.8	189.3	111	261.6	260.0
91	188.4	190.6	112	271.9	267.0
92	190.9	192.0	113	282.3	274.5
93	193.5	193.6	114	292.7	282.6
94	195.9	195.3	115	302.9	291.5
95	198.2	197.2	116	313.1	301.3
96	200.4	199.2	117	323.6	312.2
97	202.4	201.5	118	334.0	324.5
98	204.4	204.0	119	344.0	339.1
99	206.3	206.7	120	355.0	355.0
100	208.1	209.5			

$X = T_\infty - 800/750 + 1.722 \times 10^{-4} (T_\infty - 800)^2$

R = radius of earth = 6356.77 km,

$a = T_\infty - T_{120}/T_\infty$

α = thermal diffusion factor (0 for all but helium)

$\gamma = m_i \; g_{120}/\sigma \, k \, T_\infty$,

g_{120} = acceleration of gravity at 120 km = 944.655 cm/sec^2

and

k = Boltzmann's constant.

At 120 km the temperature is 355°K and the number densities are:

$$n\,(N_2) = 4.0 \times 10^{11} \text{ cm}^{-3}$$

$$n\,(O_2) = 7.5 \times 10^{10}$$

$$n\,(O) = 7.6 \times 10^{10}.$$

RELATIONSHIP OF HORIZONTAL AND VERTICAL WINDS

The horizontal component of the wind field is related to the vertical component through the continuity equation for the major species (assuming $\partial N/\partial t = 0$):

$$\frac{\partial}{\partial r}(N V_r) + \frac{2 N V_r}{r} + \frac{1}{r \sin\theta} \frac{\partial}{\partial \theta}(N V_\theta \sin\theta) = 0, \qquad \text{(C.1)}$$

where

N = major gas number density (sum of O, O_2, N_2),

V_r = radial component of wind field, and

V_θ = latitudinal component of wind field.

Rearranging and noting that

$$\frac{1}{N} \frac{\partial N}{\partial r} = -\frac{1}{H'},$$

$$\begin{aligned} \frac{\partial}{\partial \theta}(N V_\theta \sin\theta) &= -r \sin\theta \frac{\partial}{\partial r}(N V_r) - 2 N V_r \sin\theta \\ &= -N \sin\theta \left(r \frac{\partial V_r}{\partial r} - \frac{r V_r}{H'} + 2 V_r \right) . \end{aligned} \qquad \text{(C.1')}$$

Using the expansion of the vertical wind component,

$$V_r(r, \theta) = \sum_{\ell} V_\ell(r) P_\ell(n),$$

and the assumption of no latitudinal variation in N, (C.1') becomes

$$\frac{\partial}{\partial \theta}(\sin\theta\, V_\theta(r)) = -\sin\theta \sum_{\ell} B_\ell(r)\, P_\ell(\mu),$$

where

$$B_\ell(r) = \left(r \frac{\partial V_\ell(r)}{\partial r} - r \frac{V_\ell(r)}{H'(r)} + 2 V_\ell(r) \right).$$

With $\mu = \cos\theta$ and $d\mu = -\sin\theta\, d\theta$, we obtain

$$\frac{\partial}{\partial \mu}[(1-\mu^2)^{1/2} V_\theta] = \sum_{\ell} B_\ell P_\ell(\mu).$$

Integrating over μ from μ' to 1 (θ' to 0) leads to

$$V_\theta = -\sum_{\ell} \frac{B_\ell}{(1-\mu^2)^{1/2}} \int_{u'}^{1} P_\ell(\mu)\, d\mu$$

$$= -\sum_{\ell} B_\ell P_\ell^{-1}(\mu) \text{ (Magnus and Oberhetinger, 1949)} \quad \text{(C.2)}$$

where

$$P_\ell^{-1}(\mu) = \frac{1}{(1-\mu^2)^{1/2}} \int_{u'}^{1} P_\ell(\mu)\, d\mu$$

$$= -\frac{\Gamma(\ell)\, P_\ell^{1}(\mu)}{\Gamma(\ell+2)} \quad \text{(C.3)}$$

$$= \frac{P_{\ell-1}(\mu) - u P_\ell(\mu)}{(\ell+1)(1-\mu^2)^{1/2}}$$

APPENDIX D

METHOD OF SOLUTION

1. Harmonic expansion

The minor gas continuity equation modified to include motion in the background gas was shown in Appendix A to be:

$$
\begin{aligned}
\frac{\partial n}{\partial t} = {} & \frac{\partial}{\partial r}\left\{D\left[\frac{\partial n}{\partial r} + \frac{n\,(1+\alpha)}{T}\frac{\partial T}{\partial r} + \frac{n}{H}\right] + K\left[\frac{\partial n}{\partial r} + \frac{n}{T}\frac{\partial T}{\partial r} + \frac{n}{H'}\right]\right\} \\
& + \frac{2}{r}\left\{D\left[\frac{\partial n}{\partial r} + \frac{n\,(1+\alpha)}{T}\frac{\partial T}{\partial r} + \frac{n}{H}\right] + K\left[\frac{\partial n}{\partial r} + \frac{n}{T}\frac{\partial T}{\partial r} + \frac{n}{H'}\right]\right\} \\
& + V_r\left[\frac{n}{N}\frac{\partial N}{\partial r} - \frac{\partial n}{\partial r}\right] + V_\theta\,\frac{1}{r}\left[\frac{n}{N}\,\frac{\partial N}{\partial \theta} - \frac{\partial n}{\partial \theta}\right] \\
& + \frac{1}{r^2 \sin\theta}\,\frac{\partial}{\partial\theta}\left[D\sin\theta\left(\frac{\partial n}{\partial \theta} + \frac{n\,(1+\alpha)}{T}\,\frac{\partial T}{\partial \theta}\right)\right].
\end{aligned}
\tag{D.1}
$$

It was assumed in the solution of (D.1) that neither the temperature, T, nor the major component number densities, N, varied with latitude; this implies also that H, H', and D are θ independent. The minor gas number density $n(r, \theta)$ was expanded in a series of Legendre polynomials

$$
n\,(r,\,\theta) = \sum_n n_n\,(r)\,P_n\,(\mu), \tag{D.2}
$$

where

$\mu = \cos\theta$,

and a solution was sought for the n^{th} coefficient, $n_n(r)$. The horizontal and vertical components of the wind were also expanded in Legendre series and the full wind field was expressed in terms of the coefficients for the vertical component (see Appendix C):

$$V_r(r, \theta) = \sum_{\ell} V_\ell P_\ell(\mu)$$

$$V_\theta(r, \theta) = -\sum_{\ell} B_\ell P_\ell^{-1}(\mu)$$

and

$$B_\ell(r) = r\frac{\partial V_\ell}{\partial r} + r\frac{V_\ell}{N}\frac{\partial N}{\partial r} + 2V_\ell .$$

After the above simplifications and substitutions each term in (D.1) is multiplied by $P_m(\mu)$ and integrated from -1 to +1 ($\theta = 0$ to $\theta = \pi$, as a negative sign has come in through $d\mu = -\sin\theta d\theta$). Thus, the equation for the coefficient of the m^{th} harmonic becomes

$$\begin{aligned}\frac{2}{2m+1}\frac{\partial n_m}{\partial t} = &\frac{\partial}{\partial r}\left\{D\left(\frac{\partial n_m}{\partial r} + \frac{n_m(1+\alpha)}{T}\frac{\partial T}{\partial r} + \frac{n_m}{H}\right) + K\left(\frac{\partial n_m}{\partial r} + \frac{n_m}{T}\frac{\partial T}{\partial r}\right.\right.\\ &\left.\left. + \frac{n_m}{H'}\right)\right\}\frac{2}{2m+1} + \frac{2}{r}\left\{D\left(\frac{\partial n_m}{\partial r} + \frac{n_m(1+\alpha)}{T}\frac{\partial T}{\partial r} + \frac{n_m}{H}\right) + K\left(\frac{\partial n_m}{\partial r}\right.\right.\\ &\left.\left. + \frac{n_m}{T}\frac{\partial T}{\partial r} + \frac{n_m}{H'}\right)\right\}\frac{2\delta_{nm}}{2m+1} - \sum_{\ell, n} V_\ell\left[\frac{n_n}{H^*} + \frac{\partial n_n}{\partial r}\right]\int_{-1}^{+1} P_\ell(\mu) P_n(\mu) P_m(\mu)\, d\mu \qquad \text{(D.3)}\\ &+ \frac{1}{r}\sum_{\ell, n} B_\ell n_n \int_{-1}^{+1} P_\ell^{-1}(\mu)\frac{\partial P_n(\mu)}{\partial \theta} P_m(\mu)\, d\mu\\ &+ \frac{D}{r^2}\sum_{n} n_n \int_{-1}^{+1}\frac{1}{\sin\theta}\frac{\partial}{\partial\theta}\left(\sin\theta\frac{\partial P_n(\mu)}{\partial\theta}\right) P_m(\mu)\, d\mu = 0.\end{aligned}$$

Here

$$\frac{1}{H^*} = \frac{1}{T}\frac{\partial T}{\partial r} + \frac{1}{H'} = -\frac{1}{N}\frac{\partial N}{\partial r}.$$

With the substitutions

$$A_{\ell nm} = \int_{-1}^{+1} P_\ell(\mu)\, P_n(\mu)\, P_m(\mu)\, d\mu,$$

$$B_{\ell\, nm} = \int_{-1}^{+1} P_\ell^{-1}(\mu) \frac{\partial P_n(\mu)}{\partial \theta} P_m(\mu)\, d\mu,$$

and

$$C_{nm} = \int_{-1}^{+1} \frac{P_m(\mu)}{\sin\theta} \frac{\partial}{\partial \theta} \sin\theta \frac{\partial P_n(\mu)}{\partial \theta}\, d\mu$$

equation (D.3) is equivalent to (10) in section IIC:

$$\frac{2}{2m+1} \frac{\partial n_m}{\partial t} = \frac{2}{2m+1} \frac{\partial}{\partial r} \Big\{\Big\}_m + \frac{2}{2m+1} \frac{\partial}{r} \Big\{\Big\}_m - \sum_{\ell, n} V_\ell \left[\frac{n_n}{H^*} + \frac{\partial n_n}{\partial r}\right] A_{\ell nm} \tag{D.3'}$$

$$- \frac{1}{r} \sum_{\ell, n} B_\ell\, n_n\, B_{\ell nm} + \frac{D}{r^2} \sum_n n_n\, C_{nm},$$

where

$$\Big\{\Big\}_m = D \left[\frac{\partial n_m}{\partial r} + \frac{n_m (1+\alpha)}{T} \frac{\partial T}{\partial r} + \frac{n_m}{H}\right] + K \left[\frac{\partial n_m}{\partial r} + \frac{n_m}{T} \frac{\partial T}{\partial r} + \frac{n_m}{H^*}\right].$$

2. Numerical integration

a. Lindzen and Kuo algorithm

A numerical solution to (D.3') was obtained by use of an integration technique described by Lindzen and Kuo (1969). They express a differential equation of the form

$$\frac{d^2 f}{d x^2} + g(x) \frac{d f}{d x} + h(x)\, f = r(x) \tag{D.4}$$

as the finite difference equation

$$A_i f_{i-1} + B_i f_i + C_i f_{i+1} = D_i, \tag{D.5}$$

where

$$A_i = \frac{1}{(\delta x)^2} - \frac{g(x_i)}{2\delta x}, \tag{D.6a}$$

$$B_i = -\frac{2}{(\delta x)^2} + h(x_i), \tag{D.6b}$$

$$C_i = \frac{1}{(\delta x)^2} + \frac{g(x_i)}{2\delta x}, \tag{D.6c}$$

$$D_i = r(x_i), \tag{D.6d}$$

δx is the finite-difference grid interval and $i = 1, 2, 3, \ldots I - 1$. The boundary conditions

$$\frac{df}{dx} + a_1 f = b_1 \quad \text{at} \quad x = 0$$

and

$$\frac{df}{dx} + a_2 f = b_2 \quad \text{at} \quad x = 1$$

become

$$A_b f_0 + B_b f_1 = D_b$$

and

$$A_t f_{I-1} + B_t f_I = D_t.$$

The difference equation is solved by substituting

$$f_{i-1} = \alpha_{i-1} f_i + \beta_{i-1} \tag{D.7}$$

into it and obtaining

$$\alpha_i = \frac{-C_i}{A_i\ \alpha_{i-1} + B_i}$$

and

$$\beta_i = \frac{D_i - A_i\ \beta_{i-1}}{A_i\ \alpha_{i-1} + B_i}.$$

The lower boundary condition becomes

$$\alpha_0 = -\frac{B_b}{A_b} \quad \text{and} \quad \beta_0 = \frac{D_b}{A_b}.$$

Thus, knowledge of f_I provides all the f_i through (D.7); f_I may be found by substituting (D.7) into the top boundary:

$$f_I = \frac{D_t - A_t\ \beta_{I-1}}{B_t + \alpha_{I-1}\ A_t}.$$

b. Time dependent solution

The one dimensional solution to (D.3') is obtained by expressing it in the form of (D.5), by use of the finite difference approximations (Crank and Nicolson, 1947)

$$\frac{\partial^2 n}{\partial r^2} \rightarrow \frac{n_{i+1} - 2\,n_i + n_{i-1}}{(\delta\ r)^2}$$

$$\frac{\partial n}{\partial r} \rightarrow \frac{n_{i+1} - n_{i-1}}{2\ \delta\ x}$$

$$\frac{\partial n}{\partial t} \rightarrow \frac{n_i^{j+1} - n_i^j}{\delta\ t}.$$

With these substitutions it becomes

$$\frac{n_i^{j+1} - n_i^j}{\Delta t} = \frac{a_i}{2}\left[\frac{n_{i+1}^j - 2\,n_i^j + n_{i-1}^j}{(\delta\ r)^2} + \frac{n_{i-1}^{j+1} - 2\,n_i^{j+1} + n_{i-1}^{j+1}}{(\delta\ r)^2}\right]$$

$$+\frac{b_i}{4}\left[\frac{n_{i+1}^j + n_{i-1}^j}{\delta\ r} + \frac{n_{i+1}^{j+1} - n_{i-1}^{j+1}}{\delta\ r}\right] + \frac{c_i}{2}\,[n_i^j + n_i^{j+1}],$$

where a_i, b_i and c_i are the coefficients in (D.3'). Rearranging:

$$n_{i+1}^{j+1}\left[\frac{a_i}{(\delta\ r)^2} + \frac{b_i}{2\,\delta\ r}\right] + n_i^{j+1}\left[-\frac{\partial}{\delta\ t} - \frac{2\,a_i}{(\delta\ r)^2} + c_i\right] + n_{i-1}^{j+1}\left[\frac{a_i}{(\delta\ r)^2} - \frac{b_i}{2\,\delta\ r}\right]$$

$$= -\,n_{i+1}^j\left[\frac{a_i}{(\delta\ r)^2} + \frac{b_i}{2\,\delta\ r}\right] - n_i^j\left[\frac{2}{\delta\ t} - \frac{2\,a_i}{(\delta\ r)^2} + c_i\right] - n_{i-1}^j\left[\frac{a_i}{(\delta\ r)^2} - \frac{b_i}{2\,\delta\ r}\right] \tag{D.8}$$

Consistency with (D.4) requires a coefficient of unity for the second derivative so we divide by a_i. Then, putting the result in the form of (D.5) yields

$$A_i = \frac{1}{(\delta\ r)^2} - \frac{b_i/a_i}{2\,\delta\ r}, \tag{D.9a}$$

$$B_i = \frac{2}{(\delta\ r)^2} + \frac{c_i}{a_i} - \frac{2}{a_i\ \delta\ t}, \tag{D.9b}$$

$$C_i = \frac{1}{(\delta\ r)^2} + \frac{b_i/a_i}{2\,\delta\ r}, \tag{D.9c}$$

and

$$D_i = -\,A_i\,n_{i-1}^j - \left(B_i + \frac{4}{a\,\delta\ t}\right)n_i^j - C_i\,n_{i+1}^j \tag{D.9d}$$

for the coefficients.

The general solution to (D.3') is then obtained by straightforward extension of this technique utilizing an L-dimensional vector as dependent variable (L corresponds to the number of Legendre polynomials used in the expansion) and matrix coefficients. (D.3') is rewritten

$$\sum_{N=1}^{L}\left[a_{M,N}\frac{\partial^2 n_N}{\partial r^2}+b_{M,N}\frac{\partial n_N}{\partial r}+c_{M,N}\,n_N-\frac{\partial n_N}{\partial t}\right]=0$$

where

$$a_{M,N}=\delta_{MN} \tag{D.10a}$$

$$b_{M,N}=\left\{\left[\frac{\partial}{\partial r}(D)+\frac{D}{H}+\frac{K}{H'}\right]\delta_{MN}-\frac{2M+1}{2}\sum_{\ell=1}^{L}v_\ell\,A_{\ell MN}\right\}\frac{1}{D+K} \tag{D.10b}$$

$$\begin{aligned}c_{M,N}=&\left\{\left[\frac{\partial}{\partial r}\left(\frac{D}{H}\right)+K\frac{\partial}{\partial r}\left(\frac{1}{H'}\right)\right]\delta_{MN}+\frac{2M+1}{2}\,\frac{D\,C_{Mn}}{r^2}\right.\\&\left.-\frac{2M+1}{2}\sum_{\ell=1}^{L}\left[\frac{v_\ell}{H'}A_{\ell MN}+\frac{1}{r}B_\ell\,B_{\ell MN}\right]\right\}\frac{1}{D+K}\end{aligned} \tag{D.10c}$$

Then the coefficients, (D.9) become

$$A_i=\frac{\delta_{MN}}{(\delta r)^2}-\frac{b_{MN}}{2\,\delta r} \tag{D.11a}$$

$$B_i=-\frac{2\,\delta_{MN}}{(\delta r)^2}+C_{MN}-\frac{2\,\delta_{MN}}{(D+K)\,\delta t} \tag{D.11b}$$

$$C_i=\frac{\delta_{MN}}{(\delta r)^2}+\frac{b_{MN}}{2\,\delta r} \tag{D.11c}$$

$$\begin{aligned}D_i=&-\left[\frac{\delta_{MN}}{(\delta r)^2}-\frac{b_{Mn}}{2\delta r}\right]\vec{n}^{\,j}_{i-1}-\left[-\frac{2\,\delta_{MN}}{(\delta r)^2}+C_{MN}+\frac{2\,\delta_{MN}}{(D+K)\,\delta t}\right]\vec{n}^{\,j}_{i}\\&-\left[\frac{\delta_{MN}}{(\delta r)^2}+\frac{b_{MN}}{2\,\delta r}\right]\vec{n}^{\,j}_{i+1}.\end{aligned} \tag{D.11d}$$

The steady state solution can be obtained by dropping the third term in B_i and setting D_i equal to zero.

c. Evaluation of $A_{\ell MN}$, $B_{\ell MN}$, and C_{MN}

The coefficient $A_{\ell mn}$ is calculated directly

$$A_{\ell MN} = \int_{-1}^{+1} P_{\ell}(u)\, P_m(u)\, P_n(u)\, d\,u$$

in the course of the machine integration of (D.3'), using a machine supplied subroutine to perform the integration over the appropriate interval and program supplied polynomials.

The second coefficient,

$$B_{\ell MN} = \int_{-1}^{+1} P_{\ell}^{-1}(u)\, \frac{\partial P_n(u)}{\partial \theta}\, P_m(u)\, d\,u$$

is reduced to a tractable form by the substitutions

$$\frac{\partial P_n(u)}{\partial \theta} = -\sin\theta\, \frac{\partial P_n(u)}{\partial u} = -(1-u^2)^{1/2}\, \frac{\partial P_n(u)}{\partial u}$$

$$\frac{\partial}{\partial u} P_n(u) = \frac{n\,(u\,P_n(u) - P_{n-1}(u))}{(u^2-1)}$$

$$P_{\ell}^{-1}(u) = -\frac{\Gamma(\ell)}{\Gamma(\ell+2)}\, P_{\ell}'(u)$$

$$= -(1-u^2)^{1/2}\, \frac{\partial}{\partial u} P_{\ell}(u)$$

$$= -\frac{(u\,P_{\ell}(u) - P_{\ell-1}(u))}{(\ell+1)\,(1-u^2)^{1/2}}$$

Thus, $B_{\ell_{MN}}$ reduces to

$$- \int_{-1}^{+1} \frac{n\,[P_{\ell-1}(u) - u\,P_{\ell}(u)] \cdot [u\,P_n(u) - P_{n-1}(u)]\,P_m(u)\,d\,u}{(\ell + 1)\,(u^2 - 1)}$$

This integration is carried out by machine, with the singularities at ± 1.0 being avoided by using limits of ±0.99.

The coefficient

$$C_{MN} = \int_{-1}^{+1} \frac{P_m(u)}{\sin\theta} \frac{\partial}{\partial\theta}\left[\sin\theta \frac{\partial P_n(u)}{\partial\theta}\right] d\,u$$

is simplified by the observation that

$$\frac{1}{\sin\theta} \frac{\partial}{\partial\theta}\left(\sin\theta \frac{\partial P_n(u)}{\partial\theta}\right) + n\,(n+1)\,P_n(u) = 0$$

from Legendre's equation. Thus

$$C_{MN} = -\,n\,(n+1) \int_{-1}^{+1} P_m(u)\,P_n(u)\,d\,u$$

$$= -\,\frac{2\,m\,(m+1)}{2\,m+1} \quad \text{for} \quad n = m,$$

$$= \;0 \quad \text{for} \quad n \neq m.$$

PRECEDING PAGE BLANK NOT FILMED

APPENDIX E

PROGRAM USED FOR SOLUTION OF MINOR GAS CONTINUITY EQUATION

```
      IMPLICIT      REAL*8(A-H,O-Z)
       COMMON/INDEX/L, M, N, I, L1, M1, N1
      COMMON/CALC/DR, CS, RE, ALTO, TINF, EDC, TLB, ZLB, MN2, MO2,
     1  MO1, MHE
      COMMON/MOD/TEMP(41), MM(41), DENN2(41), DENO2(41), DENO1(41),
     1  DENHE(41), DENA(41)
      REAL*8
     1      MASS, MM, MN2, MO2, MO1, MHE, MBAR, NUM
      COMMON/COEF/ ALMN(6,6,6), BLMN(6,6,6)
      DIMENSION XDEN(6,6), DENS(422), ZET1(422), ZET2(422), ZET3(422)
      DIMENSION UDEN (6,6), BL(6),BP(6,6),DM1(6),DM2(6),DM3(6),DM4(6)
      DIMENSION LL(6), MV(6)
      DIMENSION AL(6,6,422), BE(6,422), F(6,421), VL(6),      A(6,6 ),
     1 B(6,6  ), C(6,6  ), DEN(6,6  ), PRO(6,6  ),PROB(6  ), DM(6),
     2 NUM(6  ), ALF(6  ), HEIGHT(422) ,FM(6) , ALP(6,6),PN(6),DPN(6)
      DIMENSION AUX(200),DH1(422),DH2(422),DH3(422)
      DIMENSION SCHTI(422), SCHTA(422), DIF(422), SHI(422), SCI(422)
      DIMENSION  VLI(422),  BLI(422),  DDHI(422),EDCI(422)
      EXTERNAL PLP,PLL
      DATA AL/9 *0./,BE/1.663E 09,2*0./,TD/-0.4/
      DENT(ALT) = DN2(ALT) + DO1(ALT) + DO2(ALT)
      SCHT(ALT, MASS)= 8.31E07*T(ALT)*((RE+ALT)**2)/(MASS*980.665*(RE
     1  **2))
      DIFC(ALT)=(1.69E19/DENT(ALT))*((T(ALT)/273.16)**0.691)
      Y(ALT) = 1./(DIFC(ALT) + EDC)
      DT(ALT)=(T(ALT+DR) - T(ALT-DR))/(2.*DR)
      TDT(ALT)=DT(ALT)/T(ALT)
      SH(ALT)=(1. + TD)*TDT(ALT)+ 1./SCHT(ALT,MHE)
      SC(ALT)=TDT(ALT) + 1./SCHT(ALT,MBAR(ALT))
      DD(ALT)=(DIFC(ALT + DR) - DIFC(ALT - DR)) /(2.*DR)
      DDH(ALT)        = (DIFC(ALT + DR) * SH  (ALT + DR)      - DIFC
     1  (ALT - DR) * SH  (ALT - DR)       ) /(2.*DR)
      DHH(ALT)        =        (SC  (ALT + DR)       -       SC
     1  (ALT - DR)       ) /(2.*DR)
      DHE(TH,I)= F(1,I)+ F(2,I)*DCOS(TH)    +  0.5*F(3,I)*
     1 (3.* DCOS(TH)    *   DCOS(TH)   -1.)
     2  + 0.5* (5.*DCOS(TH)** 3-3.*DCOS(TH))*F(4,I)
     3  + (1./8.)* (35.*DCOS(TH)**4-30.*DCOS(TH)**2 +3.)*F(5,I)
     4  + (1./8.)* (63.* DCOS(TH)**5-70.*DCOS(TH)**3+15.*DCOS(TH))
     5  *F(6,I)
    5  FORMAT('1')
  500 FORMAT(   I5, 1P7E16.6)
  250 FORMAT(  3X, 1P6E16.6 )
  251  FORMAT(T120,'A')
  252  FORMAT(T120,'B')
  253  FORMAT(T120,'C')
   50 FORMAT(  3X, 1P6E16.6 )
   51 FORMAT  (T120, 'DEN')
  175  FORMAT(  4X,     1P6E16.6   )
  176 FORMAT (1X,I3,T120,'ALPHA')
  177 FORMAT (T120, 'BETA')
  210 FORMAT('1',T5 ,'F(0,TOP)',T17,'F(1,TOP)',T29,'F(2,TOP)',T41,
     1'F(3,TOP)',T53,'F(4,TOP)')
   12  FORMAT(    /  1P6E12.2)
  325 FORMAT(//,T3,'ALT',T12,'N(HE)0', T24,'N(HE)1',T36,'N(HE)2',
     1     T48,'N(HE)3', T60, 'N(HE)4', T72, 'N(HE)5',T84,'HORIZ. FLUX'/)
  326 FORMAT (//,T3,  'ALT', T10,
     1     'HE( 0 DEG)',T22,'HE(90 DEG)',T35,'HE(180DEG)',T 53,'RH(0)',
     1 T65 ,'RH(90)', T77,'RH(180)',T95,'FLUX(0)',T107,'FLUX(90)',
```

```
     1   T119,  'FLUX(180)'/)
  150 FORMAT( 1X,-5P1F5.0,1P7E12.2)
  151 FORMAT (1X,-5P1F5.0,     1P3E12.2,   6X,1P3E12.2,6X,1P3E12.2)
  400  FORMAT(//,T3,'LAT', T12, 'HE(120)', T24, 'HE(300)',
     1  T36,  'HE(500)'/)
  450 FORMAT(1X, I5, 1P3E12.2)
      WRITE(6,5)
C  NDR IS THE NUMBER OF GRID POINTS ***********************************
C  NDIM IS THE NUMBER OF HARMONICS OR DIMENSION OF THE MATRICES *****
C  NT IS THE NUMBER OF TIME STEPS DESIRED ****************************
C  DELT IS THE VALUE OF THE TIME STEP ********************************
C  NV IS ONE IN NORMAL TIME DEPENDENT CALCULATION:IT IS SET NOT
C      EQUAL TO ONE IF STEADY STATE RESULT IS DESIRED
C  NWR IS ZERO IF NO PRINTOUT OF THE MATRICES IS DESIRED*************
C  NF IS SET TO ZERO IF THE HORIZONTAL FLUX IN UPPER BOUNDARY IS
C         NOT DESIRED
C   NEDC IS SET TO ZERO IF EDC IS DESIRED TO BE CONSTANT
      DATA   NT/ 1/,   NDIM/6/,  NDR/420/,  NV/0/,   NWR/0/
      DATA   NF/1/,   NEDC/1/
      DELT=7.2D03*24.D0
      NP2=NDR+2
      NP1=NDR+1
      DO 225  M=1,NDIM
      PN(M)=0.D0
      DPN(M)=0.D0
      DO 225  N=1,NDIM
      DO 225  L=1,NDIM
      CALL QATR(-1.D0,1.D0,1.D-2,200,PLP,ALMN(L,M,N), IER, AUX)
  225 CALL QATR(-.99D0,.99D0,.01D0,20,PLL,BLMN(L,M,N),IER,AUX)
      BLMN(2,3,3)=0.D0
      BLMN(2,1,3)=0.0D0
      BLMN(2,2,2) = 0.
      BLMN(2,3,1) = 0.
      PN(1)=1.D0
      PN(3)=-0.5D0
      PN(5)=0.375D0
      DPN(2)=-1.D0
      DPN(4)=1.5D0
      DPN(6)=-1.875D0
      EDCM = 2.5D06
      ALTE1 = 1.1D07
      ALTE2 = 1.3D07
      DO 600  I=1,NP2
      RI=I
      ALT=ALTO+RI*DR
      HEIGHT(I)=ALT
      EDCI(I)=   EDCM  *DEXP(1.10000D-06*(ALT- ALTE1))
      IF (ALT.GE. ALTE1) EDCI(I)= EDCM
      IF (ALT.GE.ALTE2) EDCI(I)=EDCM*DEXP(1.10D-06*(ALTE2-ALT))
      IF (NEDC.EQ.0)  EDCI(I)=4.D06
      SCHTI(I)=    DHH(ALT)
      SCHTA(I)=    SCHT(ALT,MBAR(ALT))
      DIF(I)  =  DIFC(ALT)
      DENS(I)   =   DENT(ALT)
      VLN   =   DENS(I)
      CALL VLL(VL,  BL,   I,   VLN,   NDIM,  2, NV)
      VLI(I)   =   VL(2)
      BLI(I)   =   BL(2)
      SHI(I)   =   SH(ALT)
      SCI(I)   =  SC(ALT)
```

```
      DDHI(I)    =    DDH(ALT)
  600 CONTINUE
      DO 501    I3=1, NDIM
      DM(I3)=0.D0
      DO 501    I4=1,NDR
      BE(I3,I4)=0.D0
  501 CONTINUE
C  BEGIN TIME LOOP ****************************************************
      DO 503   IT=1,NT
C  SET BETA (BE) AT UPPER BOUNDARY TO ZERO ***************************
      DO 504   I5=1,NDIM
      BE(I5,NDR)=0.D0
  504 CONTINUE
C CALCULATE ALPHA (AL) AT UPPER BOUNDARY *****************************
      WRITE (6,530)  IT
  530 FORMAT  (110X, 15H TIME STEP NO.=,I5)
      IF (IT.GT.2) GO TO 550
      EDC=EDCI(NDR)
      CALL CALC1(FM, BE(1,NDR),AL(1,1,NDR),NDR,NDIM,IT,NV,NF)
  550 CONTINUE
      NDR1=NDR-1
      DO 200    I2=1,NDR1
      I=    NP1    -I2
      RI = I
      ALT = ALTO + RI * DR
      DTSH = SCHTI(I)
      DTSC = SCHTA(I)
      DTDC = DIF(I)
      DTDD = (DIF(I+1)-DIF(I-1))/(2.D0*DR)
      EDC=EDCI(I)
                DTY = 1.D0/(DIF(I)+EDC)
      DTDH = DDHI(I)
      DTH=  SCHTI(I)
      DSH = SHI(I)
      DSC = SCI(I)
      H = DENS(I)   *2.*DR/(DENS(I-1)    -DENS(I+1))
      R= RE + ALT
      VL(2)   =VLI(I)
      BL(2)   =BLI(I)
      IF(IT.EQ.1.AND.NV.EQ.1)      VL(2)=0.D0
      IF (IT.EQ.1.AND.NV.EQ.1)      BL(2)=0.D0
C     GENERATE A, B, C MATRICES ************************************
      DO 100   M = 1,NDIM
      DO 100   N = 1,NDIM
      SUML = 0.
      SUMLB = 0.
      DO 11   L = 1,NDIM
   10 SUML = SUML + VL(L)      * ALMN(L,N,M)
   11 SUMLB = SUMLB + VL(L)      * ALMN(L,N,M) /      H +BL(L)*
     1 BLMN(L,N,M) / R
      RM = M-1
      CMN=0.
      IF(M.EQ.N)CMN=-2.*RM*(RM+1.)/(2.*RM+1.)
      DE=0.
      IF(M.EQ.N) DE=1.
      RN=N-1
                X=(2.*RN+1.)/2.
      BRA = (DTDD + DTDC* DSH + EDC/   H ) * DE
      A(N, M    ) = DE / (DR*DR) -(1. / (2.*DR))* (BRA-X*SUML) *   DTY
      B(N,M) = -2. * DE/(DR*DR) + DTY * ((DTDH + EDC * DTH) * DE + DTDC
```

```
     1 * CMN*X    /(   R*   R) - SUMLB*X)
      C(N,   M   ) = DE / (DR*DR) + (1. / (2.*DR)) * DTY* (BRA-SUML*X)
      BP(N,M)=        B(N,M)    +DE*   (2.DO/DELT)*DTY
      IF (IT.EQ.1)  GO TO 100
      B(N,M) =        B(N,M)   -DE*   (2.DO/DELT)*DTY
  100 CONTINUE
      IF (NWR.EQ.0)    GO TO 520
      WRITE (6,251)
      WRITE(6,250)   A
      WRITE (6,252)
      WRITE (6,250)  B
      WRITE(6,253)
      WRITE(6,250)   C
      WRITE(6,176)   I
      WRITE(6,175)  ((AL(N,M,I),N=1,NDIM),M=1,NDIM)
  520 CONTINUE
C  CALCULATE ALPHA (AL) FOR GRID PT. (I-1) *************************
C AFTER THE SECOND TIME STEP (IT.GT.2) ALPHA (AL) NEED NOT BE RECAL-
C CULATED ***********************************************************
      IF (IT.GT.2)   GO TO 570
C
      CALL MINV(AL(1,1,I),NDIM,     D,    LL,MV)
      CALL GMPRD(C,      AL(1,1,I),    PRO, NDIM,NDIM,NDIM)
      CALL GMADD(PRO,      B,       XDEN,    NDIM,NDIM)
      IF (NWR.EQ.0)    GO TO   522
      WRITE(6,176)   I
      WRITE(6,175)  ((AL(N,M,I),N=1,NDIM),M=1,NDIM)
      WRITE(6,51)
      WRITE (6,50) XDEN
  522 CONTINUE
      CALL SMPY(XDEN,    -1.DO,   DEN,   NDIM,NDIM,    0)
      CALL SMPY(A,      1.DO,     UDEN,    NDIM,     NDIM,   0)
      CALL MINV(A,   NDIM,      D,    LL,    MV)
      CALL GMPRD(A,DEN,    AL(1,1,I-1),   NDIM,NDIM,NDIM)
C  CALCULATE D(DM),(EQUATION 4), ***********************************
  570 CONTINUE
C  IF FIRST TIME STEP(IT.EQ.1),SKIP CALCULATION OF D****************
      IF (IT.EQ.1)   GO TO 510
C AT THIS PT.,IN THE FIRST AND SECOND TIME STEPS (IT.LE.2),A HAS
C       ALREADY BEEN INVERTED ***************************************
C AFTER THE SECOND TIME STEP, A HAS NOT BEEN INVERTED**************
C  AT THIS POINT, UDEN IS THE SAME AS THE UNIVERTED A MATRIX *******
      IF (IT.GT.2)   GO TO 610
      CALL GMPRD (UDEN,F(1,I-1),   DM,    NDIM,    NDIM,     1)
      GO TO 620
  610 CONTINUE
      CALL GMPRD (A,    F(1,I-1),   DM,    NDIM,   NDIM,     1)
  620 CONTINUE
      CALL GMPRD(BP,     F(1,I),    DM1,  NDIM,   NDIM,     1)
      CALL GMPRD(C,      F(1,I+1),     DM2,   NDIM,     NDIM,     1)
      CALL GMADD (DM,    DM1,    DM3,   NDIM,   1)
      CALL GMADD (DM3,    DM2,    DM1, NDIM,   1)
      CALL SMPY    (DM1,   -1.DO,   DM, NDIM,1,   0)
C CALULATE BETA (BE) AT GRID PT. (I-1) *****************************
C  ALPHA(I-1) HAS NOT BEEN INVERTED YET, ALPHA(I) HAS BEEN INVERTED**
      CALL GMPRD (C,      AL(1,1,I),      ALP,     NDIM,     NDIM,   NDIM)
      CALL SMPY  (ALP,   -1.DO,   UDEN,   NDIM,    NDIM, 0)
      CALLGMPRD (UDEN, BE(1,I),   NUM,     NDIM,    NDIM,     1)
      CALL GMSUB (NUM,   DM,   ALF,    NDIM,     1)
      CALL SMPY   (ALF,   -1.DO,    PROB,    NDIM, 1,    0)
C  IN THE FIRST AND SECOND TIME STEPS(IT.LE.2) A HAS ALREADY BEEN
C      INVERTED: SO SKIP TO 630 ***************************************
      IF (IT.LE.2) GO TO 630
      CALL MINV   (A,    NDIM,    D,  LL,    MV)
  630 CONTINUE
      CALL GMPRD (A,    PROB,    BE(1,I-1),    NDIM, NDIM,   1)
  510 CONTINUE
  200 CONTINUE
```

```
C THIS IS THE END OF THE INTERMEDIATE STEPS:THE DENSITIES WILL NEXT BE
C      CALCULATED ******************************************************
C   SET BOUNDARY CONDITION AT LOWER BOUNDARY ***********************
      F(1,1)    =    1.663D09
      DO  497  I1=2,NDIM
      F(I1,1)=0.D0
  497 CONTINUE
C   INVERT ALPHA (AL) AT LOWER BOUNDARY; THE REST OF THE AL'S HAVE
C         ALREADY BEEN INVERTED ************************************
C  AFTER THE SECOND TIME STEP,  THIS NEED NOT BE DONE
      IF (IT.GT.2)  GO TO  580
      CALL MINV(AL(1,1,1),NDIM,    D,  LL,   MV)
  580 CONTINUE
      DO 300 J=1,NDR
      K=J
      CALL GMSUB (F(1,K),    BE(1,K), DM4,   NDIM,   1)
      CALL GMPRD(AL(1,1,K),    DM4    ,     F(1,K+1),NDIM,NDIM,1)
      DH1(K)= DHE(0.0D0,   K)
      DH2(K)= DHE(1.5708D0,   K)
      DH3(K)= DHE(3.1416D0,   K)
      ZET1(K) = DH1(K)/(DENS(K)  + DH1(K))
      ZET2(K) = DH2(K)/(DENS(K)  + DH2(K))
      ZET3(K) = DH3(K)/(DENS(K)  + DH3(K))
  300 CONTINUE
      HEIGHT(1)=81.E05
      WRITE(6,325)
      BIGPHI=0.D0
      DO 125 I= 1,NDR
      R=RE+HEIGHT(I)
      PHI=0.D0
      PHI1=      0.D0
      DO  128  I9=1,NDIM
      PHI=  PHI    +  F(I9,I)*DPN(I9)
      PHI1=  PHI1   + F(I9,I)*PN(I9)
  128 CONTINUE
      PHI=-PHI   *DIF(I)/R
      PHI1   =-PHI1*BLI(I)*0.5D0
      PHI=PHI    +PHI1
      BIGPHI=BIGPHI+PHI*1.D05
  125 WRITE(6, 150) HEIGHT(I),(F(J,I), J=1,NDIM) ,    PHI
      WRITE(6,326)
      DO 126 I=1,NDR
      IF (I.GE.NDR1)  GO TO 127
      IF (I.EQ.1)     GO TO 127
      FLUX1= -( DIF(I)   +EDCI(I))*(DH1(I+1)-DH1(I-1))/(2.D0*DR)
     1-DH1(I)   *(SHI(I)   *DIF(I)   +SCI(I)   *EDCI(I)   )+DH1(I)   *VLI(I)
      FLUX2= -( DIF(I)   +EDCI(I))*(DH2(I+1)-DH2(I-1))/(2.D0*DR)
     1    -DH2(I)   *(SHI(I)   *DIF(I)   +SCI(I)   *EDCI(I))
      FLUX3= -( DIF(I)   +EDCI(I))*(DH3(I+1)-DH3(I-1))/(2.D0*DR)
     1-DH3(I)   *(SHI(I)   *DIF(I)   +SCI(I)   *EDCI(I)   )-DH3(I)   *VLI(I)
      GO TO 126
  127 FLUX1=0.D0
      FLUX2=0.D0
      FLUX3=0.D0
  126 WRITE(6,151)    HEIGHT(I),
     1 DH1(I),DH2(I),DH3(I), ZET1(I), ZET2(I), ZET3(I) ,FLUX1,
```

```
     1       FLUX2,FLUX3
      WRITE(6,400)
      DO 350 II=1,19
      RI=II
      DHL1   = DHE((RI-1.D0)*0.174533D0,40)
      IF (II.EQ.1)  R1=DHL1
      IF (II.EQ.19) R2=DHL1
      DHL2   = DHE((RI-1.D0)*0.174533D0,220)
      IF  (II.EQ.1)  R3=DHL2
      IF  (II.EQ.19)  R4=DHL2
      DHL3   = DHE((RI-1.D0)*0.174533D0,420)
      IF (II.EQ.1)  R5=DHL3
      IF (II.EQ.19)  R6=DHL3
      LA   = 10*(II-1)
  350 WRITE(6, 450)  LA   ,DHL1   , DHL2,DHL3
      R1=R2/R1
      R2=R4/R3
      R3=R6/R5
      WRITE (6,130)
  130 FORMAT(//T12, 'RATIOS OF POLE DENS.',T60,'INTEG. FLUX AT EQ.'/)
      WRITE (6,131)  R1, R2,R3, BIGPHI
  131 FORMAT ( 6X, 1P3D12.2,T60,1P1D14.4//)
  503 CONTINUE
      WRITE (6,650)
      WRITE (6,652)
  651 FORMAT (1X, -5P1F5.0, 1P6D14.2,-5P2F14.4,1P1D12.2)
  650 FORMAT(////,T3,'ALT(KM)',T15,     'EDC',T29,'DIFC',T43,
     1  'VL/',T57,  'BL/',  T71, 'VL',T85,'BL',T99,'1/SC',  T113,
     1    '1/SH', T125,'X/N')
  652 FORMAT (T13,      '(CM*CM/SEC)',T27,'(CM*CM/SEC)',T41,
     1    '(SH*DIFC)',T55,'(SH*DIFC)',T69,'(CM/SEC)',T83,'(CM/SEC)',
     1    T99,    '(KM)',   T113,   '(KM)'/)
      X8=DENS(220)*100.D0
      DO 640  I7=1,NDR
      ALT=HEIGHT(I7)
      EDC=EDCI(I7)
      DTDC=DIF(I7)
      VLHD=VLI(I7)/(SHI(I7)*DTDC)
      BLHD=BLI(I7)/(SHI(I7)*DTDC)
      RINV1=1.D0/SCI(I7)
      RINV2=1.D0/SHI(I7)
      X9=X8/DENS(I7)
      WRITE (6,651)   ALT,  EDC,   DTDC,    VLHD, BLHD, VLI(I7),BLI(I7)
     1    ,RINV1,        RINV2 ,X9
  640 CONTINUE
      STOP
      END
      BLOCK DATA
      IMPLICIT     REAL*8(A-H,O-Z)
      COMMON/MOD/TEMP(41),MM(41),DENN2(41),DENO2(41),DENO1(41),
     A DENHE(41),DENA(41),MN2,MO2,MO1,MHE,MA
      REAL*8
     1      MASS, MM, MN2, MO2, MO1, MHE, MBAR
      DATA TEMP    /3*186.0,5*185.9,2*185.8,188.4,190.9,193.5,195.9,
     A 198.2,200.4,202.4,204.4,206.3,208.1,212.2,215.7,220.0,224.6,
     B 229.0,233.4,237.9,242.3,246.8,251.1,261.6,271.9,282.3,292.7,
     C 302.9,313.1,323.6,334.0,344.4,355.0/,MM    /4*28.96,5*28.95,
     D 2*28.94,28.92,28.89,28.87,28.83,28.78,28.70,28.61,28.52,28.42,
```

pag:

```
E 28.30,28.18,28.02,27.99,27.92,27.87,27.82,27.78,27.74,27.71,
F 27.66,27.57,27.49,27.41,27.34,27.26,27.19,27.13,27.08,27.04,27.01
G/,DENN2     /            2.478E 14,2.072E 14,1.733E 14,1.449E 14,
H 1.212E 14,1.014E 14,8.480E 13,7.095E 13,5.934E 13,4.965E 13,
I 4.103E 13,3.544E 13,2.831E 13,2.349E 13,1.947E 13,1.626E 13,
J 1.362E 13,1.146E 13,9.673E 12,8.178E 12,6.817E 12,5.704E 12,
K 4.804E 12,4.060E 12,3.453E 12,2.950E 12,2.529E 12,2.174E 12,
L 1.875E 12,1.620E 12,1.365E 12,1.164E 12,9.983E 11,8.606E 11,
M 7.460E 11,6.513E 11,5.723E 11,5.057E 11,4.478E 11,4.008E 11 /
 DATA DENO2    /            6.649E 13,5.559E 13,4.648E 13,3.888E 13,
A 3.251E 13,2.721E 13,2.275E 13,1.906E 13,1.598E 13,1.332E 13,
B 1.101E 13,9.188E 12,7.361E 12,6.146E 12,5.190E 12,4.296E 12,
C 3.553E 12,2.936E 12,2.423E 12,1.994E 12,1.644E 12,1.359E 12,
D 1.131E 12,9.443E 11,7.932E 11,6.693E 11,5.665E 11,4.809E 11,
E 4.093E 11,3.492E 11,2.903E 11,2.443E 11,2.066E 11,1.757E 11,
F 1.501E 11,1.292E 11,1.119E 11,9.744E 10,8.501E 10,7.495E 10/
G ,DENO1     /            8.700E 10,8.930E 10,9.210E 10,9.500E 10,
H 9.800E 10,1.015E 11,1.055E 11,1.105E 11,1.165E 11,1.250E 11,
I 1.420E 11,1.680E 11,2.060E 11,2.660E 11,3.410E 11,4.100E 10,
J 4.515E 11,4.800E 11,4.935E 11,5.000E 11,4.945E 11,4.760E 11,
K 4.425E 11,4.050E 11,3.610E 11,3.210E 11,2.835E 11,2.510E 11,
L 2.230E 11,2.000E 11,1.812E 11,1.642E 11,1.487E 11,1.347E 11,
M 1.235E 11,1.125E 11,1.020E 11,9.250E 10,8.400E 10,7.600E 10 /
 DATA DENHE    /            1.663E 09,1.391E 09,1.163E 09,9.725E 08,
A 8.132E 08,6.807E 08,5.691E 08,4.761E 08,3.982E 08,3.332E 08,
B 2.753E 08,2.282E 08,1.886E 08,1.568E 08,1.306E 08,1.091E 08,
C 9.144E 07,7.692E 07,6.492E 07,5.492E 07,4.575E 07,4.421E 07,
D 4.275E 07,4.138E 07,4.008E 07,3.886E 07,3.768E 07,3.656E 07,
E 3.551E 07,3.450E 07,3.304E 07,3.171E 07,3.048E 07,2.934E 07,
F 2.829E 07,2.731E 07,2.639E 07,2.554E 07,2.474E 07,2.400E 07/
G ,DENA      /            2.965E 12,2.479E 12,2.073E 12,1.734E 12,
H 1.450E 12,1.213E 12,1.014E 12,8.486E 11,7.098E 11,5.939E 11,
I 4.868E 11,4.046E 11,3.363E 11,2.795E 11,2.329E 11,1.945E 11,
J 1.630E 11,1.371E 11,1.157E 11,9.800E 10,8.154E 10,6.823E 10,
K 5.746E 10,4.857E 10,4.130E 10,3.528E 10,3.025E 10,2.601E 10,
L 2.242E 10,1.938E 10,1.633E 10,1.393E 10,1.194E 10,1.029E 10,
M 8.923E 09,7.791E 09,6.846E 09,6.049E 09,5.357E 09,4.795E 09 /
 END
 BLOCK DATA
 IMPLICIT      REAL*8(A-H,O-Z)
 COMMON/CALC/DR, CS, RE, ALTO, TINF, EDC, TLB, ZLB, MN2, MO2,
1  MO1, MHE
 REAL*8
1      MN2, MO2, MO1, MHE
 DATA DR/1.00E 05/,CS/2.12E-15/,RE/6356.77E 05/,ALTO/80.00E 05/,
1 TINF/1100./,EDC/4.00E 06/,TLB/355./,ZLB/120.00E 05/,MN2/28./,
2 MO2/32./,MO1/16./,MHE/4./
 END
 FUNCTION MBAR(ALT)
 IMPLICIT      REAL*8(A-H,O-Z)
 REAL*8
1      MASS, MM, MN2, MO2, MO1, MHE, MBAR
 MEAN MASS FROM 80 KM TO TOP
 COMMON/CALC/DR, CS, RE, ALTO, TINF, EDC, TLB, ZLB, MN2, MO2,
1  MO1, MHE
 COMMON/MOD/TEMP(41), MM(41), DENN2(41), DENO2(41), DENO1(41),
1  DENHE(41), DENA(41)
  COMMON/INDEX/L, M, N, I, L1, M1, N1
 REAL*8
1      MASS, MM. MN2, MO2, MO1, MHE, MBAR
```

```
      IF (ALT - ZLB) 25, 25, 45
   25 MBAR = MM(I)
      GO TO 50
   45 MBAR = (DN2(ALT) * MN2 + DO2(ALT) * MO2 + DO1(ALT) * MO1 +
     1 DHE(ALT) * MHE) / (DN2(ALT) + DO2(ALT) + DO1(ALT) + DHE(ALT))
   50 RETURN
      END
      SUBROUTINE VLL(VL, BL, II,VLN,NDIM,IT,NV)
      IMPLICIT     REAL*8(A-H,O-Z)
      DIMENSION VL(3),      BL(3)
      COMMON/INDEX/L,M,N,I,L1,M1,N1
      COMMON/CALC/DR, CS, RE, ALTO, TINF, EDC, TLB, ZLB, MN2, MO2,
     1  MO1, MHE
      REAL*8
     1      MASS, MM, MN2, MO2, MO1, MHE, MBAR
      DT(ALT) = (T(ALT+DR) - T(ALT -DR))/(2.*DR)
      TDT(ALT) = DT(ALT)/T(ALT)
      SCHT(ALT, MASS)= 8.31E07*T(ALT)*((RE+ALT)**2)/(MASS*980.665*(RE
     1  **2))
      SC(ALT) = TDT(ALT) + 1./SCHT(ALT,MBAR(ALT))
      DENT(ALT) = DN2(ALT) + DO2(ALT) + DO1(ALT)
      DHH(ALT)        =       (SC   (ALT + DR)               SC
     1  (ALT - DR)        ) /(2.*DR)
      RI = II
      ALT = ALTO + RI * DR
      DSC=DHH(ALT)
      SC1=SC(ALT)
      R = RE + ALT
      H = DENT(ALT)*2.*DR/(DENT(ALT-DR)-DENT(ALT+DR))
      ZB =   80.D05
      ZT = 602.D05
      VW =   100.D0
      BETA = 1.8D-07
      DO 56 I1=1,NDIM
      VL(I1)    = 0.
      BL(I1)=0.D0
   56 CONTINUE
      IF (IT.EQ.1.AND.NV.EQ.1)  GO TO 50
      IF (ALT - ZB) 10, 20, 20
   10 VL(2)     = 0.
      BL(2)=0.D0
      GO TO 50
   20 IF (ALT - ZT) 25, 35, 35
   25 DX=(ALT-200.D05)
      ALN= BETA *DX
      VL(2)     = (VW/2.)*(1. +DERF(ALN))
      X2=(VW/1.77245) * BETA *DEXP(-ALN*ALN)
      BL(2)=R*(X2     -VL(2)*SC1+2.*VL(2)/R)
      GO TO 50
   35 VL(2)     = VW
      BL(2)=VL(2)    *(2.- R*SC1)
   50 RETURN
      END
      SUBROUTINE CALC1 (FM,   BET,   ALPHA,NDR,NDIM,IT,NV,NF)
      IMPLICIT REAL*8(A-H,O-Z)
      REAL*8
     1      MASS, MM, MN2, MO2, MO1, MHE, MBAR, NUM
```

```
      COMMON/CALC/DR, CS, RE, ALTO, TINF, EDC, TLB, ZLB, MN2, MO2,
     1 MO1, MHE
      COMMON/INDEX/L, M, N, I, L1, M1, N1
      COMMON/ COEF/ ALMN(6,6,6), BLMN(6,6,6)
      DIMENSION VL(6)      , BL(6)
      DIMENSION UAMM(6,6), UDENF(6,6)
      DIMENSION XAMM(6,6),XDENF(6,6)
      DIMENSION LLA(6), MMA(6), LLN(6), MMN(6)
      DIMENSION AMM(6,6),BMM(6,6),ABM(6,6),ADM(6),NUMF(6),DM(6),BET(6),
     1 AL(6,6,1),DENF(6,6),FM(6), ALPHA(6,6)
      REAL*8   NUMF
      DT(ALT) = (T(ALT + DR) - T(ALT - DR))/(2.*DR)
      TDT(ALT) = DT(ALT)/T(ALT)
      SCHT(ALT, MASS)= 8.31E07*T(ALT)*((RE+ALT)**2)/(MASS*980.665*(RE
     1 **2))
      SH(ALT) = (1. - .4)*TDT(ALT) + 1./SCHT(ALT,MHE)
      SC(ALT)=TDT(ALT) + 1.D0/SCHT(ALT,MBAR(ALT))
      DENT(ALT)=DN2(ALT)+DO1(ALT)+DO2(ALT)
      DIFC(ALT)=(1.69D19/DENT(ALT))*((T(ALT)/273.16)**0.691)
      FNDR=NDR
      ALT1=ALTO+FNDR*DR
      ALT2=ALTO+(FNDR+1.D0)*DR
      NP1=NDR+1
      DA=DIFC(ALT1)
      DB=DIFC(ALT2)
      DC=1.D0/(DA+EDC)
      DD=1.D0/(DB+EDC)
      SH1=SH(ALT1)
      SH2=SH(ALT2)
      SC1=SC(ALT1)
      SC2=SC(ALT2)
      WRITE (6,701)   DA,  DB,  DC,  DD
      WRITE (8,701)  SH1,  SH2,  SC1,   SC2
  701 FORMAT  (D20.10,  D20.10,D20.10,  D20.10)
      R1=RE+ALT1
      R2=RE+ALT2
      AM = -1.D0/DR     +DA*SH1*DC/2.D0+EDC*SC1*DC/2.D0
      BM =  1.D0/DR     +DB*SH2*DD/2.D0+EDC*SC2*DD/2.D0
      WRITE (6,702)    AM,   BM
      WRITE (8,702)    AM, BM
  702 FORMAT   (5X, 4H AM=,D20.10,  4H BM=,D20.10)
      DATA DM/3*0./
      VLN1=       DENT(ALT1)
      VLN2=       DENT(ALT2)
      CALL VLL(VL,BL,NDR,VLN1,NDIM,IT,NV)
      VTL=VL(2)
      CALL VLL(VL,BL,NP1,VLN2,NDIM,IT,NV)
      VTT=VL(2)
C     WRITE (6,703)  ALMN
C     WRITE (6,704)  BLMN
  703 FORMAT (10X,6H ALMN=,3D20.10)
  704 FORMAT (5X, 6H BLMN=,3D20.10)
      WRITE (6,707)  VL
      WRITE(8,707)  BL
  707 FORMAT(5X,6H VLBL=,3D20.10)
      WRITE (6,707)  BL
      WRITE (8,707)  VL
C     MAKE AM A MATRIX = AMM(N,M)
C     MAKE BM A MATRIX = BMM(N,M)
      IF (NF.EQ.0.AND.IT.EQ.1)   GO TO 710
```

```
      EPS1    =    R1      /  SCHT(ALT1,MHE)
      EPS2    =    R2    /SCHT(ALT2,MHE)
      VBAR1=     1.D04*  DSQRT(0.6192D0*T(ALT1))
      VBAR2   = 1.D04 *DSQRT(0.6192D0*T(ALT2))
      HF1  = (1.D0   +   (8.4D0/EPS1))*VBAR1 /(EPS1**2)
      HF2  = (1.D0   +   (8.4D0/EPS2))*VBAR2 /(EPS2**2)
      WRITE (6,902) HF1
      WRITE (8,902) HF1
      HF1=HF1*DC
      HF2=HF2*DD
      DO 11  M= 1,NDIM
      DO 11 N = 1,NDIM
      RM=M-1
      X=RM*(RM+1)
      DELTA = 0.
      IF(N.EQ.M) DELTA=2.D0/(2.D0*RM+1.D0)
      AMM(N,M) =(AM+X*HF1/2.D0)*DELTA   -(DC/2.D0)*VTL*ALMN(2,N,M)
   11 BMM(N,M) =(BM+X*HF2/2.D0)*DELTA   -(DD/2.D0)*VTT*ALMN(2,N,M)
      GO TO 720
  710 CONTINUE
      DO 10  M= 1,NDIM
      DO 10 N = 1,NDIM
      RM=M-1
      DELTA = 0.
      IF(N.EQ.M) DELTA=2.D0/(2.D0*RM+1.D0)
      AMM(N,M) = AM * DELTA -(DC/2.D0)*VTL       *ALMN(2,N,M)
   10 BMM(N,M) = BM * DELTA -(DD/2.D0)*VTT       *ALMN(2,N,M)
  720 CONTINUE
      WRITE (6,708) AMM
      WRITE (6,708) BMM
  708 FORMAT (10X,8H AMMBMM=,3D20.10)
      WRITE (8,708) AMM
      WRITE (8,708) BMM
      CALL MINV(AMM,  NDIM,    DETF,     LLN, MMN)
  902 FORMAT (5X, 3H K=,1P1D13.5)
      CALL GMPRD(AMM,BMM,UDENF,      NDIM,    NDIM,    NDIM)
      CALL SMPY(UDENF,-1.D0,ALPHA,     NDIM,    NDIM,    0)
      WRITE (6,901)  ALPHA
  901 FORMAT (5X, 7H ALPHA=,3D20.10)
      WRITE (8,901)  ALPHA
      RETURN
      END
      FUNCTION DN2(ALT)
      IMPLICIT      REAL*8(A-H,O-Z)
      REAL*8
     1     MASS, MM, MN2, MO2, MO1, MHE, MBAR
      N2 DENSITY FROM 80 KM TO TOP
      COMMON/CALC/DR, CS, RE, ALTO, TINF, EDC, TLB, ZLB, MN2, MO2,
     1  MO1, MHE
      COMMON/MOD/TEMP(41), MM(41), DENN2(41), DENO2(41), DENO1(41),
     1  DENHE(41), DENA(41)
      I = (ALT -ALTO) / DR + .5
      IF (ALT - ZLB) 25, 25, 45
   25 DN2 = DENN2(I)
      GO TO 50
   45 DN2 = DJN2(ALT)
   50 RETURN
      END
      FUNCTION DO2(ALT)
      IMPLICIT      REAL*8(A-H,O-Z)
```

```
      REAL*8
     1     MASS, MM, MN2, MO2, MO1, MHE, MBAR
C     O2 DENSITY FROM 80 KM TO TOP
      COMMON/CALC/DR, CS, RE, ALTO, TINF, EDC, TLB, ZLB, MN2, MO2,
     1  MO1, MHE
      COMMON/MOD/TEMP(41), MM(41), DENN2(41), DENO2(41), DENO1(41),
     1  DENHE(41), DENA(41)
      I = (ALT -ALTO) / DR + .5
      IF (ALT - ZLB) 25, 25, 45
   25 DO2 = DENO2(I)
      GO TO 50
   45 DO2 = DJO2(ALT)
   50 RETURN
      END
      FUNCTION DO1(ALT)
      IMPLICIT      REAL*8(A-H,O-Z)
      REAL*8
     1     MASS, MM, MN2, MO2, MO1, MHE, MBAR
C     O1 DENSITY FROM 80 KM TO TOP
      COMMON/CALC/DR, CS, RE, ALTO, TINF, EDC, TLB, ZLB, MN2, MO2,
     1  MO1, MHE
      COMMON/MOD/TEMP(41), MM(41), DENN2(41), DENO2(41), DENO1(41),
     1  DENHE(41), DENA(41)
      I = (ALT -ALTO) / DR + .5
      IF (ALT - ZLB) 25, 25, 45
   25 DO1 = DENO1(I)
      GO TO 50
   45 DO1 = DJO1(ALT)
   50 RETURN
      END
      FUNCTION DHE(ALT)
      IMPLICIT      REAL*8(A-H,O-Z)
      REAL*8
     1     MASS, MM, MN2, MO2, MO1, MHE, MBAR
C     HE DENSITY FROM 80 KM TO TOP
      COMMON/CALC/DR, CS, RE, ALTO, TINF, EDC, TLB, ZLB, MN2, MO2,
     1  MO1, MHE
      COMMON/MOD/TEMP(41), MM(41), DENN2(41), DENO2(41), DENO1(41),
     1  DENHE(41), DENA(41)
      I = (ALT -ALTO) / DR + .5
      IF (ALT - ZLB) 25, 25, 45
   25 DHE = DENHE(I)
      GO TO 50
   45 DHE = DJHE(ALT)
   50 RETURN
      END
       FUNCTION T(ALT)
      IMPLICIT      REAL*8(A-H,O-Z)
      REAL*8
     1     MASS, MM, MN2, MO2, MO1, MHE, MBAR
C     TEMPERATURE FROM 80KM TO TOP
      COMMON/CALC/DR, CS, RE, ALTO, TINF, EDC, TLB, ZLB, MN2, MO2,
     1  MO1, MHE
      COMMON/MOD/TEMP(41), MM(41), DENN2(41), DENO2(41), DENO1(41),
     1  DENHE(41), DENA(41)
      I = (ALT -ALTO) / DR + .5
      IF(ALT- 80.E05) 15,15,20
   15 T = 186.0
      GO TO 50
```

```
20 IF (ALT - ZLB) 25, 25, 45
25 T = TEMP(I)
   GO TO 50
45 T = TJ(ALT)
50 RETURN
   END
   FUNCTION DJN2(ALT)
   IMPLICIT      REAL*8(A-H,O-Z)
   J65 N2 DENSITY
   COMMON/CALC/DR, CS, RE, ALTO, TINF, EDC, TLB, ZLB, MN2, MO2,
  1  MO1, MHE
   REAL*8
  1      MASS, MM, MN2, MO2, MO1, MHE, MBAR
   GLB = 980.665 / ((1. + ZLB / RE)**2)
   ZETA = (ALT - ZLB) * (RE + ZLB) / (RE + ALT)
   X = (TINF-800.) / (750. + 1.722E-04 * (TINF-800.)**2)
   A = 1.- TLB / TINF
   S = 0.0291 *DEXP (-X * X / 2.)
   SIGMA = ( S + 1.50 E-4) * 1.E-5
   EXPSZ =DEXP(-SIGMA * ZETA)
   GAMMA = MN2 * GLB / (SIGMA * 8.314E 07 * TINF)
   DJN2 = 4.008E 11 * ((1. - A) / (1. - A * EXPSZ)) ** (1. + GAMMA) *
  1 DEXP (-SIGMA * GAMMA * ZETA)
   RETURN
   END
   FUNCTION DJO2(ALT)
   IMPLICIT      REAL*8(A-H,O-Z)
   J65 O2 DENSITY
   COMMON/CALC/DR, CS, RE, ALTO, TINF, EDC, TLB, ZLB, MN2, MO2,
  1  MO1, MHE
   REAL*8
  1      MASS, MM, MN2, MO2, MO1, MHE, MBAR
   GLB = 980.665 / ((1. + ZLB / RE)**2)
   ZETA = (ALT - ZLB) * (RE + ZLB) / (RE + ALT)
   X = (TINF-800.) / (750. + 1.722E-04 * (TINF-800.)**2)
   A = 1.- TLB / TINF
   S = 0.0291 *DEXP (-X * X / 2.)
   SIGMA = ( S + 1.50 E-4) * 1.E-5
   EXPSZ =DEXP(-SIGMA * ZETA)
   GAMMA = MO2 * GLB / (SIGMA * 8.314E 07 * TINF)
   DJO2 = 7.495E 10 * ((1. - A) / (1. - A * EXPSZ)) ** (1. + GAMMA) *
  1 DEXP (-SIGMA * GAMMA * ZETA)
   RETURN
   END
   FUNCTION DJO1(ALT)
   IMPLICIT      REAL*8(A-H,O-Z)
   J65 O  DENSITY
   COMMON/CALC/DR, CS, RE, ALTO, TINF, EDC, TLB, ZLB, MN2, MO2,
  1  MO1, MHE
   REAL*8
  1      MASS, MM, MN2, MO2, MO1, MHE, MBAR
   GLB = 980.665 / ((1. + ZLB / RE)**2)
   ZETA = (ALT - ZLB) * (RE + ZLB) / (RE + ALT)
   X = (TINF-800.) / (750. + 1.722E-04 * (TINF-800.)**2)
   A = 1.- TLB / TINF
   S = 0.0291 *DEXP (-X * X / 2.)
   SIGMA = ( S + 1.50 E-4) * 1.E-5
   EXPSZ =DEXP(-SIGMA * ZETA)
   GAMMA = MO1 * GLB / (SIGMA * 8.314E 07 * TINF)
```

```
      DJO1 = 7.600E 10 * ((1. - A) / (1. - A * EXPSZ)) ** (1. + GAMMA) *
     1 DEXP (-SIGMA * GAMMA * ZETA)
      RETURN
      END
      FUNCTION DJHE(ALT)
      IMPLICIT     REAL*8(A-H,O-Z)
C     J65 HE DENSITY
      COMMON/CALC/DR, CS, RE, ALTO, TINF, EDC, TLB, ZLB, MN2, MO2,
     1 . MO1, MHE
      REAL*8
     1      MASS, MM, MN2, MO2, MO1, MHE, MBAR
      ALPHA = -0.4
      GLB = 980.665 / ((1. + ZLB / RE)**2)
      ZETA = (ALT - ZLB) * (RE + ZLB) / (RE + ALT)
      X = (TINF-800.) / (750. + 1.722E-04 * (TINF-800.)**2)
      A = 1.- TLB / TINF
      S = 0.0291 *DEXP (-X * X / 2.)
      SIGMA = ( S + 1.50 E-4) * 1.E-5
      EXPSZ =DEXP(-SIGMA * ZETA)
      GAMMA = MHE * GLB / (SIGMA * 8.314E 07 * TINF)
      DJHE = 2.400E 07 * ((1. - A) / (1. - A * EXPSZ)) ** (1. + ALPHA
     1 + GAMMA) *DEXP(-SIGMA * GAMMA * ZETA)
      RETURN
      END
      FUNCTION TJ (ALT)
      IMPLICIT     REAL*8(A-H,O-Z)
      REAL*8
     1      MASS, MM, MN2, MO2, MO1, MHE, MBAR
C     J65 TEMPERATURE
      COMMON/CALC/DR, CS, RE, ALTO, TINF, EDC, TLB, ZLB, MN2, MO2,
     1  MO1, MHE
      X = (TINF-800.) / (750. + 1.722E-04 * (TINF-800.)**2.)
      S = 0.0291 *DEXP(-X*X/2.)
      SIGMA = ( S + 1.50 E-4) * 1.E-5
      ZETA = (ALT - ZLB) * (RE + ZLB) / (RE + ALT)
      TJ = TINF - (TINF - TLB) *DEXP (-SIGMA * ZETA)
      RETURN
      END
```